Master's thesis

NTNU
Norwegian University of Science and Technology
Faculty of Medicine and Health Sciences
Department of Clinical and Molecular Medicine

Mirjam Dürkoop

Studying the immunomodulatory effects of SARS-CoV-2 viral proteins in human lung epithelial cell lines

Master's thesis in Molecular Medicine
Supervisor: Hany Zakaria Meås
Co-supervisor: Markus Haug
June 2021

NTNU
Kunnskap for en bedre verden

CEMIR
Centre of Molecular Inflammation Research

Mirjam Dürkoop

Studying the immunomodulatory effects of SARS-CoV-2 viral proteins in human lung epithelial cell lines

Master's thesis in Molecular Medicine
Supervisor: Hany Zakaria Meås
Co-supervisor: Markus Haug
June 2021

Norwegian University of Science and Technology
Faculty of Medicine and Health Sciences
Department of Clinical and Molecular Medicine

NTNU
Norwegian University of
Science and Technology

Abstract

The novel coronavirus disease 2019 (COVID-19), caused by the severe acute respiratory syndrome coronavirus 2 (SARS-CoV-2), presents a wide spectrum of clinical manifestations which range from asymptomatic or cold-like symptoms to severe pneumonia and multisystem failure with fatal outcome. Disease severity correlates with dysregulated host immune responses, characterized by delayed or missing antiviral type I and III interferon (IFN) responses and excessive inflammatory responses. Several viral proteins are proposed to inhibit IFN production, among these SARS-CoV-2 Orf3a, Orf6 and Orf9b. However, most studies have so far focused on viral protein inhibition of type I IFN (IFNα/β) responses in cell types that are of low relevance, and most mechanisms are not yet fully characterized. Here, we studied immunomodulatory effects of SARS-CoV-2 Orf3a, Orf6 and Orf9b proteins in human lung epithelial cell lines (A549, Calu-3) as a relevant cell model for SARS-CoV-2 infection and focused on effects on type III IFN (IFN-λ1/2/3) induction. For this, we used lentiviral transduction to generate cell lines stably expressing the viral proteins upon doxycycline treatment. We demonstrate that A549 and Calu-3 cells respond to transfection of poly(I:C), a dsRNA mimic and common RIG-I/MDA5 agonist, by inducing antiviral and inflammatory immune responses. Inflammatory cytokine and chemokine production was not found altered in lung epithelial cells expressing viral proteins. But interestingly we found a slight reduction in IFN-λ2 secretion from A549 cells expressing Orf3a, Orf6 or Orf9b compared to wildtype cells. Combined, our findings suggest exclusive anti-IFN activity by SARS-CoV-2 Orf3a, Orf6 and Orf9b, but lower type III IFN antagonistic effects compared to what has previously been proposed for type I IFNs. This highlights the distinct role of type III IFNs in maintaining antiviral immunity at the airway epithelium, and the importance of further in-depth studies. Deeper understanding of the immune responses in severe COVID-19 is strongly needed to develop effective therapeutic approaches and to prepare us with knowledge for future pandemic coronavirus outbreaks.

Acknowledgements

This Master thesis was performed at the Research Group on Molecular Mechanisms of Mycobacterial and HIV-1 Infections at the Centre of Molecular Inflammation Research (CEMIR), part of the Faculty of Medicine and Health Sciences at the Norwegian University of Science and Technology (NTNU) in Trondheim.

First of all, I would like to thank my main supervisor, Dr. Hany Meås, for his great support throughout the whole thesis. He has been one of the most enthusiastic and motivating persons I ever worked with. Not only did he teach me to not take results or cell culture contaminations personally, but he also made me ENJOY the work. Thank you! I would also like to thank my co-supervisor, Dr. Markus Haug, and principal investigator, Prof. Trude Helen Flo, for their continuous trust and great support. I was overwhelmed by the warm and fun atmosphere in the group meetings, and I valued a lot how much they trusted me and my work. I wish them all the best for their future projects and am very excited to hear more about it! Also great thanks to Claire, Anne, Ragnhild, Marit and all the other group members for making me feel so welcome, teaching me really valuable skills and helping me whenever I had a question.

I would also like to thank all my fellow classmates and friends for making these two years extraordinary, despite the COVID-19 pandemic. Even though we could not meet as much as we wanted, we still made the best out of it with bonfires in the forest or game nights. Special thanks also to my boyfriend and greatest lab partner, Håvard, who supported me throughout every phase of this project, helped me stay sane and always had good ideas ready. Thank you!

Above all, I want to thank my family for their trust and continuous encouragement throughout all my years of study. Even though we live quite far away from each other, and COVID-19 made it so difficult for us to meet, I always felt your support and love. Thank you!

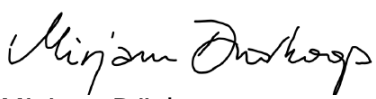

Mirjam Dürkoop
Trondheim, June 2021

Table of Contents

List of Figures

Abbreviations

ACE2	Angiotensin-Converting Enzyme 2
ANOVA	Analysis of variance
ARDS	Acute respiratory distress syndrome
AP-1	Activator protein 1
ATCC	American Type Culture Collection
BALF	Bronchoalveolar Lavage Fluid
BMDM	Bone-marrow derived macrophage
BSA	Bovine Serum Albumin
CARD	two caspase activation recruitment domains
CMV	Cytomegalovirus
COVID-19	Coronavirus disease-19
CRS	Cytokine release syndrome
CXCL	Chemokine (C-X-C) Ligand
DAMP	Damage-associated molecular pattern
DC	Dendritic cell
DEAE	Diethylaminoethyl cellulose
DMEM	Dulbecco's Modified Eagle's Medium
DMSO	Dimethyl sulfoxide
DNA	Deoxyribonucleic acid
DPBS	Dulbecco's Phosphate Buffered Saline
DPP4	Dipeptidyl peptidase 4
DTT	dithiothreitol
EDTA	Ethylenediaminetetraacetic acid
ELISA	Enzyme-linked Immunosorbent Assay
FBS	Fetal Bovine Serum
FCS	Fetal Calf Serum
GAPDH	Glyceraldehyde 3-phosphate dehydrogenase
GFP	Green fluorescent protein
GOI	Gene of interest

GV	GoStix Value
HAECs	human air-liquid airway epithelial cells
HEK293T	Human embryonic kidney 293T cells
HIV-1	Human immunodeficiency virus 1
HMVEC	Human lung microvascular endothelial cells
HRP	Horseradish peroxide
IAV	Influenza A virus
IFIT	Interferon Induced Protein with Tetratricopeptide Repeats 1
IFN	Interferon
IFNAR	Interferon Alpha Receptor
IFNLR	Interferon Lambda Receptor
IFU	Infectious Units
IKK	IκB kinase
IL	Interleukin
IRF	Interferon regulatory factor
ISG	Interferon-stimulated gene
ISGF3	Interferon-stimulated gene factor 3
ISRE	Interferon-stimulated Response Element
JAK	Janus kinases
LB	Lysogeny broth
LDH	Lactate Dehydrogenase
LTR	Long-terminal repeat
LV	Lentivirus
MAVS	Mitochondria antiviral-signaling protein
MDA5	Melanoma differentiation gene 5
MDM	Monocyte-derived macrophages
MERS	Middle Eastern Respiratory Syndrome
MERS-CoV	Middle Eastern Respiratory Syndrome Coronavirus
MOI	Multiplicity of infection

MTS	3-(4,5-dimethylthiazol-2-yl)-5-(3-carboxymethoxyphenyl)-2-(4-sulfophenyl)-2H-tetrazolium
MTT	3-(4,5-dimethylthiazol-2-yl)-2,5-diphenyltetrazolium bromide
NADH	Nicotinamide adenine dinucleotide hydrogen
NF-kB	Nuclear factor kappa-light-chain enhancer of activated B cells
NK cell	Natural Killer cell
NLRP	Nucleotide-binding oligomerization domain
NSP	Non-structural protein
OAS	2',5'-oligoadenylate synthetase
OD	Optical Density
ORF	Open Reading Frame
SDS-PAGE	sodium dodecyl sulphate–polyacrylamide gel electrophoresis
PAMP	Pathogen-associated molecular pattern
PBMC	Peripheral blood mononuclear cells
PBS	Phosphate Buffered Saline
RT-qPCR	Quantitative Reverse Transcriptase Polymerase Chain Reaction
PEG	Polyethylene glycol
PES	Phenazine ethosulfate
PRR	Pattern Recognition Receptor
iPSC	induced pluripotent stem cell
PVDF	polyvinylidene difluoride
RCL	Replication-competent lentivirus
RIG-I	Retinoic-acid inducible gene I
RLR	RIG-I like receptor
RNA	Ribonucleic acid
RdRP	RNA-dependent RNA polymerase
RPMI	Roswell Park Memorial Institute 1640 Medium
RT	Reverse Transcriptase
RTC	Replicase/transcriptase complex
SARS-CoV	Severe Acute Respiratory Syndrome-Coronavirus

SARS-CoV-2	Severe Acute Respiratory Syndrome-Coronavirus 2
SEM	Standard Error of Mean
STAT	Signal transducers and activators of transcription
TBK1	TANK-binding kinase 1
TBS-T	Tris Buffered Saline with Tween-20
TEER	Transepithelial electrical resistance
THP 1	Human monocytic cell line
TLR	Toll-like Receptor
TMB	Tetramethylbenzidine
TNF	Tumor-necrosis factor
TOM70	Mitochondrial surface receptor
TRAF	TNF receptor-associated factor
TRIF	TIR-domain-containing adapter-inducing interferon-β
VSV-G	G protein of vesicular stomatitis virus
WHO	World Health Organization
WT	wildtype

1. Introduction

1.1. SARS-CoV-2 and Innate Immunity

The ongoing COVID-19 pandemic is caused by the novel severe acute respiratory syndrome coronavirus 2 (SARS-CoV-2). First detected in December 2019, SARS-CoV-2 has so far infected more than 171 million people and caused over 3.6 million deaths worldwide, as reported by the World Health Organization (WHO)[1]. The majority of infected individuals are either asymptomatic or develop mild, cold-like symptoms[2]. However, about 20% of COVID-19 patients develop severe symptoms with 15% developing severe pneumonia and 5% reaching a highly critical state with acute respiratory distress syndrome (ARDS), lung damage and multiorgan failures with fatal outcomes[3, 4]. No antiviral treatment for COVID-19 has yet been approved. A detailed understanding of the underlying immunological pathology is strongly needed to understand COVID-19 pathogenesis, reveal possible targets for new antiviral treatments and prepare us with knowledge for future outbreaks of potentially new pandemic coronaviruses.

1.1.1. SARS-CoV-2 virology

Coronaviruses were first isolated in the mid-1960s and comprise a large group of enveloped, positive-sense, single-stranded RNA ((+)ssRNA) viruses that cause disease in both animals and humans, accounting for 10-35% of the common-cold upper respiratory tract infections in humans[5]. Some of these viruses, including the novel SARS-CoV-2, have become highly infectious to humans and caused several epidemic outbreaks in the past like MERS, SARS, and the ongoing COVID-19 pandemic[6-8]. All three causative agents (MERS-CoV, SARS-CoV, SARS-CoV-2) are *betacoronaviruses* and are genetically quite similar (homology: ~80% to SARS-CoV, ~50% to MERS-CoV). However, while SARS-CoV and SARS-CoV-2 are from the B lineage (*Sarbecoviruses*), MERS-CoV is from the C lineage (*Merbecoviruses*)[8, 9]. Another main difference between the three CoVs is that both SARS-CoV and SARS-CoV-2 infect host cells via angiotensin-converting enzyme 2 (ACE2) while MERS-CoV enters the cell by binding to dipeptidyl peptidase 4 (DPP4)[10]. In addition, SARS-CoV-

2 is indicated to spread more efficiently than SARS-CoV which could be mediated by structural differences in its surface proteins enabling stronger binding to ACE2[9].

The viral envelope of SARS-CoV-2 consists of a large number of glycosylated Spike (S) proteins, Envelope (E) proteins, and Membrane (M) proteins (***Figure 1***). The S protein determines the tropism and transmissibility of the virus by mediating cell entry through interaction with the host receptor ACE2[10]. In addition to ACE2, SARS-CoV-2 requires the TMPRSS2 protease to efficiently infect the host cell[11]. ACE2 is highly expressed on cells in the lung, gastrointestinal tract, liver and kidney (proteinatlas.org), and mainly SARS-CoV-2 mainly infects ciliated epithelial cells in nasal mucosa and bronchus, and type II alveolar pneumocytes in lung alveoli[12, 13]. The nucleocapsid protein (N) is located inside the viral particle and forms complexes with the genomic RNA[14]. It has been shown to play a critical role in enhancing the efficiency of the S protein and transmissibility[15]. Finally, the viral genome represents the longest viral RNA known (ca. 30 kb) and consists of 14 open-reading frames (ORFs) encoding for two large polyproteins that are cleaved into 16 non-structural proteins (NSP), and 13 ORFs at the 3' end encoding for the four structural proteins and nine different accessory proteins[16].

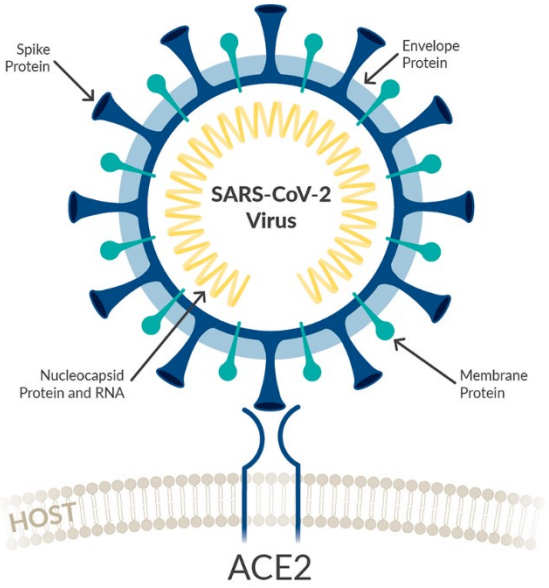

Figure 1) The general structure of SARS-CoV-2. *The figure was taken from caymanchem.com.*

1.1.2. Life cycle of SARS-CoV-2

SARS-CoV-2 is mainly transmitted through respiratory droplets or direct contact with an infected person[16]. The virus infects ACE2- and TMPRSS2-expressing epithelial cells in the lung with the use of its S protein[10, 11]. Following cell entry by receptor-mediated endocytosis and endosomal acidification, SARS-CoV-2 releases its genome into the cell cytoplasm. Highly regulated in space and time, the 16 NSPs are encoded, followed by the accessory proteins (ORFs) and structural proteins (S, E, M, N) (***Figure 2***). At first, Orf1a and Orf1b are translated into two large polyproteins, pp1a and pp1ab,

respectively. The two polyproteins are autoproteolytically cleaved by the two viral cysteine proteases NSP3 (papain-like protease) and NSP5 (3C-like protease), resulting in the release of the remaining NSPs. NSP1 is released first and recruits the host cell translation machinery, followed by NSP2-16 which form the viral replicase/transcriptase complex (RTC). NSP12 comprises the RNA-dependent RNA polymerase (RdRP) and is, together with its two cofactors NSP7 and NSP8, responsible for the generation of new genomic RNA as well as transcription of sub-genomic (sg) mRNAs. These sg mRNAs are then translated into structural (S, M, E, N) and accessory proteins (Orf3a, Orf4, Orf6, Orf7a, Orf7b, Orf8, Orf9b and Orf10). Accessory proteins are not primarily required for viral replication, and an increasing number of studies have proposed modulating functions to enhance virulence and support viral immune evasion (more under **1.2.2**)[17-19]. The structural proteins (S, M, E, N) are expressed at last and allow virus assembly and budding. New virus particles are finally released from the infected cell, ready to infect neighboring cells.[10, 20]

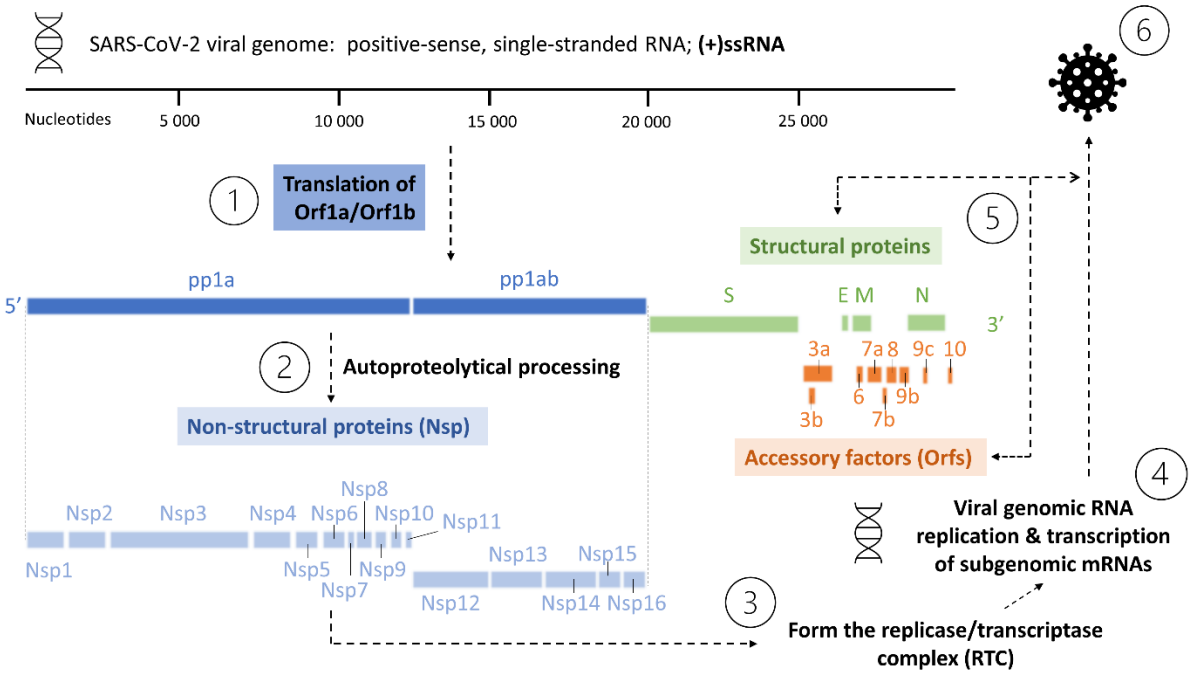

Figure 2) Viral replication cycle of SARS-CoV-2. Upon viral entry and release of the SARS-CoV-2 genomic (+) stranded RNA into the cytoplasm, the host ribosomes translate Orf1a/Orf1b into two large polyproteins, pp1a and pp1ab (1). These are processed into 16 different non-structural proteins (nsps) (2) that make up the replicase/transcriptase complex (RTC) (3). The RTC generates new viral genomic RNA and a set of sub-genomic (sg) mRNAs. The sg mRNAs encode for structural (S, E, M, N) and several accessory proteins (Orfs) (5). Newly produced viral genomic RNA is packaged into new viral particles that are finally released from the infected host cell (6). The figure was made with PowerPoint and based on the overview presented by V'Kovski, Nature Reviews Microbiology, 2020[20].

1.1.3. Induction of innate immune responses against Coronaviruses

Innate immunity is the first line of host immune defense against viral or bacterial infections. These responses are initiated as soon as the host cell is infected and are amplified by innate immune cells, e.g. neutrophils, macrophages, dendritic cells.

Upon coronavirus infection, viral ssRNA and dsRNA intermediates can be recognized as pathogen-associated molecular patterns (PAMPs) via host pattern recognition receptors (PRRs) that mediate expression of pro-inflammatory cytokines, chemokines, and type I and III Interferons (IFNs)[21-23]. The IFN responses induce expression of numerous antiviral effectors in the infected host and neighboring cells[24]. Furthermore, both pro-inflammatory cytokine, chemokine and antiviral IFN responses mediate adaptive immunity which is required to establish long-term immune memory and fight infections that escaped initial innate immune barriers via humoral and cell-mediated immune responses[25-27]. Innate immune responses are initiated by sensing of viral ssRNA or dsRNA intermediates by PRRs located on the endosome, e.g. Toll-like receptors (TLRs) 3, 7 and 8[28, 29], or in the cytoplasm, for example the retinoic-acid inducible gene I (RIG-I)-like receptors (RLRs) (e.g. RIG-I and melanoma differentiation gene 5 (MDA5))[30-33] (***Figure 3***). Besides intracellular sensing of viral nucleic acids, it has been shown that the envelope (E) protein of SARS-CoV-2 can be sensed by TLR2 on the surface of human bone marrow-derived macrophages and human peripheral mononuclear cells (PBMCs)[34]. However, in human lung epithelial cells, SARS-CoV-2 has been found to be mainly sensed by RIG-I and MDA5 in the cytoplasm[30-32, 35]. ***Figure 5*** shows the RLR-dependent signaling pathway leading to the induction and production of type I and III IFNs. In detail, when RLRs become activated, they interact with adapter mitochondria antiviral signaling protein (MAVS) via their two caspase activation recruitment domains (CARD)[36, 37], subsequently recruiting TANK-binding kinase 1 (TBK1) and inducible IkB kinase (IKKi)[38]. The two IKK-related kinases phosphorylate and activate interferon regulatory factor 3 and 7 (IRF3, 7)[36, 38]. Activated IRF3 and 7 are subsequently translocated into the nucleus where they serve as transcription factors for type I and III IFN gene expression[36, 39]. In addition to IFN induction, MAVS signaling also activates the two transcription factors activator protein 1 (AP-1) and nuclear factor kappa-light-chain enhancer of activated B cells (NF-kB) in response to viral infection

which are mainly required to induce expression of inflammatory cytokine and chemokines (e.g. Interleukin 1 (IL-1), IL-6, Tumor necrosis factor (TNF)-a, CXCL8/IL-8)[36]. Sensing of viral nucleic acids via TLRs on the endosome results in the recruitment of adapter proteins TRIF and MyD88 that mediate activation of IRFs, AP-1 and NF-kB transcription factors[22, 40]. In the nucleus, homo- and heterodimers of IRFs activate type I and III IFN expression as well as inflammatory cytokines and chemokines while NF-kB and AP-1 are specifically required to activate expression of inflammatory cytokines and chemokines[22, 33, 41].

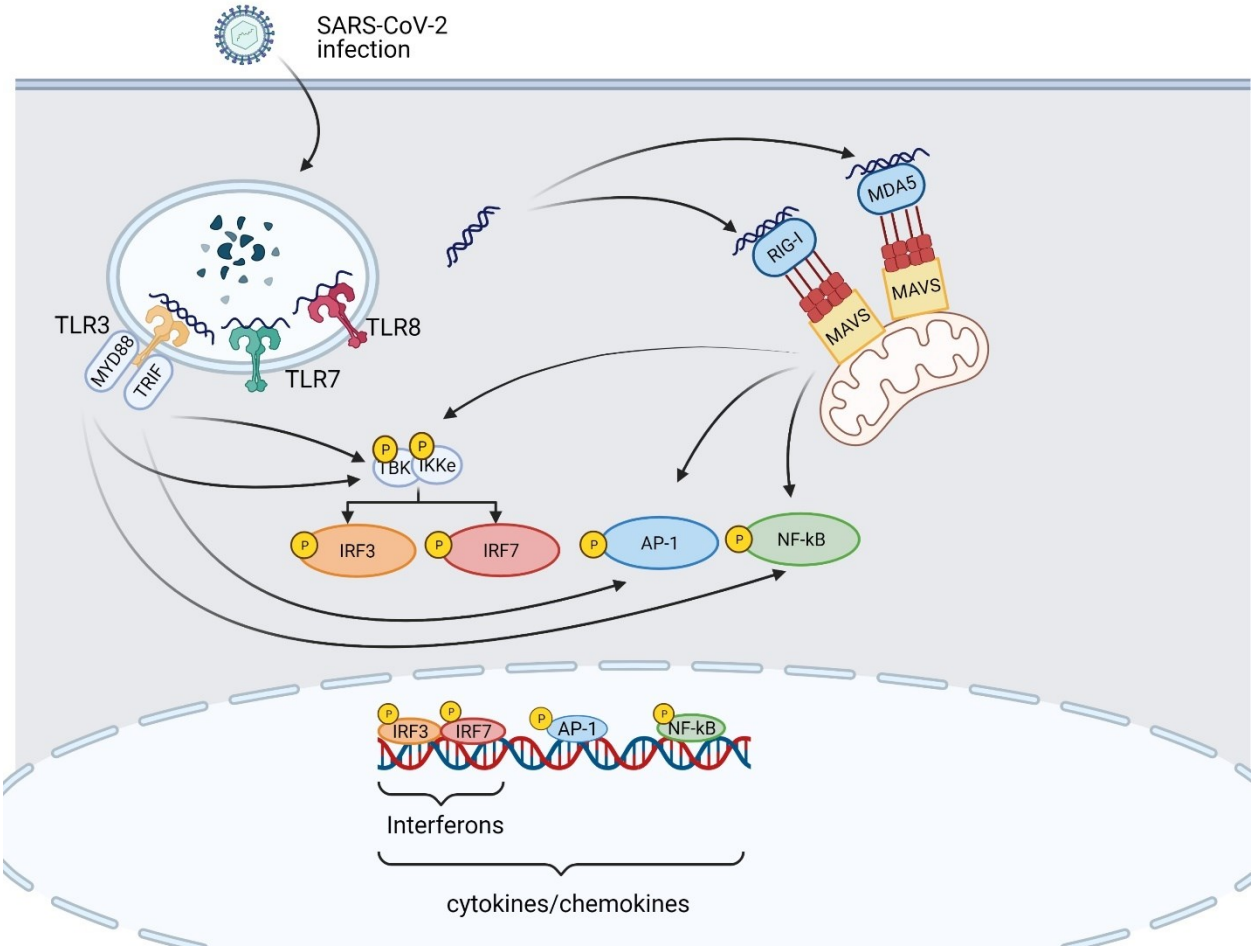

Figure 3) General overview of PRRs sensing RNA viral PAMPs (ssRNA or dsRNA) at the endosome or in the cytoplasm. *TLR3, 7, 8 and RLRs (e.g. RIG-I, MDA5) can sense viral PAMPs in endosome or cytoplasm and activate important transcription factors via different signaling pathways (not shown). Translocation of transcription factors into the nucleus activates expression of type I and III IFNs and pro-inflammatory cytokines and chemokines. The figure was made with BioRender.*

1.1.4. The Type I and III Interferon (IFN) responses

Type I and III IFNs are central during antiviral immunity and are secreted by the host cell early upon infection. Type I IFNs comprise multiple IFN-α subtypes and single

IFN-β, -ε, -κ and -ω with IFN-α2 and -β being the most commonly characterized antiviral type I IFN subtypes. Type III IFNs comprise IFN-λ1, -λ2 and -λ3 and are structurally related to IL-10 family cytokines.[25] The induction and signaling pathways of type I and III IFNs are overlapping, and they share several functions[42]. Autocrine or paracrine signaling through their respective receptors induces expression of a broad spectrum of antiviral effector proteins in the infected host cell and neighboring cells which subsequently act to restrict viral replication and support viral clearance via several mechanisms[24]. ***Figure 5*** gives an overview of the most important steps during RIG-I/MDA5-mediated type I and III IFN induction and signaling pathways. Both type I and III IFNs are produced upon PRR sensing of PAMPs and downstream activation of IRFs and NF-kB[33]. When released from the cell, they activate the expression of several hundred IFN-stimulated genes (ISGs) and important antiviral effectors (e.g. Mx1, OAS, IFIT1, Protein kinase R) via autocrine or paracrine signaling through their respective receptors[24]. In detail, type I IFNs signal through a shared heterodimeric receptor (IFNAR1/IFNAR2)[43] while type III IFNs bind to the IFNL receptor, comprised of IFNLR1 and IL10Rβ subunits[44, 45]. Both receptors signal through the Janus activated kinase (JAK)-Signal transducers and activators of transcription (STAT) signaling pathway. Downstream phosphorylation of STAT1 and STAT2 as well as recruitment of IRF9 leads to the formation of the transcription factor complex ISGF3. ISGF3 translocates to the nucleus where it binds IFN-stimulated response elements (ISREs), subsequently activating expression of ISGs and antiviral responses.[45]

Importantly, the target cells of type I and III IFN signaling are dependent on the expression of the respective **signaling receptors** which comprises one of their major differences[25]. While type I IFN receptors are ubiquitously expressed, i.e. that almost any kind of cell can respond to type I IFN signaling, type III IFN receptor expression is mainly restricted to epithelial cells of the respiratory, gastrointestinal and female reproductive tract and to some extent in innate immune cells, e.g. neutrophils[25, 46]. Consequently, type III IFNs are especially important to protect epithelial barriers from viral infections, while type I IFN signaling results in more systemic responses[25]. Strikingly, IFNLR1-deficient mice infected with influenza A virus (IAV) exhibited higher viral titers compared to mice lacking IFNAR1, suggesting that type III IFNs

are particularly important to contain respiratory viral infections[47]. Furthermore, the ability of type III IFNs to protect the lung epithelium has been correlated with limitation of viral spread from the upper airways to the lower airways, thus decreasing the development of more serious lower respiratory tract infections[47, 48]. Interestingly, the different expression of type I and III IFN receptors also affects their roles in promoting additional **inflammatory responses**. In fact, through their ubiquitously expressed signaling receptors, type I IFNs can act on a wide range of immune cells and were found to directly trigger expression of inflammatory cytokines and chemokines[46]. Type III IFN signaling in neutrophils, in contrast, was found not to induce inflammatory responses but rather resolve inflammation by suppressing neutrophil infiltration and dampening tissue-damaging responses in neutrophils[49, 50]. Other research on distinct features of type I and III IFNs has revealed that the **location of PRRs** affects the type of IFN produced[51-53]. For example, MAVS localization at the mitochondria results in type I IFN production, whereas MAVS localization at the peroxisome results in type III IFN production[52, 53]. Interestingly, abundance of peroxisomes has been shown to correlate with cell polarization[53]. Lastly, emerging research suggests that type I and III IFNs are **differentially regulated**, since their genes contain distinct promoters and transcription factor binding sites[46]. Furthermore, the promoters of IFN- λ1, - λ2 and - λ3 are different, suggesting differential induction as well[46]. Examples for this are emerging and regulation of type I and III IFNs as well as type III IFN subtypes remains to be explored.

Altogether, the features of type I and III IFNs reveal important distinct functions during viral infections, with type III IFNs specifically acting as pro-barrier cytokines and type I IFNs being more inflammatory and modulating systemic responses. Whereas more is known about type I IFNs with regards to induction and effector responses in various cell types during viral infection and in general, further research is warranted on the role of type III IFNs.

1.2. Dysregulation of Innate Immunity by SARS-CoV-2

SARS-CoV-2 has developed several strategies to evade above-mentioned innate immune responses to protect its own life cycle. In general, evasion of innate

immunity is reflected at the immunological level by dysregulated inflammatory and antiviral responses directly influencing the clinical course of the infection. Understanding the complex interplay between SARS-CoV-2 and the host is crucial to develop successful antiviral treatments and prevent and/or treat severe COVID-19. Furthermore, knowledge about SARS-CoV-2 biology will help to quickly characterize future coronaviruses with pandemic potential, detecting and preventing their outbreak earlier.

1.2.1. Immunological features of severe COVID-19

Severe COVID-19 has been characterized by undetectable serum levels of type I and III IFNs and an exacerbated inflammatory response, evidenced by high levels of inflammatory markers in the blood (C-reactive protein, ferritin, D-dimers), an increased neutrophil-to-lymphocyte ratio and increased serum levels of pro-inflammatory cytokines and chemokines[17, 20, 54-59]. The dysfunctional IFN response, unable to inhibit viral replication and spread, and the exacerbated inflammatory response has been suggested to lead to a "storm" of cytokines, clinically manifested by severe acute respiratory distress syndrome (ARDS), lung and multiorgan damage, intravascular coagulation and eventually death[57, 60, 61]. Of note, the broad spectrum of symptoms suggests that not only infected epithelial cells at the primary site of infection (mostly lung) contribute to the immunopathology of severe and fatal COVID-19. Infection of epithelial cells in the gastrointestinal tract, liver or even central nervous system can further contribute to the clinical manifestations of severe COVID-19[62, 63]. Additionally, SARS-CoV-2 infection of endothelial cells and viral modulation of complement and coagulation regulators was found to additionally enhance hyperinflammation and dysregulation of antiviral immune responses while also causing vascular leakage, intravascular coagulation, and clot formation (thrombosis)[64, 65]. However, here we focus on the dysregulation of innate immune responses in lung epithelial cells.

Recent publications highlight the importance of dysfunctional IFN responses during SARS-CoV-2 infection. Several studies have shown that serum samples from patients with severe COVID-19 had undetectable levels of type I and III IFNs[54, 55]. Consistently, transcriptional profiling of SARS-CoV-2 infected primary human airway

epithelial cells (pHAE) showed a complete lack of type I and III IFN responses[56]. Furthermore, SARS-CoV-2 infection studies of the permissive Calu-3 and hACE2-A549 human lung epithelial cell lines discovered a delay in type I and III IFNs production that failed to restrict viral replication[17, 30, 32, 55]. Additionally, comparing average remaining activity of type I and III IFN induction pathways in HEK293T cells before and after SARS-CoV-2 infection revealed lower inhibition of the type III IFN induction pathway compared to the type I IFN pathway[66]. Interestingly, several studies found that SARS-CoV-2 replication could be restricted when permissive cells were pre-treated with type I or III IFNs[55, 66-68]. These findings show that IFN-induced responses would suffice to fight SARS-CoV-2 infection and that during severe COVID-19, SARS-CoV-2 fails to induce the production of the important antiviral mediators. But how does SARS-CoV-2 antagonize the type I and III IFN response? In fact, several accessory and non-structural proteins of SARS-CoV-2 are found to have antagonistic functions by inhibiting important mediators in PRR- and type I and III IFN-signaling pathways leading to aberrant ISG expression and antiviral effector responses[17, 18, 69]. The functions of some of these will be discussed in detail under **1.2.2**. In addition to viral evasion strategies, transcriptomic screenings of serum samples from severe COVID-19 patients suggested additional underlying mechanisms of the dysregulated IFN response in severe COVID-19. Zhang *et al.* found that patients with life-threatening COVID-19 had undetectable levels of type I and III IFNs and that 3.5% of them had loss-of-function mutations in genes associated to the type I and III IFN response pathways (*TLR3, TLR7, TBK1, IRF7, IRF3, IFNAR1/2*, …). Among patients with asymptomatic/mild COVID-19, they found detectable levels of type I and III IFNs and only 0.2% loss-of-function mutations in one of the 13 gene loci.[70] Another possible cause of type-I IFN deficiency in life-threatening COVID-19 was suggested to be the generation of type-I IFN auto-antibodies, as reported by Bastard *et al.* in a broad cohort-study[71]. The study found that 13.7% of these patients, again having low levels of type I IFNs in serum, had developed auto-antibodies with interferon-neutralizing activity. In contrast, none of asymptomatic/mild COVID-19 patients with normal IFN levels developed such auto-antibodies. Interestingly, 94% of all patients with detected auto-antibodies were

male, suggesting that genetic mutations on the X-chromosome could favor the emergence of auto-antibodies.[71]

Infected epithelial cells produce the earliest wave of cytokines to respond to the infection and trigger inflammatory responses and chemokines to recruit immune cells to the site of viral infection[72]. In patients with severe COVID-19, serum levels of circulating IL-6, TNF-α, IL-8/CXCL8, CCL2 and CCL8 are highly elevated and continue to circulate beyond the clearance of the virus[55, 73]. The high elevation of CCL2 and CCL8 as well as CXCL2 and CXCL8 lead to recruitment of monocyte-derived macrophages and neutrophils, respectively[55]. Significant increase of macrophages in the lung alveolar space was evidenced by *ex vivo* analysis of lung tissue from fatal COVID-19 cases[74] and high levels of circulating neutrophils was shown by serum analysis of severe COVID-19 patients[75]. Surprisingly, even though macrophages do not express hACE2 and are most likely not infected by SARS-CoV-2, they have been associated as key players for the exacerbated cytokine response[60]. In fact, single-cell analysis of bronchioalveolar lavage fluid (BALF) from patients with COVID-19 showed that disease severity correlated with stronger epithelium-immune cell interactions and specifically highly inflammatory macrophages and activated cytotoxic T lymphocytes compared to mild COVID-19 cases[76]. Another study of bulk and single-cell RNA sequencing data from BALF further suggested that inflammatory macrophages and IFN-γ secreting T cells in the lung alveoli form positive feedback loops and by that promote lung inflammation and severe pneumonia[77]. Lastly, a recent study demonstrated that the early responses of infected epithelial cells have direct consequences on immune activation evidenced by the ability of pro-inflammatory mediators from infected Calu-3 lung epithelial cells directly inducing pro-inflammatory (primary) macrophage activation[30].

Altogether, COVID-19 severity is driven by delayed or missing type-I and -III IFN responses consequently allowing the virus to replicate and spread and inducing elevated levels of cytokines and chemokines resulting in high inflammation. If the immune system cannot fight the infection at this stage, persistent lung inflammation will lead to ARDS, damage of the vasculature and at last lung and multiorgan failure with fatal outcome[57, 60, 61].

1.2.2. Immunomodulatory functions of SARS-CoV-2 Orf3a, Orf6 and Orf9b

A combination of proteomics-based interaction studies with functional studies in HEK293T cells suggest at least 13 viral proteins with proposed antagonistic functions against innate immune responses[17, 18, 69]. This study focuses on IFN-antagonistic effects of SARS-CoV-2 Orf3a, Orf6 and Orf9b. However, several other viral proteins (Nsp1, Nsp5, Nsp13, Nsp14, Nsp15) have been proposed to contribute to the inflammatory phenotype of severe COVID-19 and interact with host proteins that are necessary to elicit a functional type I IFN response[19, 69, 78-81].

To this date, the mechanistic functions of SARS-CoV-2 viral proteins are only partially understood. However, several proteomics studies have identified host interaction partners and localizations of SARS-CoV-2 viral proteins in infected cells, such as the recent study by Meyers *et al.* from February 2021[78] or two SARS-CoV-2 protein interaction maps published by Gordon *et al.* in July and December 2020[69, 79]. Together, these studies propose a direct link between several SARS-CoV-2 viral proteins employing direct antagonistic effects on the host's innate immune pathways and contributing to the clinical course of COVID-19. Furthermore, they revealed insight into the cellular localizations of the viral proteins, providing additional information about their roles and functions in the host cell[69, 78, 79]. An overview of SARS-CoV-2 Orf3a, Orf6 and Orf9b, their host interaction partners and proposed immunomodulatory functions are demonstrated in ***Figure 4*** and will be discussed in detail in the text. In ***Figure 5***, current knowledge on type I and III antagonism of SARS-CoV-2 Orf3a, Orf6 and Orf9b was collected and visualized.

Several studies have suggested that SARS-CoV-2 Orf6 and Orf9b are potent type I IFN antagonists[17, 19, 67, 69, 78, 79, 82, 83]. In fact, **SARS-CoV-2 Orf6** seems to antagonize both IFN induction and signaling pathways by preventing trafficking of the required transcription factors (IRF3, ISGF3) from the cytosol into the nucleus (see ***Figure 5***)[69]. It has been suggested that type I and III IFN signaling pathways could be inhibited by the interaction of Orf6 with the nuclear import complex Nup98/RAE1, recently identified as high-confidence binding partners[69]. In fact, transient transfection of SARS-CoV-2 Orf6 in HEK293T cells confirmed the direct interaction with Nup96/RAE1 and that Nup98 binding to Orf6 blocked STAT1 nuclear translocation[67]. Another study showed that SARS-CoV-2 Orf6 could also prevent

expression of a transfected IFN-β Luciferase reporter plasmid in HEK293T cells at a step post-IRF3 phosphorylation and along the RIG-I/MDA5-MAVS-IRF3 axis, suggesting that Orf6 also prevents type I IFN induction[19]. Interestingly, proximity proteomics revealed that Orf6 could interact with MAVS through proximity[78], suggesting a mechanistic relationship between the two proteins that could result in downregulation of the IFN induction pathways.

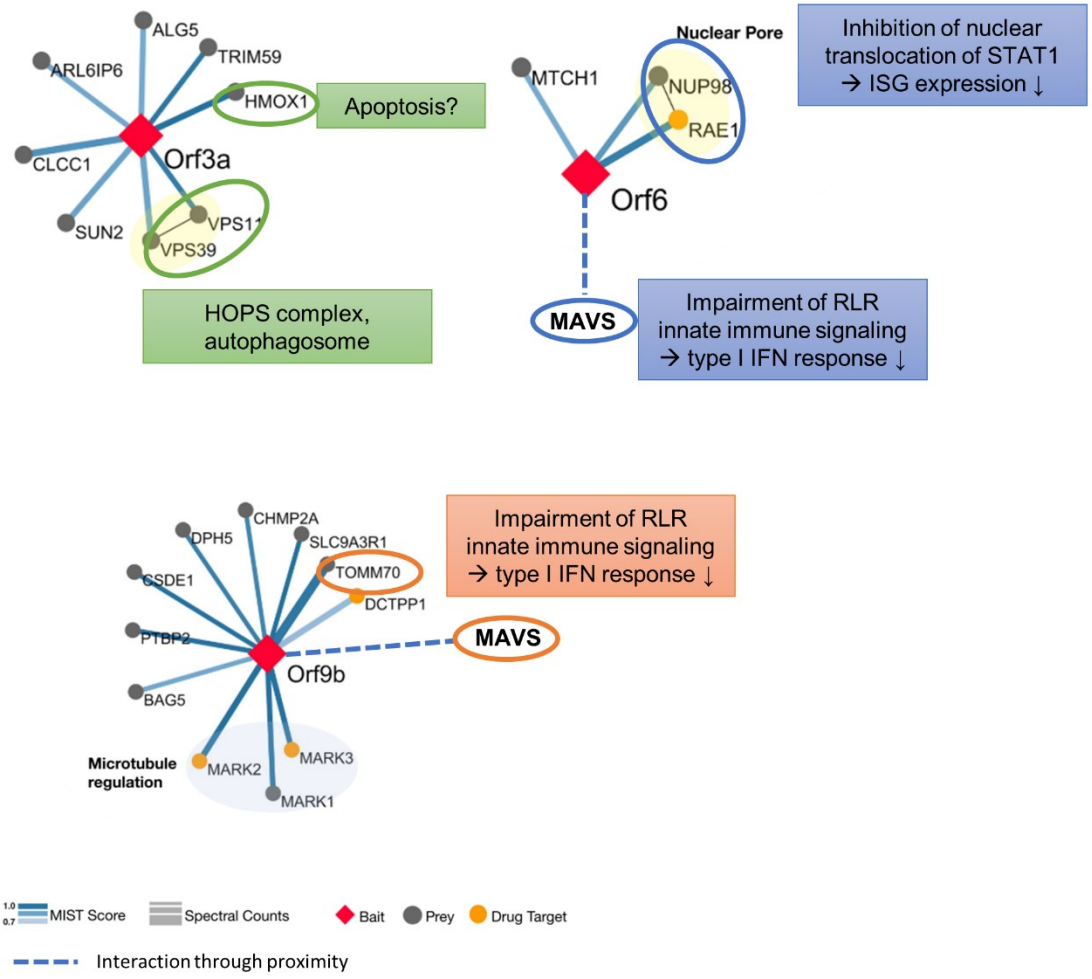

Figure 4) Interaction maps of SARS-CoV-2 Orf3a, Orf6 and Orf9b and possible immunological consequences of host-pathogen interactions. *The interaction maps were adapted from Gordon et al.[69] and additional proximity interactions included[78].*

SARS-CoV-2 Orf9b has also been suggested to impair IFN induction along the RIG-I/MDA5-MAVS-IRF3 axis[79, 82]. Several studies found that expression of transfected IFN-β Luciferase reporter plasmids was significantly reduced in presence of Orf9b in HEK293T cells[82, 84]. Immunoprecipitation assays pulled down translocase of outer membrane 70 (TOM70) together with SARS-CoV-Orf9b[79, 82]. Importantly, Tom70

interacts with MAVS upon RNA virus infection and mediates phosphorylation of IRF3 by recruiting TBK1/IRF3 to the mitochondria[84]. Consistent to the pull-down assays, transient transfection of HEK293T cells with SARS-CoV-2 Orf9b-Flag identified direct interaction with TOM70 at the mitochondria, evidenced by confocal microscopy using anti-Flag and anti-TOM70 antibodies[82]. Combined, inhibition of TOM70 by Orf9b could directly prevent IRF3 activation and thus expression of type I and III IFNs.

SARS-CoV-2 Orf3a was found to be primarily localized at the late endosomes where it has been described to target and block autophagy by preventing autophagosome-lysosome fusion[66, 85]. Recently, Orf3a has also been described in the context of innate immune manipulation by inhibiting IFN-β secretion from transiently transfected HEK293T cells[66]. Luciferase reporter assays determined that Orf3a could downregulate expression of reporter assays for NF-kB and IRF3[66], which are both required for the induction of type I and III IFNs, and also inflammatory cytokines (NF-kB). The same study suggested that Orf3a might also antagonize IFN signaling pathways, since they found that HEK293T cells transiently transfected with Orf3a reduced the activation of a transfected reporter plasmid for ISRE[66] – the promoter site to which ISGF3 binds and induces transcription of ISGs. In addition, previous research on SARS-CoV Orf3a, to which SARS-CoV-2 Orf3a is 85.1% similar[69], showed that SARS-CoV Orf3a could activate the NRLP3 inflammasome, inducing the release of highly inflammatory IL-1b[86]. Furthermore, SARS-CoV Orf3a was also suggested to downregulate IFN signaling pathways, specifically by inducing degradation of IFNAR1[87] and suppressing STAT2 phosphorylation[18]. Interestingly, SARS-CoV Orf3a was shown to upregulate fibrinogen secretion from lung epithelial cells[88] which is associated with systemic inflammation[89] and, when dysfunctional, can cause thrombosis[90]. This hints towards the pathology of severe COVID-19 suggesting that SARS-CoV-2 Orf3a could have similar functions. More research is needed to characterize the mechanisms by which SARS-CoV-2 Orf3a could interfere with type I and III IFN responses and promote exacerbated inflammation or cytokine storm. Summarizing all the proposed IFN-modulating functions of SARS-CoV-2 Orf3a, Orf6 and Orf9b leaves an interesting network of host-pathogen connections (***Figure 5***).

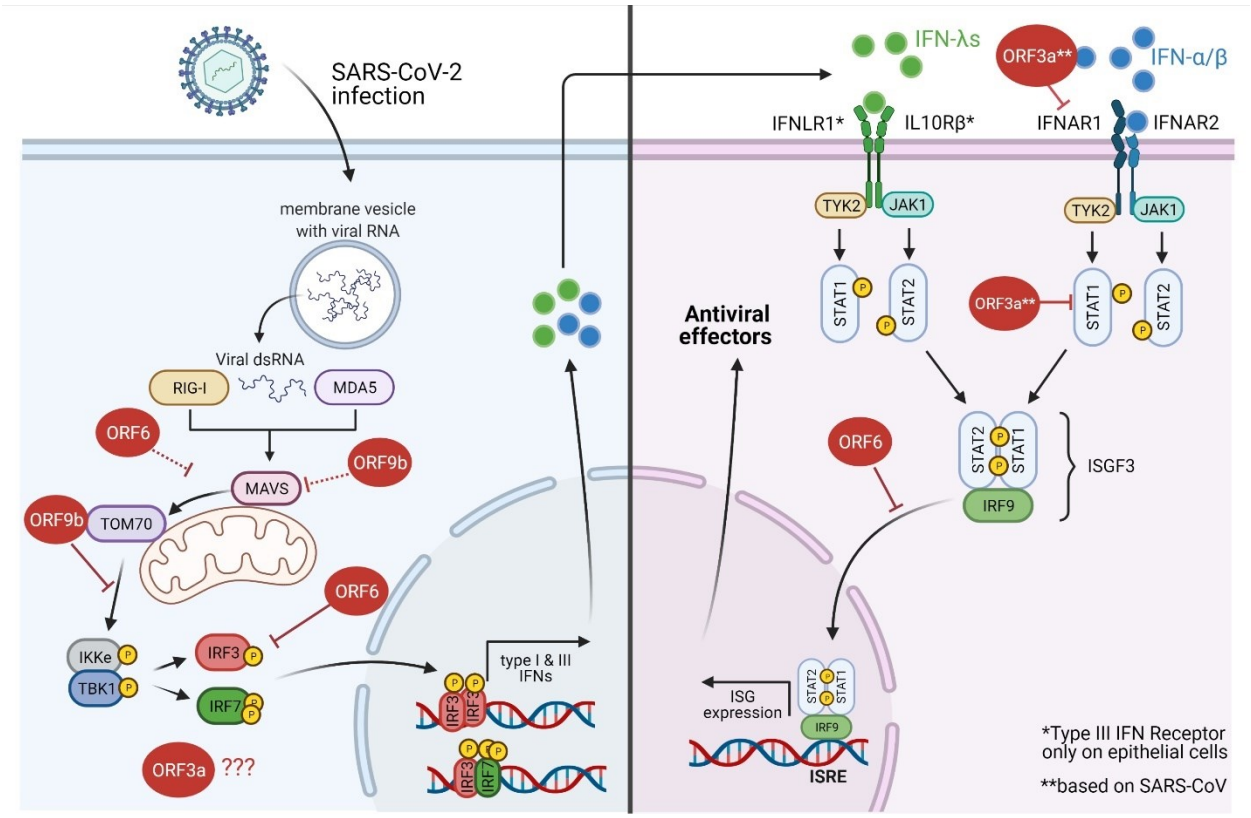

Figure 5) Summary of antagonism of type I and III IFN signaling by SARS-CoV-2 Orf3a, Orf6 and Orf9b. *The inhibitory steps are indicated for the individual viral proteins. Punctuated arrows indicate mechanisms that are not yet fully understood. The figure was made with BioRender.*

Importantly, to this date, our knowledge is mostly based on findings from HEK293T cells (human embryonic kidney epithelial cells). Although HEK293T cells are one of the most commonly used cell lines in molecular biology studies, they have several characteristics that limit them to study SARS-CoV-2 and innate immunity at the lung epithelium. First, they express markers of several kinds of tissues and resemble mostly embryonic adrenal precursor structures[91]. Considering that SARS-CoV-2 primarily infects the human adult lung, this raises concerns about the physiological relevance of HEK293T cells to study SARS-CoV-2 biology. In addition, they do not express hACE2 (proteinatlas.org) nor important viral sensing PRRs, like TLR3[92] or RIG-I[93], and do not contain the genes for type I and III IFNs (*IFNA2, IFNB1, IFNL1-3*) (proteinatlas.org). This explains why many of the above-mentioned functional protein studies are based on luciferase reporter assays that required transfection of all components of the IFN signaling pathways and IFN genes[17, 18, 82, 83], raising concerns about the relevance of these studies. In addition, we do not yet understand

how individual SARS-CoV-2 viral proteins interfere with type III IFN responses, also because our knowledge on type III IFNs is limited. Since type III IFNs are specifically important to protect epithelial barriers[25], it is crucial to characterize mechanisms by which SARS-CoV-2 viral proteins inhibit type III IFN responses.

Therefore, this study aimed to investigate the effects of SARS-CoV-2 Orf3a, Orf6 and Orf9b on modulating type III IFN production in a physiologically more relevant setting by generating A549 and Calu-3 lung epithelial cell lines stably expressing the viral proteins upon doxycycline treatment. For this, we obtained lentiviral strep-tagged expression plasmids for most SARS-CoV-2 viral proteins from Nevan Krogan's lab – the team who published the first SARS-CoV-2 protein interaction map using the same plasmids[69]. We believe that this study will not only give further insight into the immunomodulatory functions of SARS-CoV-2 viral proteins in physiologically relevant cell lines, but also into if and how type III IFN responses might be modulated and thus contribute to the clinical course of COVID-19. A deeper understanding of the pathoimmunology of COVID-19 is needed to develop effective therapeutic approaches and to prepare us with knowledge for future pandemic coronavirus outbreaks. The results from this study could contribute to these efforts.

2. Aims and Objectives

For this study, we obtained lentiviral strep-tagged expression plasmids for 26 out of 29 predicted SARS-CoV-2 viral proteins from Nevan Krogan's lab[69]. Based on literature and proposed functions, we generated a priority list of seven SARS-CoV-2 proteins (Nsp1, Nsp5, Nsp13, Nsp15, Orf3a, Orf6, Orf9b) that have previously been suggested to interfere with the host type I IFN response, thus contributing directly to the immunopathology of COVID-19. Since most of these studies are based on cell types that are less relevant for studying SARS-CoV-2 biology and many mechanisms are still unresolved, the aim of this study was to generate human lung epithelial cell lines stably expressing the selected viral proteins upon doxycycline treatment. Furthermore, since type III IFNs play a critical role in protecting lung epithelial cells from viral infections and have not yet been studied in the context of viral protein modulation, the study aimed to investigate the role of the selected SARS-CoV-2 viral proteins in modulating innate immune pathways leading to type III IFN production. Better understanding of the interactions between the host cell and SARS-CoV-2 is important to explain the underlying immune responses of COVID-19 and identify possible therapeutic targets.

The objectives of this study were to:

1. Clone and validate lentiviral expression plasmids for seven different SARS-CoV-2 viral proteins (Nsp1, Nsp5, Nsp13, Nsp15, Orf3a, Orf6, Orf9b).
2. Optimize and validate a lentiviral transduction protocol to create A549 and Calu-3 human lung epithelial cell lines stably expressing the selected SARS-CoV-2 viral proteins upon doxycycline treatment.
3. Determine the production of inflammatory cytokines and type III IFNs in A549 and Calu-3 cells in response to PRR-ligand stimulation using synthetic viral ligands.
4. Investigate the effects of SARS-CoV-2 Orf3a, Orf6 and Orf9b expression in A549 and Calu-3 cells on production of type III IFNs and inflammatory cytokines in response to synthetic PRR-ligand stimulation.

3. Materials and Methods

3.1. Cell culture

3.1.1. Cell lines and culture conditions

Human embryonic kidney (HEK) 293T cells (CRL-1573; American Type Culture Collection (ATCC)) are adherent cells originating from human embryonic kidney tissue. They were cultured in Dulbecco's Modified Eagle's Medium (DMEM with 4.5 g/L glucose and *L*-glutamine) (Cat#12-604F, Lonza™) supplemented with 10% heat-inactivated fetal bovine serum (FBS) (Gibco), 2 mM *L*-glutamine (Sigma-Aldrich) and optionally 100 U penicillin/0.1 mg/mL streptomycin (Gibco). Human THP-1 monocyte cells (TIB-202; ATCC) are suspension cells, derived from a one-year-old infant with acute monocytic leukemia. They were cultured in Gibco Roswell Park Memorial Institute 1640 Medium (RPMI-1640) (Cat#2192645, Gibco by Life Technologies) supplemented with 10% heat-inactivated FBS, 2 mM L-glutamine, 0.05 mM β-mercaptoethanol (Sigma-Aldrich) and optionally 100 U penicillin/0.1 mg/mL streptomycin. Human lung epithelial Calu-3 cells are adherent cells and originate from a 25-year-old man with adenocarcinoma. They were obtained as a gift from Denis Kainov's lab. Calu-3 cells were cultured in DMEM supplemented with 10% heat-inactivated FBS, 2 mM L-glutamine and optionally 100 U penicillin/0.1 mg/mL streptomycin. Human lung epithelial A549 cells (CCL-185; ATCC) are adherent cells originating from a 58-year-old man with lung carcinoma. They were cultured in DMEM supplemented with 10% heat-inactivated FBS, 2 mM L-glutamine and 100 U penicillin/0.1 mg/mL streptomycin, when necessary. The cells were tested for mycoplasma contamination by laboratory technician Anne Marstad.

3.1.2. General cell culture procedures

Thawing of cells

The stock vial was taken out of the liquid nitrogen storage tank and rapidly thawed in a 37°C water bath. The vial was decontaminated with 70% ethanol and the cell suspension was transferred into a 15-mL centrifuge tube containing 9 mL of prewarmed complete growth medium. The cell suspension was centrifuged at room temperature for 5 minutes at 1500 rpm. The cell pellet was resuspended in complete

growth medium and added to complete growth medium in the recommended cell culture flask.

Cryopreservation of cells

Cells were frozen when at 70-80% confluency. To freeze the cells, complete growth medium was supplemented with 10% additional FBS and 10% Dimethyl sulfoxide (DMSO) (Sigma-Aldrich). Cells were pelleted by centrifugation at 300 x *g* for 5 minutes, gently resuspended in freezing medium and added to pre-labelled cryovials. Using a freezing container (Nalgene® Mr. Frosty) filled with isopropyl alcohol, the cells were frozen down at a crucial cooling rate of 1°C/min until reaching the desired storage temperature of -80°C for short-term storage or in liquid nitrogen for long-term storage.

Passaging cells

HEK293T, Calu-3 and A549 cells were maintained until 70-80% confluency and THP-1 cells were kept at a density of 2.0 – 8.0 x 10^5 cells/mL. HEK293T, A549 and THP-1 cells were passaged every 2-3 days at a ratio of 1:20 – 1:30 (HEK293T), 1:4 – 1:8 (A549) and 1:2 – 1:3 (THP-1), respectively. Calu-3 cells were growing slowly after thawing and approximately one passage (1:2 to 1:3) was necessary per week. The frequency of sub-culturing was adapted over time and cell media changed every 2-3 days.

To sub-culture adherent cells from a T75 flask, complete growth medium was aspirated, and cells were washed with 5 mL pre-warmed Dulbecco's Phosphate-Buffered Saline (DPBS) (Lot Nr. RNBJ7475, Sigma Aldrich). To detach adherent cells from the flask surface, 1 mL of 0.25% Trypsin/EDTA (Lonza™) was added, and cells were incubated until complete detachment was visible. Trypsinization was stopped by adding 5 mL of pre-warmed complete growth medium and the cell suspension was transferred into a 15-mL centrifuge tube. The cells were pelleted at room temperature for 5 minutes at 300 x *g* and the pellet resuspended in complete growth medium. The pellet was resuspended in 4 mL of complete growth medium and cell number and viability assessed, if necessary. According to the passaging ratio, the

volume was calculated and added to a cell culture flask with pre-warmed complete growth medium.

To sub-culture suspension cells at a ratio of 1:2, half of the cell suspension was removed from the culture flask and replaced with fresh pre-warmed complete growth medium.

Assessment of cell number and viability

To check the cell number and estimate cell viability, the trypan blue exclusion test was used. From the cell suspension, 10 µl were mixed with 10 µl filtered trypan blue and a final volume of 10 µl of the mixture were added to EVE™ cell counting slides (Cat# EVS-050, NanoEntek America, Inc.). Finally, cell number and viability were assessed with the EVE™ Automated Cell Counter (Cat#EVE-MC, NanoEntek America, Inc.).

3.2. Plasmid DNA cloning

3.2.1. Selected DNA plasmids

DNA plasmids used in this study comprised lentiviral expression plasmids encoding the genes-of-interest (GOI) (see ***Table 1***), as well as packaging and envelope plasmids for 2nd and 3rd generation lentivirus production (see ***Table 2***). Lentiviral expression plasmids for 26 of the 29 predicted SARS-CoV-2 viral proteins tagged with a Strep-II tag were obtained as a gift from Nevan Krogan's lab[69]. 2nd and 3rd generation lentiviral packaging and envelope plasmids were obtained as a gift from Didier Trono, cloned prior to the start of this study and stored at -20°C.

Table 1) List of both inducible and non-inducible lentiviral expression plasmids and their encoded SARS-CoV-2 viral proteins.

SARS-CoV-2 viral protein	pLVX-TetOne-Puro plasmids (inducible)	pLVX-Puro plasmids (non-inducible)
NSP1	pLVX-TetOne-Puro-nCoV2019-nsp1-2xStrep	pLVX-Puro-nCoV2019-nsp1-2xStrep
NSP5	pLVX-TetOne-Puro-nCoV2019-nsp5-2xStrep	pLVX-Puro-nCoV2019-nsp5-2xStrep
NSP13	pLVX-TetOne-Puro-nCoV2019-nsp13-2xStrep	pLVX-Puro-nCoV2019-nsp13-2xStrep

NSP15	pLVX-TetOne-Puro-nCoV2019-nsp15-2xStrep	pLVX-Puro-nCoV2019-nsp15-2xStrep
ORF3A	pLVX-TetOne-Puro-nCoV2019-orf3a-2xStrep	pLVX-Puro-nCoV2019-orf3a-2xStrep
ORF6	pLVX-TetOne-Puro-nCoV2019-orf6-2xStrep	pLVX-Puro-nCoV2019-orf6-2xStrep
ORF9B	pLVX-TetOne-Puro-nCoV2019-orf9b-2xStrep	pLVX-Puro-nCoV2019-orf9b-2xStrep
GFP (control)	pLVX-TetOne-Puro-GFP-2xStrep	pLVX-Puro-GFP-2xStrep

Table 2) Packaging and envelope plasmids required for 2nd- and 3rd-generation lentivirus production.

Packaging/ Envelope Plasmids	**Details**	**Source**
PSPAX2	2nd generation lentiviral packaging plasmid	A gift from Didier Trono (Addgene plasmid #12260)
PMDLG/PRRE	3rd-generation lentiviral packaging plasmid	A gift from Didier Trono (Addgene plasmid #12251)
PRSV-REV	3rd-generation lentiviral packaging plasmid	A gift from Didier Trono (Addgene plasmid #12253)
PMD2.G	2nd- and 3rd-generation lentiviral envelope plasmid (VSV-G)	A gift from Didier Trono (Addgene plasmid #12259)

3.2.2. Bacterial transformation

To prepare the lentivirus expression plasmids for each selected SARS-CoV-2 viral protein, the plasmid DNA received from Krogan's lab was cloned using One Shot™ Stbl3™ chemically competent *E. coli* (#C7373-03; Invitrogen) and according to the protocol available at Thermo Fisher Scientific (MAN0001497). Following the instructions from Krogan's lab, 2 µg of plasmid DNA were mixed with 5 µL of water per well, incubated at room temperature, mixed to resuspend, and stored at -20°C. For transformation, 1 µL of the diluted DNA was added to respective vials of One Shot™ cells, mixed gently and incubated on ice for 30 minutes. Cells were then heat-shocked for 45 seconds at 42°C without shaking, followed by incubation on ice for 2 minutes to reduce damage of the cells. 250 µL of pre-warmed S.O.C medium

(#15544034; Invitrogen) was added, and the vial shaken horizontally for 1 hour at 225 rpm in a pre-heated shaking incubator (37°C). Finally, 50 µL and 200 µL from each transformation were spread on pre-warmed LB agar plates containing ampicillin (recipe see **Supplementary A**) and grown overnight at 37°C. Colonies were picked using a sterile pipette tip and added to a sterile 15-mL tube with a dual-position cap containing 5 mL LB medium and ampicillin (100 µg/mL) (recipe see **Supplementary A**). The bacterial culture was incubated at 30°C for 20-24 hours under shaking (150 rpm). A control (only LB medium + ampicillin) was included to check for potential ampicillin-resistant bacteria contamination in the medium. The next day, the culture was expanded to 100 mL into an autoclaved Erlenmeyer flask and incubated another 20-24 hours at 30°C and 150 rpm. The bacterial culture was then used for plasmid preparation and to make a glycerol stock for long-term storage of transformed cells. For this, 500 µL of bacteria culture were mixed with 500 µL 50% glycerol (in MilliQ water) on ice and immediately frozen down to -80°C.

3.2.3. Plasmid purification

After bacterial transformation and culture expansion, plasmids were prepared using the ZymoPURE™ II Plasmid Midiprep Kit (#D4200, ZymoPure™) and according to the manufacturer's instructions. Up to 100 mL of bacterial culture were centrifuged in two steps at $\geq$ 3,400 x *g* for 10 minutes for highest possible plasmid DNA yield. All steps were followed precisely after the manufacturer's instructions, including multiple steps of bacterial cell lysis, DNA isolation, washing and elution using a spin-column based method. Instead of the common vacuum protocol, the centrifugation option was used to process and wash the lysate on the spin-column until elution. The optional step for EndoZero Plasmid DNA was included to avoid endotoxin contaminations. The plasmid DNA was kept at -20°C until further use. To assess plasmid quantity and purity, the NanoDrop 1000 Spectrophotometer and Software ND-1000 3.8.1 was used.

3.3. Lentiviral transduction of human lung epithelial cell lines

3.3.1. General principles

Lentiviral transduction

Lentiviral transduction employs the function of lentiviruses as gene-delivery vehicles to mediate stable integration of a gene of interest (GOI) into the host genome of a target cell in order to express the GOI permanently[94]. Lentiviruses are enveloped, (+)ssRNA viruses and members of the *retroviridae* family. Retroviruses possess the unique ability to integrate their viral genome into the genome of a host cell. First, an enzyme called reverse transcriptase converts the (+)ssRNA into cDNA which is then transported into the nucleus and finally integrated into the host cell genome by the help of a viral integrase. Lentiviruses are unique members of retroviruses, because of their ability to productively infect dividing and non-dividing cells. Consequently, they have become particularly attractive for human gene therapy or functional studies of primary cells or other non-dividing cells, like neurons.[95-98]

The best-known lentivirus is the human immunodeficiency virus 1 (HIV-1) and many of its viral elements are present in recombinant lentiviruses. However, because of the high pathogenicity of HIV-1, several adaptations are required to minimize the possibility of accidentally generating replication-competent lentiviruses (RCLs) from recombinant lentiviruses[96, 99-103]. In short, only essential genes for viral replication are preserved, the viral elements are split onto multiple separate plasmids and/or the flanking regions of the transgene are optimized[103, 104]. To produce recombinant lentiviral vectors, a mix of packaging, envelope and transfer plasmids are co-transfected into packaging cells (e.g. HEK293T). The packaging plasmid(s) carry the genes for the reverse transcriptase (RT) and integrase (IN) enzymes (encoded by *Pol*), the viral core proteins (encoded by *Gag*) and the regulatory Rev protein (encoded by *Rev*). The envelope plasmid often carries the gene for the glycoprotein of vesicular stomatitis virus (VSV-G) instead of the HIV-1 glycoprotein to allow infection of a broad variety of cell types[101, 105, 106]. Finally, the "transfer" plasmid carries the GOI, flanked by long-terminal repeats (LTRs) which are required for integration. After transfection of the plasmids into the packaging cells, viral packaging proteins are expressed and recognize lentiviral genomic RNA transcripts, carrying the GOI, via the packaging sequence ψ. This induces budding and

subsequently release of infectious virions into the cell culture supernatant. Harvested lentiviruses can then be used to transduce the target cells, which could be any kind of cell that is of interest for the study. After uptake via receptor-mediated endocytosis and release of the viral RNA and proteins into the cytoplasm, it becomes reverse transcribed into cDNA by the viral RT, the cDNA transported into the nucleus where it is finally integrated into the genome with help of the viral integrase. Finally, the protein of interest is translated from corresponding mRNA in the cytoplasm.[107, 108]

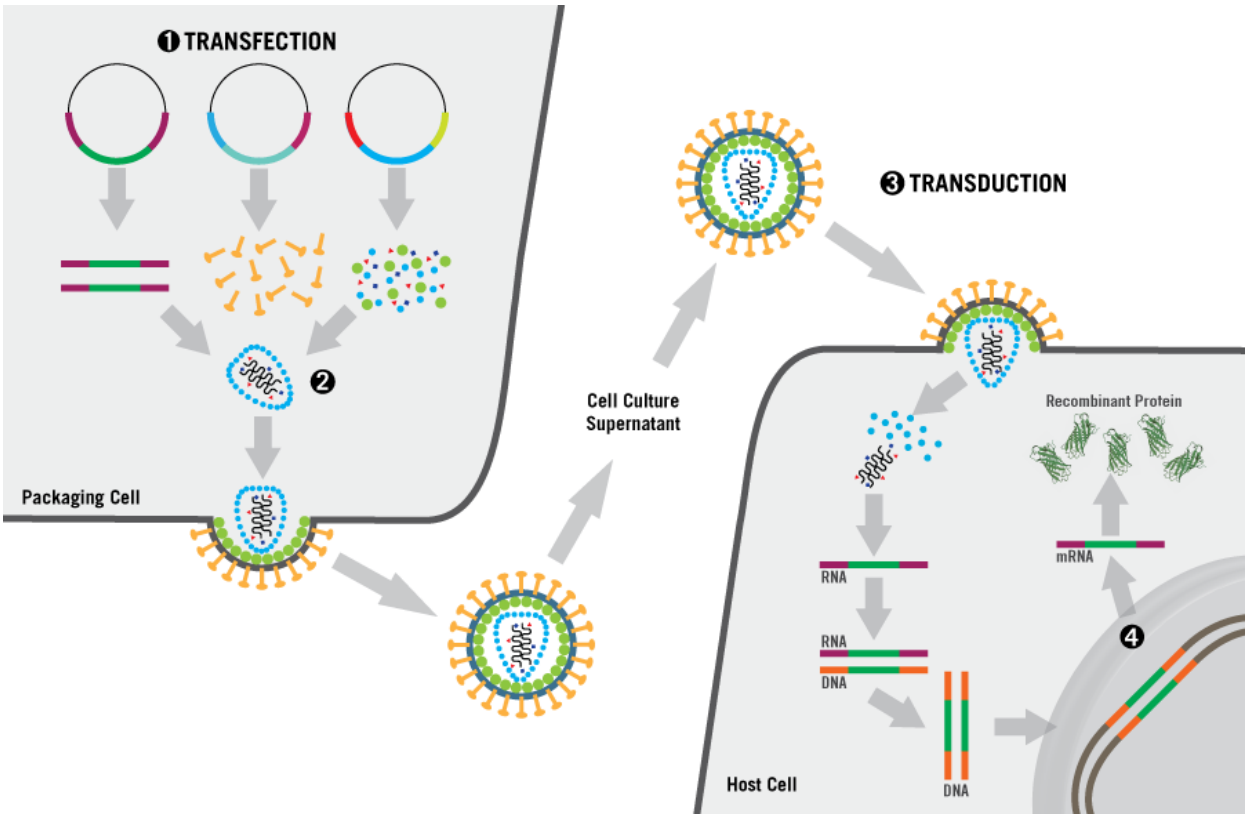

Figure 6) Overview of lentivirus production and transduction. *1) The packaging, envelope and transfer plasmids are co-transfected into packaging cells, e.g. HEK293T cells. 2) Viral particles form and are released into the cell culture supernatant. 3) The cell culture supernatant containing infective virions is added to target cells. 4) In the target cell, the transgene is integrated into the genome and is expressed in the cytoplasm, e.g. to study its functions. The figure was taken from sopachem.com.*

To produce safe lentiviral vectors, different generations of lentiviral packaging systems were made (***Table 3***). The **1st generation lentiviral packaging system** is no longer used because of biosafety risks since it includes the genomic components for the virulence proteins Vif, Vpr, Vpu and Nef which mainly enhance virulence and are not required for lentiviral vector functions[103, 104]. The **2nd-generation lentiviral packaging system** excludes these virulence proteins, including only separate plasmids encoding for Pol (RT, IN), Gag, Rev and Tat, besides the envelope protein

VSV-G[103]. However, the Pol, Tat, Rev and Gag lentiviral proteins are expressed from a single packaging plasmid, rendering the 2nd generation system less safe than newer generations because only one recombination event could lead to RCLs[100]. In addition, the transgene is flanked by intact long-terminal repeats (LTRs) that depend on the regulatory Tat protein to activate transcription and raise potential safety concerns because of accidental production of RCLs[99]. As a solution, the **3rd generation packaging system** separates Rev from Gag-Pol and exchanges the promoter region of the LTRs with a constitutive promoter (e.g. CMV) to exclude Tat, significantly reducing the chance to produce RCLs[99, 100]. Finally, a **4th-generation packaging system** comprises a total set of five packaging, regulatory and envelope plasmids by separating Pol, Gag and Rev-Tat and introducing an additional regulatory plasmid encoding a transactivator protein (tTA)[108, 109]. Several factors render this new vector design as highly safe from RCL production. Segregation of lentiviral proteins onto five plasmids as well as introduction of a trans-lentiviral system by splitting gag and pol onto separate plasmids significantly reduces the risk of RCL production. Furthermore, the double transactivation system enabled by transfection of an additional plasmid encoding for a Tet-Off transactivator protein (tTA) significantly increases viral titers and reduces the risk of RCLs[108-110]. In detail, tTA is only expressed in absence of tetracycline (e.g. doxycycline)[110] and subsequently activates expression of Gag, Pro, Tat and Rev[108]. Expression of Tat then allows activation of the U3 promoter region of the 5'LTR and induces expression of viral transcripts necessary for the viral lifecycle[108].

Table 3) Overview of the different generations of lentiviral systems.

Features	2nd Generation	3rd Generation	4th Generation
Envelope plasmids	Interchangeable, often VSV-G	Interchangeable, often VSV-G	Interchangeable, often VSV-G
Packaging plasmids	All on one: 1) Gag, Pol, Rev, Tat	Two: 1) Gag, Pol 2) Rev	Three plasmids: 1) Gag 2) Vpr, Pol 3) Rev, Tat 4) tTA (requires absence of tetracycline)

Transfer plasmids	Requires Tat to activate 5'LTR promoter by binding to U3 region	Does not require Tat	Requires Tat to activate 5'LTR promoter by binding to U3 region
LTR viral Promoter	Intact	U3 deletion	Intact
Safety	Safe: 3 separate plasmids	Safer: 4 separate plasmids; elimination of Tat; self-inactivating lentiviruses (SIN)	Safest: 6 separate plasmids; separation of Gag and Pol; additional trans-expression step

Doxycycline-inducible expression system

Further optimization of lentiviral transduction is the use of tetracycline-inducible lentiviral expression plasmids to allow controlled gene expression[111]. The tetracycline-inducible expression system comprises both Tet-On and Tet-Off Systems, where the transgene is expressed either in presence of the tetracycline-derivate doxycycline (Tet-On) or in absence of doxycycline (Tet-Off). The idea originates from the mechanism of tetracycline resistance development in *E. coli* and was first described by Gossen *et al.* in 1992[110]. In this study, we used the Lenti-X Tet-One inducible expression system (***Figure 7***). In addition to the transgene, the lentiviral vector integrates a gene encoding for the Tet-On® 3G transactivator protein that is constitutively expressed. However, only in presence of Doxycycline, the Tet-On 3G® protein undergoes the necessary conformational change to bind to the pTRE3G that controls the expression of the transgene.[108, 111]

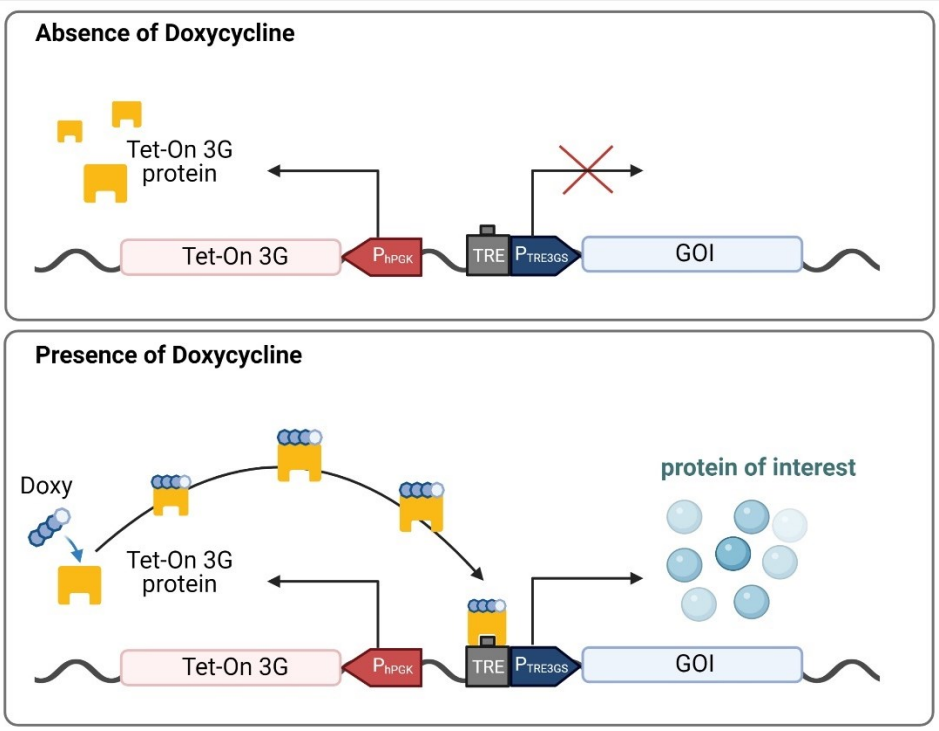

Figure 7) The mechanism of the inducible Tet-On expression system. *Only in presence of the tetracycline-derivate doxycycline, the Tet-On 3G® transactivator protein can bind the TRE element of the TRE3G Promoter and induce the expression of the GOI. The figure was made with BioRender.*

3.3.2. HEK293T cell transfection

pLVX-TetOne-Puro and pLVX-Puro expression plasmids were validated by transient transfection in HEK293T cells using GeneJuice® transfection reagent (#70967-4, EMD Millipor Corp.) and the provided protocol (User Protocol TB289, EMD Millipore Corp.). For pLVX-TetOne-Puro plasmid validation, cells were incubated with and without 0.50 µg/mL Doxycycline (#D3072-1ML, Sigma Aldrich) for 24-48 hours. A negative control with un-transfected HEK293T cells was always included. At first, 0.75×10^5 HEK293T cells/well were seeded in complete growth medium (500 µL/well) in a 24-well plate, followed by incubation for 24 hours (37°C, 5% CO_2) to allow the cells to attach and reach 50-60% confluency. For each transfection, 3 µL of GeneJuice® transfection reagent was mixed in 100 µL serum-free medium (Opti-MEM™, Gibco™), vortexed and incubated for 5 minutes at room temperature. 1 µg of SARS-CoV-2 plasmid preparations was added, diluted carefully by pipetting, and incubated for 15 minutes at room temperature. Finally, the entire volume of the complete mixture was added dropwise to each well containing the cells. After 2-8 hours, the medium was exchanged with new complete growth medium containing

0.50 µg/mL Doxycycline in case of pLVX-TetOne-Puro expression plasmid validation. The cells were incubated for 24-48 hours at 37°C (5% CO_2) to allow the proteins to accumulate in the cells. The cells were lysed in 150 µL RIPA buffer for Western blot analysis.

3.3.3. Lentivirus production in HEK293T cells

2nd generation lentiviral packaging

2nd generation lentiviral packaging included three plasmids: the envelope plasmid (pMD2.g), the packaging plasmid (pPAX2) and the transfer plasmid (pLVX-TetOne-Puro). HEK293T cells were seeded at a density of 0.15 x 10^6/mL in a 6-well plate (2 mL/well) and incubated for 24 hours (37°C, 5% CO_2). Cells were transfected with three 2nd generation plasmids at a ratio of 0.67 µg (pMD2.6), 1.00 µg (pPAX2) and 1.33 µg (pLVX-TetOne-Puro) using GeneJuice® transfection reagent, following the general transfection protocol described under **3.3.2**. Co-transfection was performed by preparing a mastermix of the packaging and envelope plasmid for all transfections. To facilitate accurate pipetting (10 µL/well), the plasmid mix was diluted in complete growth media. After preparation of the GeneJuice® Transfection Reagent/serum-free media mixture according to the general protocol, 10 µL of the plasmid mastermix was added together with 1.33 µg of each transfer plasmid. After incubation for 15 minutes at room temperature, the complete mixture was added to each well containing the cells in complete growth medium (no Pen/Strep).

3rd generation lentiviral packaging

3rd-generation packaging system included four plasmids: the envelope plasmid (pMD2.g), two packaging plasmids (pMDLg/pRRE and pRSV-rev) and the transfer plasmid (pLVX-TetOne-Puro). Co-transfection of all four plasmids in HEK293T cells was performed similar to the protocol explained for 2nd generation packaging. The two packaging plasmids and the envelope plasmid were already provided as a single mix with the right ratio of the three plasmids. For transfection in a 6-well plate, 1.00 µg of the packaging/envelope plasmid mix was added to the GeneJuice®/serum-free medium mixture together with 1.00 µg of transfer plasmid DNA and finally added to the cells in complete growth medium (no Pen/Strep).

4th generation lentiviral packaging

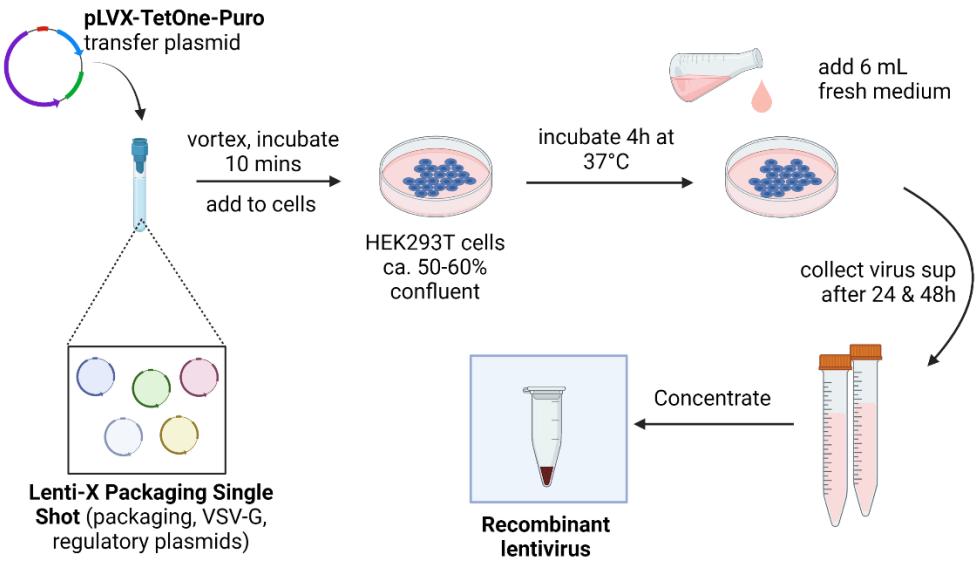

Figure 8) Step-by-step workflow for 4th-generation packaging of lentiviruses in HEK293T cells. *The figure was made with BioRender.*

4th-generation lentiviral packaging involved five different packaging/envelope plasmids that were pre-mixed with transfection reagent in so-called Lenti-X™ Packaging Single Shots (#631282; TakaraBio Inc.). The protocol was performed according to the manufacturer. At first, 3.0 x 10^6 HEK293T cells were seeded in 8 mL complete growth medium (no Pen/Strep) in a 10-cm tissue culture plate. After 24-hour incubation at 37°C (5% CO_2), the cells were 50-60% confluent and ready for transfection. In a sterile tube, 7 µg transfer plasmid DNA were diluted in 600 µL sterile water and mixed thoroughly by vortexing. The diluted DNA (600 µL) was then added to a tube of Lenti-X™ Packaging Single Shots and vortexed at high speed for 20 seconds until the pellet was dissolved completely. The sample was incubated for 10 minutes at room temperature and centrifuged for 2 seconds at the end. Finally, the entire mixture of plasmid DNA-containing nanoparticle complexes was added to the cells, distributed by gently rocking the culture dish back and forth and incubated for at least 4 hours at 37°C (5% CO_2). An additional 6 mL of fresh complete growth medium was added, and the cells incubated at 37°C (5% CO_2) until harvesting after 24h and 48h.

Concentration of lentiviral supernatant

First, virus-containing supernatant was filtered through a 0.45 µm PES filter (VWR) and stored at 4°C between harvesting timepoints and until concentration. Lentivirus was concentrated using Lenti-X™ Concentrator and according to the manufacturer's instructions (#631232; Clontech). In detail, 1 part of Lenti-X™ Concentrator was mixed with 3 parts of filtered lentiviral supernatant, mixed by gentle inversion, and incubated at 4°C for at least 30 minutes. The sample was centrifuged at 1,500 x g for 45 minutes at 4°C, followed by careful removal of the supernatant and gentle resuspension in 1/10th of the original volume using the complete growth medium of the target cells. The concentrated virus sample was directly titrated and stored at -80°C in single-use aliquots.

3.3.4. Titration of lentiviruses

To validate lentivirus production and prepare transduction of target cells, the lentiviral titers were assessed by HIV-1 p24 Enzyme-linked Immunosorbent Assay (ELISA) or Lenti-X GoStix® Plus. Both methods measure the amount of p24, the capsid protein of HIV-1 and any HIV-1 derived lentivirus, from which infectious units (IFUs) were calculated.

HIV-1 p24 ELISA

The HIV-1 p24 ELISA Assay (#XB-1000, XpressBio) is a typical "sandwich" ELISA that employs the high specificity of a murine anti-HIV-1 p24 capture antibody immobilizing the p24 antigen on the surface of the microtiter well, and a biotinylated mouse anti-HIV-1 p24 detection antibody that forms a complex with the immobilized p24 antigen. A fully detailed description of the principles of a "sandwich" ELISA can be found under **3.6.1**. The protocol was provided by the manufacturer and the procedure was similar to **0**. A difference was that p24 ELISA wells were pre-coated with the p24 capture antibody and incubation with the capture antibody was not necessary for this assay. The amount of pre-coated well strips was selected based on the number of standards, lentivirus samples and blank control – all measured in duplicates, respectively. To inactivate all infective viruses, 1:100 and 1:10,000 dilutions of lentivirus harvests in DMEM (200 µL) were incubated in 21 µL lysis buffer

(provided) for 5 minutes at room temperature. 220 µL of the sample preparations were added to pre-coated ELISA wells. The p24 standard was diluted in DMEM to 200 ng/mL, followed by a 2-fold dilution series of 7 standards. 200 µL of each standard dilution was added to 20 µL lysis buffer in the pre-coated ELISA wells. For the blank control, only DMEM was added to 20 µL lysis buffer in one pre-coated ELISA well. The samples, standards and controls were incubated for 60 minutes at 37°C, followed by a wash step of three cycles in 350 µL wash buffer (20X, diluted in deionized water). The detection antibody (100 µL) was incubated for 1 hour at 37°C, followed by another wash step of three cycles. 100 µL Streptavidin HRP conjugate was incubated at room temperature for 30 minutes, followed by a wash step. Right after, the Substrate Solution (100 µL) was added and incubated for < 30 min in the dark at room temperature until appropriate color change was observed. The reaction was stopped by adding 100 µL of Stop Solution (1 N H_2SO_4). The read-out was performed at 450 nm using a plate reader. The blank control was subtracted from each value and p24 concentrations calculated based on the standard curve and dilution factor. Quantitative analysis of the results was performed directly by the Microplate Reader Software viral titers were visualized with GraphPad Prism Software Version 9.1.2.

Lenti-X™ GoStix™ Plus

Similar to p24 ELISA, viral titer determination with Lenti-X™ GoStix™ Plus (#631280; TakaraBio Inc.) estimated p24 concentration. 20 µL of lentivirus supernatant was applied to the sample well (S) of the Lenti-X™ GoStix™ Plus cassette. Three drops of Chase Buffer were added, and the lateral flow test was run for 10 minutes at room temperature. A control band (C) appeared to show that the test functioned properly and a test band (T) if the sample contained sufficient lentivirus. The test was quantified using the Lenti-X GoStiX Plus Smartphone App measuring so-called GoStix Values (GV), which were equivalent to the concentration of p24 [ng/mL].

Calculating Infectious units (IFUs) from p24 values

Lentiviral titers were calculated from p24 values determined by p24 ELISA or Lenti-X™ GoStix™ Plus, respectively. To convert p24 concentration to viral titers given as

Infectious Units (IFU)/mL, a theoretical conversion factor from Didier Trono was used[112]. He assumed that there are approximately 2000 p24 molecules in one lentiviral particle (LP) (2000 x molecular weight/Avogrado) or 1000 LPs per pg of p24. He further assumed that a successfully packaged LP will have an infectivity index of about 1 IFU per 100-1000 LPs. Thus, one may theoretically assume that there are 10 to 100 IFU/pg of p24. In the end, this can be formulated by the following equation: $viral\ titer\ \left[\frac{IFU}{mL}\right] = p24\left[\frac{pg}{mL}\right] \times 100$.

If lentivirus samples were concentrated, the concentration factor was included in the calculation.

3.3.5. Lentiviral transduction and selection

Transduction of suspension cells by "spinofection"

Transduction of THP-1 cells was performed in 6-well plates with 3 mL/well. At first, 1 x 10^6 THP-1 cells were added to 15-mL tubes and centrifuged at 300 x *g.* The cell pellet was resuspended in 1 mL virus supernatant (no MOI considered) containing 8 µg/mL polybrene and centrifuged at 1200 x g for 90 minutes at room temperature. A negative transduction control was included and comprised THP-1 cells incubated with media only. The cell pellet was resuspended in the same virus supernatant and added to 2 mL pre-warmed complete growth media in a 6-well plate.

Transduction of adherent cells by "reverse transduction"

"Reverse transduction" implied seeding target cells on top of viral supernatant in a 6-well plate. In theory, this supposedly forces the low-density viral particles to encounter the high-density adherent cells on their way to the flask bottom, thus assuring close contact between the cells and the viral particles. For each transduction in a 6-well plate, 0.15 x 10^6 HEK293T cells were harvested from cell culture by trypsinization, centrifugation (300 x *g*, 5 min) and resuspended in 1.0 mL complete growth medium containing 8 µg/mL polybrene. The cell suspension was added to 0.5 mL of virus supernatant in a 6-well plate (no MOI considered). A negative control was included with 0.5 mL complete growth medium instead of virus supernatant.

Transduction of adherent cells by centrifugation

A549 and Calu-3 cells were harvested by trypsinization, centrifugation (300 x *g*, 5 min) and resuspension in 4 mL complete growth medium. 0.20 x 10^6 A549 cells and 0.60 x 10^6 Calu-3 cells were seeded in a 6-well plate (2 mL/well) and incubated overnight (37°C, 5% CO_2) to allow the cells to attach to the well bottom and reach a confluency of 50-60%. The viral supernatants were thawed gently and resuspended to an MOI = 5 in 2 mL complete growth medium containing 8 µg/mL polybrene. The old media was aspirated from the cells and 2 mL of the virus-containing medium was added to each well with cells. A negative control was incubated with complete growth medium only. The cells were centrifuged at 1,200 x *g* for 90 minutes at 32°C. To remove toxic polybrene, the transduction media was exchanged with fresh complete growth medium after incubation for 6 hours (37°C, 5% CO_2).

Puromycin selection and expansion of polyclonal cell lines

After transduction, cells were incubated for 48-72 hours at 37°C and 5% CO_2. Cells were washed with PBS and incubated in 2 mL complete growth medium containing the appropriate concentration of puromycin (determined by kill curve experiment). The cells were observed every 1-2 days either visually (adherent cells) or by cell viability assessment (suspension cells). Dead cells were removed by media change every 2-3 days and viable cells were expanded. After 2 weeks, the cells were cultured in complete growth medium with 0.50 µg/mL puromycin. After successful validation of expression of the GOIs by Western blot analysis and/or fluorescence microscopy, aliquots of cells were cryopreserved and stored at -80°C for long-term storage.

3.3.6. Optimization and validation of lentivirus transduction and selection

Puromycin kill curve

Since each mammalian cell line responds differently to selection antibiotics like puromycin, a kill curve was performed to determine the right concentration of puromycin for A549, Calu-3 and THP-1 cells. The right concentration was thereby defined as the concentration of puromycin that kills wildtype cells but not transduced cells which carry a puromycin selection gene. Wildtype A549, Calu-3 and THP-1 cells were seeded in a 24-well plate. A549 and Calu-3 cells were incubated overnight to

allow the cells to adhere. The cells were then incubated in complete growth medium containing the concentrations indicated. All experiments included a negative control (no antibiotic). The cells were incubated with puromycin for 2-3 days and number of viable cells/mL assessed by Trypan Blue Exclusion.

Doxycycline titration

To determine the optimal concentration of doxycycline to induce expression of the GOI, A549-GFP cells were incubated in complete growth medium containing doxycycline for the concentrations indicated. 0.75 x 10^5 GFP-A549 cells were seeded in a 24-well plate (500 µL/well) and incubated at 37C (5% CO_2) overnight to allow the cells to attach. The medium was gently aspirated and exchanged with new complete growth medium containing the different concentrations of doxycycline and incubated for 24-96 hours. GFP expression levels assessed by fluorescence microscopy.

3.4. Pattern Recognition Receptor (PRR) stimulation assays

In a 24-well plate (500 uL/well), 0.04 x 10^6 A549 and 0.15 x 10^6 Calu-3 cells were seeded accordingly and incubated for 24 hours prior to stimulation. To induce viral protein expression in transduced cell lines, the cells were incubated in doxycycline-containing media for 24 hours. For TLR3 and TLR8 stimulation, 5 µg/mL polyinosinic:polycytidylic acid (poly(I:C)) (#VPIC-42-01; Invivogen) or 5 µg/mL poly-uridine (polyU) (#PLU-35-03; Invivogen), respectively, were first incubated with 5 µg/mL poly-L-arginine (#P7762; Sigma Aldrich) for 10 minutes and added to the cells in 500 µL complete growth medium. For TLR7 stimulation, 5 µg/mL CL264 (#C64-38-01A; Invivogen) was added to the cells in 500 µL complete growth medium. For RIG-I/MDA5 stimulation, 5 µg/mL poly(I:C) was transfected using Lipofectamine RNAiMAX (#13778-075; Invitrogen). In detail, 5 µg/mL poly(I:C) was incubated in double the volume of Lipofectamine RNAiMAX for 10-15 minutes and then added to the cells in 500 µL complete growth medium. The ligands were incubated for the indicated time-points and supernatant harvested for analysis (ELISA, LDH assay). Supernatant for ELISA was stored at -20°C. Supernatant for

LDH assays was used directly. Stimulation prior to MTS assays were performed in 96-well plates and volumes or number of seeded cells adapted accordingly.

3.5. Western Blot Analysis

3.5.1. Basic principle

Western blot analysis is commonly used to detect and analyze proteins from cell or tissue lysates. At first, the cells are lysed and denatured in lysis buffer followed by gel electrophoresis, e.g. sodium dodecyl sulfate polyacrylamide gel electrophoresis (SDS-PAGE). During SDS-PAGE, the samples are prepared in lysis buffer containing SDS resulting in denatured and negatively charged polypeptides, allowing their separation through the acrylamide mesh of the gel along an electric current. Here, the acrylamide concentration is crucial since it determines the resolution of the gel electrophoresis: low molecular weight proteins require a higher acrylamide concentration while high molecular weight proteins a lower acrylamide concentration. To enable immunodetection of the proteins, they need to be transferred from the gel on to a nitrocellulose (NC) or polyvinylidene difluoride (PVDF) membrane. This is performed by electroblotting which, again, employs an electric current to move the negatively charged proteins towards a positively charged anode where the membrane is placed. After blotting, the proteins need to be visualized and this is performed by incubating the membrane with a primary and secondary antibody. The primary antibody is usually the protein-specific antibody while the secondary antibody is specific to the primary antibody and gives the detection signal, e.g. by chemiluminescence, fluorescence or autoradiography. Secondary antibodies that are detected by chemiluminescence are typically conjugated with an enzyme like horseradish peroxidase (HRP) that catalyzes the oxidation of a substrate, e.g. luminol. The oxidized, chemiluminescent substrate eventually emits light at a certain wavelength that is detected.

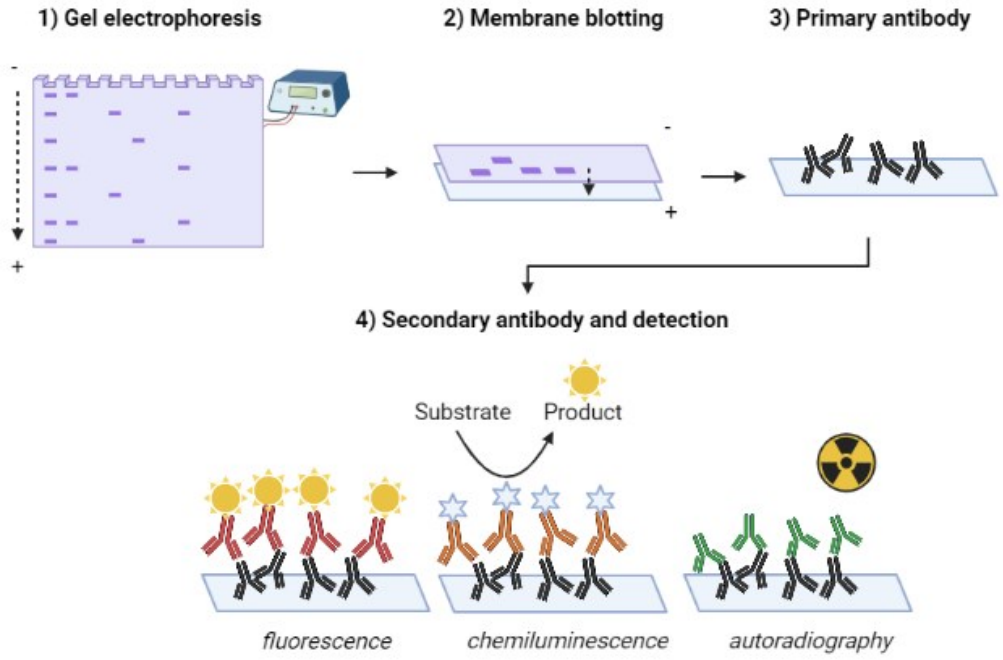

Figure 9) The basic steps of western blotting. *1) Protein samples are loaded onto a gel and separated by their molecular weight while moving through the gel along an electric current. 2) The separated proteins are then blotted on to a membrane. 3) After incubation with a protein-targeting primary antibody, 4) a secondary antibody is added to detect the proteins. Detection can occur in many different ways, depending on the nature of the secondary antibody. The figure was illustrated using BioRender.*

3.5.2. Standard procedure

At first, cells were washed in pre-warmed PBS, lysed in RIPA buffer containing proteinase inhibitor by scarping, rotation for 15 min (4°C) and centrifugation for 20 min at 10000 rpm (4°C). The protein-containing supernatant was collected into labelled Eppendorf tubes and either used directly or stored at -20°C. To prepare protein samples for SDS-PAGE, 30 µL were incubated in 7.5 µL NuPAGE® LDS Sample Buffer (4X) (#NP0007; Invitrogen) mixed with 0.1 M dithiothreitol (DTT) (1:100) (#R0861; Thermo Scientific) and heated at 85°C for 10 minutes. The samples were quickly centrifuged after heating and 25 µL of each denatured and reduced protein sample was loaded in each well of NuPAGE® 4-12% Bis-Tris Gel (#WG1402BOX; Invitrogen) in 1X NuPAGE® MES SDS Running buffer (#NP0002; Invitrogen). To monitor protein electrophoresis, 5 µL of SeeBlue™ Plus2 Pre-stained Protein Standard (#LC5925; Invitrogen) was loaded in one well per gel. To determine the size of the proteins after visualization of the blotted membrane, 0.5 µL of the MagicMark™ XP Western Blot Protein Standard (#LC5602; Invitrogen) was loaded in one well per gel. The gel was run at 100 V for 30 minutes and 150 V for 90 minutes

and monitored continuously. The gel transfer to nitrocellulose membrane was carried out using iBlot® 2 NC Regular Stacks (#IB23001; Invitrogen) at 20 V for 9 minutes using the iBlot® 2 Gel Transfer Device (#IB21001; Invitrogen). After protein transfer, the membrane was washed in Tris Buffered Saline with Tween-20 (TBS-T) under agitation for 5 minutes.

The membrane was then incubated in 5% bovine serum albumin-fraction V (BSA) in TBS-T for 1 hour under agitation. To remove excess BSA, the membrane was washed 3 times for 5 minutes in TBS-T under agitation before incubation with the primary antibody. The primary mouse Anti-Strep II antibody (#NBP2-43735; Novus Bio) was diluted in 20 mL 5% BSA (in TBS-T) by 1:5000, added to the membrane and incubated under agitation at 4°C overnight. The primary mouse Anti-GAPDH antibody (#2118; Abcam) was diluted by 1:5000 and incubated under agitation for 1 hour at 4C. Prior to adding the secondary antibody, the membrane was washed in TBS-T 3 times for 5 minutes under agitation. The secondary goat-anti-mouse Ig/HRP antibody (#P047; Dako Denmark A/S) was diluted in 15 mL 5% BSA (in TBS-T) by 1:5000, added to the membrane and incubated under agitation for 1 hour. The membrane was washed 3 times (5 min) in TBS-T under agitation. The membrane was incubated with SuperSignal West Femto Chemiluminescent Substrate (#35096; Thermo Fisher Scientific) for 2-3 minutes, transferred onto and covered with a transparent film and visualized at an exposure time of 30 sec to 1 min using the chemiluminescent channel of the Odyssey® Fc (Li-Cor) and the Image Studio V5.2 software. To remove the primary and secondary antibodies against the proteins of interest and allow assessment of the GAPDH loading control, the membrane was stripped using a mild stripping buffer (1.5% glycine, 0.1% SDS, 1.0% Tween, pH 2.2). For this, the membrane was first washed 3 times (5 min) in TBS-T under agitation, then the stripping buffer was added twice for 10 min and finally the membrane was washed in PBS twice (10 min) and in TBS-T once (10 min). The membrane was now ready for incubation with the primary anti-GAPDH antibody.

3.6. Enzyme-linked Immunosorbent Assay (ELISA)

3.6.1. Basic principle

Enzyme-linked Immunosorbent Assay (ELISA) employs the highly specific interaction between antibodies and antigens to detect and quantify proteins, peptides, hormones, or antibodies in a substance. Sandwich ELISA uses a capture and detection antibody, both binding specifically to different epitopes of the antigen of interest. In detail, the capture antibody is first coated onto a microtiter plastic plate. The plate is then incubated in bovine serum albumin (BSA) to block non-specific binding sites on the plate surface. Then, the antigen is added and becomes immobilized by binding to the capture antibody on the plate surface. Unbound antigens are removed by thorough washing and the detection antibody is added, specifically binding to another epitope of the antigen. Critically, the detection antibody is complexed with biotin molecules, a water-soluble B complex vitamin specifically binding to the bacterial protein streptavidin. Thus, addition of the enzyme horseradish peroxidase (HRP) complexed with streptavidin results in the HRP enzyme binding to the biotin molecules on the detection antibody. Then, the HRP substrate Tetramethylbenzidine (TMB) is added and becomes oxidized by HRP, resulting in a color change that is proportional to the amount of antigens in the well. Addition of the stop solution H_2SO_4 stops the enzyme reaction, and the solution turns from blue to yellow. Color intensity is finally measured at 450 nm with a correction of 570 nm using a plate reader. Using a standard curve of an available standard, the concentration of antigen can finally be determined.

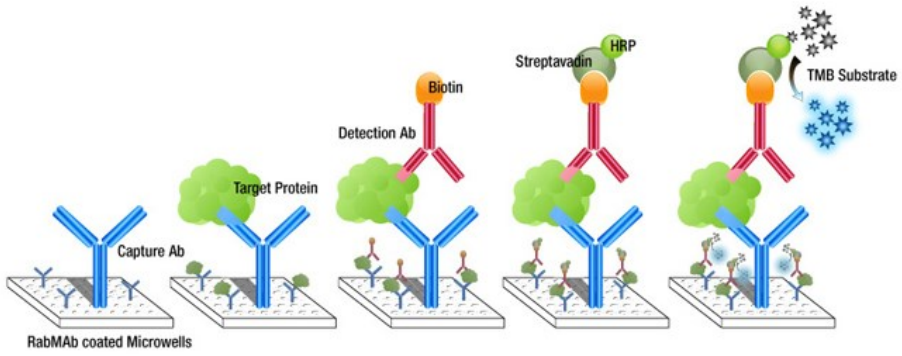

Figure 10) The basic principle of a "sandwich" ELISA. *The antigen is immobilized by a capture antibody and binds a biotinylated secondary antibody. Interaction with Streptavidin-HRP and incubation with TMB Substrate allows final detection of the antigen. With the help of a standard curve, the concentration of the antigen can be determined. Figure from epitomics.com.*

3.6.2. Standard procedure

DuoSet ELISA was performed for IL-6 (#DY206; R&D), IL-8 (#DY208; R&D), IL-29/IL-28B (IFN-λ1/3) (#DY1589B; R&D) and IL-28A (IFN-λ2) (#DY1587; R&D). The standard procedure was followed based on the manufacturer's description. The assay was carried out in 96-well half-area plates (#3690, Corning®) with half the volumes recommended by R&D Systems. In-house experiments could show that the half-volume setup produces the same strong signals when carried out in half-area plates. In detail, the wells were first coated with capture antibody (50 µL/well diluted in PBS) overnight. The plate was washed in three cycles with 150 µL wash buffer (0.1% Tween-20 in PBS) using the automated Tecan plate washer. The wells were then incubated with 150 µL of reagent diluent (1% BSA in PBS), sealed with the adhesive film and incubated for 2 hours at room temperature. A 2-fold dilution series of each standard (7 dilutions) in reagent diluent was prepared with the highest concentration as noted by the manufacturer. A replica plate with optimized sample dilutions in reagent diluent was prepared, containing 60 µL of diluted samples in the same order as planned for the ELISA setup. Sample dilutions were determined in a preliminary assay and ranged from undiluted, 1:2 to 1:10. After blocking the wells, the ELISA plate was washed three times in wash buffer and 50 µL of each standard dilution and sample dilution was added to the coated ELISA plate using a multichannel pipette. The plate was covered with adhesive film and incubated at room temperature overnight. After 4-24 hours, the wells were incubated with the detection antibody (50 µL/well in reagent diluent). The plate was covered with adhesive film and incubated at room temperature for 2 hours. After washing in three cycles, 50 µL of Streptavidin-HRP conjugate (40-fold dilution in reagent diluent) was added to each well and incubated in the dark at room temperature for 20 minutes. After washing three times, 50 µL of TMB substrate solution (1:1 dilution of Reagent A and B) (#421101; BioLegend) was added to each well and incubated in the dark for <20 minutes at room temperature. The color change was monitored continuously and stopped by adding 25 µL Stop Solution (1 N H_2SO_4). The plate was finally analyzed at 450 nm with wavelength correction of 570 nm using a microplate reader (BioRad). The blank was subtracted from each value and cytokine concentration calculated based on the standard curve. The standard curve was generated with the Microplate

Manager® Software Version 5.2 (BioRad). The data was analyzed and visualized using GraphPad Prism Software Version 9.1.2.

3.7. Cytotoxicity/Cell viability assays

3.7.1. Lactate Dehydrogenase (LDH) assay

The LDH assay is a colorimetric method that measures lactate dehydrogenase (LDH) activity in the supernatant of dead or plasma membrane-damaged cells. Cell death is associated with the rupture and damage of the plasma membrane, followed by the release of cytoplasmic enzymes in the culture supernatant. One of such enzymes is the LDH enzyme which catalyzes the conversion of lactic acid to pyruvic acid while converting NAD+ to NADH/H+. The LDH assay includes a catalyst (diaphorase) that transfers the H/H+ from the NADH/H+ product of the LDH reaction to a tetrazolium salt INT that gets immediately reduced to a formazan dye. The dye product is water soluble and has an absorbance maximum at 500 nm. The amount of dye produced is directly proportional to the number of dead cells.

The LDH assay was performed using the LDH Cytotoxicity Detection Kit (#PT3947-1; Clontech Inc.) and according to the manufacturer's instructions. Immediately before use, the LDH Reaction Mixture was prepared by mixing 3.5 mL Dye Solution with 77.8 uL Catalyst (1:45 dilution). 40 µL of the Mixture was distributed to each well and incubated at room temperature for 30 minutes in the dark. Absorbance was measured at 490 nm using a microplate reader (BioRad). Furthermore, to obtain highly sensitive results, a reference wavelength of 655 nm was used to subtract background noise that might have occurred due to nonspecific absorbance such as excess cell debris, fingerprints, or others. Finally, the blank measure was subtracted from all sample measures. The data was analyzed and visualized using GraphPad Prism Software Version 9.1.2.

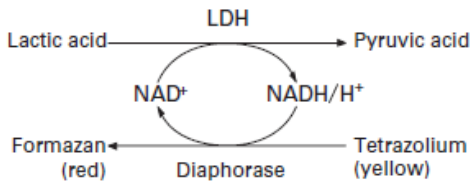

Figure 11) Redox-reaction during LDH assay. *The LDH assay quantifies a formazan product by absorbance measurement that is directly proportional to LDH-releasing dead cells. The figure was taken from the manufacturer's protocol.*

3.7.2. MTS Assay

The MTS assay is a colorimetric method that measures metabolic activity of viable cells in proliferation or cytotoxicity assays. Similar to the traditional MTT assay or the LDH assay described above, the MTS assay measures the quantity of a formazan product as measured by absorbance at 490 nm. The MTS assay includes a stable solution of the MTS tetrazolium compound [3-(4,5-dimethylthiazol-2-yl)-5-(3-carboxymethoxyphenyl)-2-(4-sulfophenyl)-2H-tetrazolium] and an electron coupling reagent (phenazine ethosulfate; PES). When adding the MTS tetrazolium solution to cells in culture, the compound is bio-reduced by viable and metabolically active cells and forms a soluble, colored formazan product. The reaction is carried out by NAD(P)H-dependent dehydrogenase enzymes that are active in metabolically active cells. The quantity of formazan produced is thus directly proportional to the number of viable and metabolically active cells in culture and is measured by absorbance at 490 nm.

The MTS assay was performed using the CellTiter 96® Aqueous One Solution Cell Proliferation Assay (#G3581; Promega) and according to the manufacturer's instructions. The following controls were included: an untreated control, a mock control (only transfection reagent) and a negative control (medium only). Transfected samples were assessed in biological duplicates. Controls were assessed from single wells. 50 µL One Solution Reagent was added to 100 µL complete growth medium and cells in each well and incubated for 3 hours at 37C (5% CO2). Absorbance was recorded directly after at 490 nm using a microplate reader (Bio-Rad). A reference wavelength of 655 nm was used to subtract background noise. The background absorbance from medium only was subtracted from all sample measures. The data was finally analyzed and visualized using GraphPad Prism Software Version 9.1.2.

3.8. Fluorescence microscopy

GFP protein expression was visualized using the EVOS™ Fluorescence microscope M7000 (#AMF7000, Invitrogen) equipped with an EVOS LED GFP Cube (Invitrogen) that catches light near 482 and 524 nm.

4. Results

4.1. Human lung epithelial cells are the main target of SARS-CoV-2

To formulate the aim of this study, SARS-CoV-2 infection studies were performed by Researcher Markus Haug to determine which cells are permissive to infection and thus allow the virus to replicate and express viral proteins. He infected human lung epithelial Calu-3 cells, Vero E6 African green monkey kidney epithelial cells and monocyte-derived macrophages (MDMs) derived from human peripheral blood mononuclear cells (PBMCs) (MOI 0.3:1; clinical isolate from St. Olavs hospital). After 24 and 48 hours, cell supernatants were harvested for virus RNA analysis from productively infected cells by RT-qPCR. Infected cells were harvested and stained after 48 hours for S-protein expression analysis by Flow Cytometry. Intracellular S-protein staining was performed after cell fixation, SARS-CoV-2 inactivation, cell permeabilization and with anti-CoV S antibody (Sino Biological) and Alexa647 anti-rabbit secondary antibody (Thermo Fisher). RT-qPCR was performed using NTNU lysis buffer and RNA isolation and qPCR protocol. Analysis of intracellular Spike protein expression and viral genome amplification levels suggested that MDMs were not infected by SARS-CoV-2 as observed by ct values of around 35 or above. Both VeroE6 and Calu-3 epithelial cells were infected as soon as after 24 hpi as evidenced by low ct values in RT-qPCR and high expression of Spike protein in infected cells (***Figure 12A, C-D***). No Spike protein expression was detected in MDMs after 48 hpi and the viral genome could not be amplified from the cell supernatant at 24 and 48 hpi (***Figure 12A-B***). We concluded that MDMs are not permissive to productive SARS-CoV-2 infection. The aim of this study was narrowed down to human lung epithelial cells (Calu-3, A549).

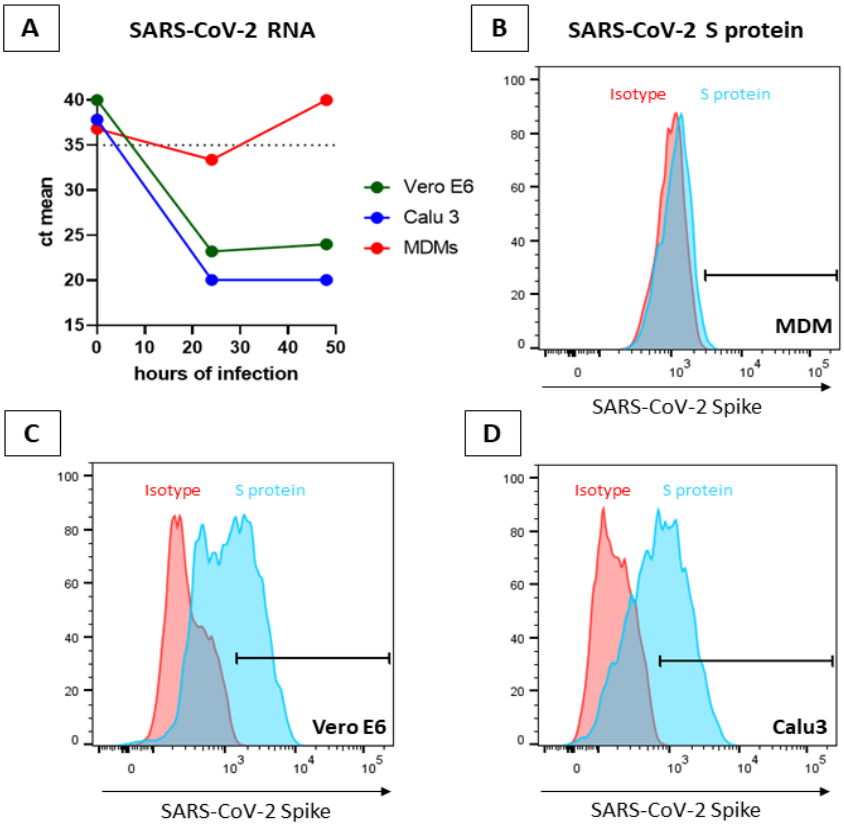

Figure 12) SARS-CoV-2 infection of primary MDMs and epithelial cancer cell lines (Vero E6, Calu-3). *Cells were infected with SARS-CoV-2 for 24 and 48 hours and analyzed by Flow Cytometry (A-C) and RT-qPCR (D) by Researcher Markus Haug. qPCR results are given as mean from technical duplicates from one experiment, the experiment was repeated twice. Cells were considered uninfected when ct values were >35. Flow Cytometry was performed on fixed and permeabilized cells with anti-SARS-CoV-2 Spike (blue) or istotype (red) primary antibody staining (1:50) and Alexa647 anti-rabbit secondary antibody (1:2000). Representative histograms from one of two experiments are shown.*

4.2. Validation of inducible and non-inducible expression plasmids

We obtained lentiviral expression plasmids for 26 out of 29 SARS-CoV-2 viral proteins as a gift from Nevan Krogan[69]. He and his team codon optimized mature Nsps and predicted Orf/accessory proteins and cloned them into pLVX-TetOne-Puro or pLVX-Puro plasmid backbones including a purification 2xStrep tag. For this study, seven viral proteins (Nsp1, Nsp5, Nsp13, Nsp15, Orf3a, Orf6, Orf9b) were chosen for generating A549 and Calu-3 lung epithelial cell lines based on their proposed ability to interfere with the type I IFN response. The obtained expression plasmids were transformed in Stbl3 cells, purified, transfected into HEK293T cells, incubated in presence or absence of doxycycline for 48 hours, and finally analyzed by anti-Strep Western Blot (***Figure 13***). Except from SARS-CoV-2 Nsp15, the expression of all

selected viral proteins from pLVX-TetOne-Puro plasmids could be demonstrated and molecular masses are consistent to the ones listed by Krogan's lab[69] (***Suppl. Table 1***). Of note, SARS-CoV-2 Nsp1, Nsp5 and Orf3a expression from pLVX-TetOne-Puro plasmids were detected both in presence and absence of doxycycline, suggesting that the Tet-On Promoter was leaky. pLVX-Puro expression plasmids for SARS-CoV-2 Orf3a and Orf9b could both be validated in HEK293T cells. However, expression of GFP from pLVX-GFP-Puro plasmid could not be determined, since no band could be detected during Western blot. Furthermore, no GFP fluorescence from pLVX-GFP-Puro transfected HEK293T cells was detected by fluorescence microscopy (data not shown).

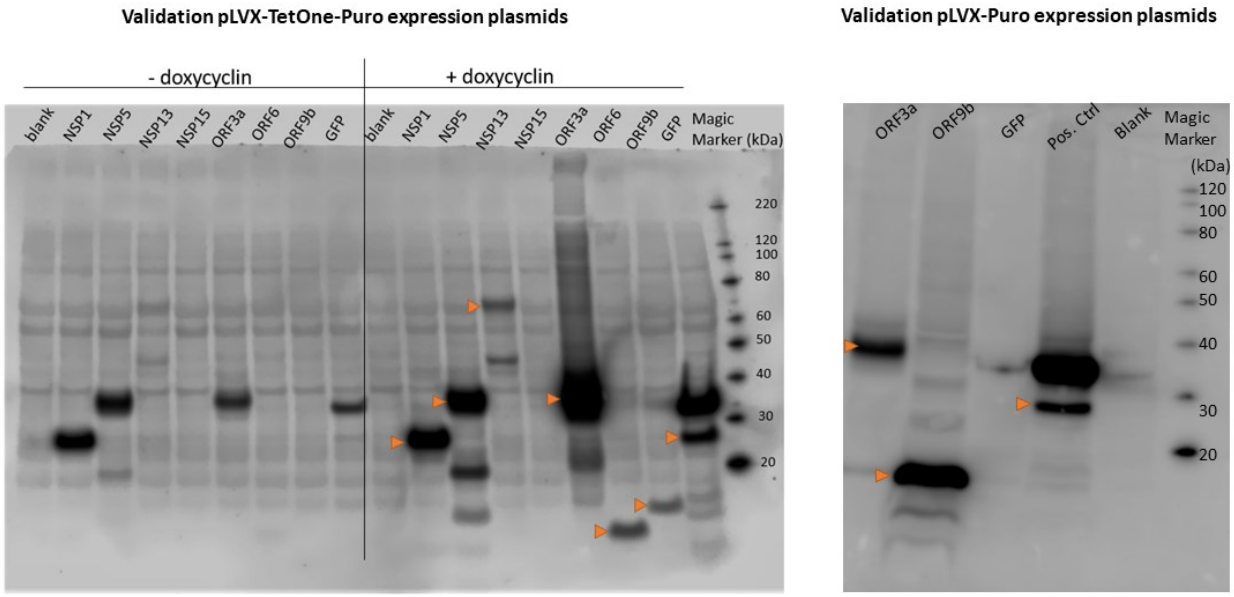

Figure 13) Lentiviral expression plasmids for SARS-CoV-2 viral proteins are functional when transiently expressed in HEK293T cells. *The plasmids were transfected in HEK293T cells in presence or absence of doxycycline for 48 hours. Cell lysates were analyzed by western blotting using a primary antibody against the Strep II tag of all proteins. pLVX-TetOne-GFP was used as positive control to validate pLVX-Puro expression plasmids. Untransfected HEK293T cells were used as negative controls (blank).*

4.3. Optimization and validation of lentivirus production, transduction and selection

To successfully produce lentiviruses (LVs) and transduce A549 and Calu-3 cells with the selected viral proteins, several steps of optimization were required. Optimization steps included a) the choice of lentiviral packaging system for successful LV production b) the choice of transduction method for each cell line for efficient cellular

uptake of viral particles, c) puromycin kill curves for puromycin selection after transduction and d) doxycycline titration for inducible expression of the GOI. Finally, successfully transduced target cells were validated by fluorescence microscopy (GFP fluorescence) and anti-Strep western blot analysis.

4.3.1. 4th-generation packaging system produces functioning lentiviral particles

The first step was to determine the optimal packaging system for LV production with pLVX-TetOne-Puro lentiviral vectors carrying the genetic information for the selected SARS-CoV-2 viral proteins and puromycin resistance gene. To produce recombinant LVs, 2nd-, 3rd- and 4th-generation LV packaging plasmids were co-transfected into HEK293T cells, LVs harvested after incubation of 1-3 days and concentrated using Lenti-X Concentrator. To validate the LVs and packaging system, LV titers were determined by either p24 ELISA or Lenti-X GoStix® Pro. Both titration methods measured the amount of the viral p24 capsid protein [ng/mL] from which theoretical infectious units per milliliter [IFU/mL] were calculated.

Both 2nd and 3rd packaging protocols resulted in high viral titers (IFU/mL $>10^7$) (***Figure 14A*** *and* ***B****)*, however cell transduction was not successful, as reflected by complete cell death (0% viable cells, ***Figure 14B*** and ***D***) after transduction and puromycin selection of THP-1 cells for up to six days. Of importance, very high viral titers were also determined for empty LV particles (only packaging and envelope plasmids). 4th-generation viral titers, determined by Lenti-X GoStix® Plus, were measured for all viral proteins except Nsp1 and ranged from 4.5×10^6 to 1.4×10^7 IFU/mL (***Figure 14E***). Importantly, Lenti-X GoStix® titration was less accurate then p24 ELISA and values should not be directly compared. Only transduction with 4th-generation LVs resulted in successful transduction of several cell lines (***Figure 14F*** and ***Figure 18***) and selection at high survival rate.

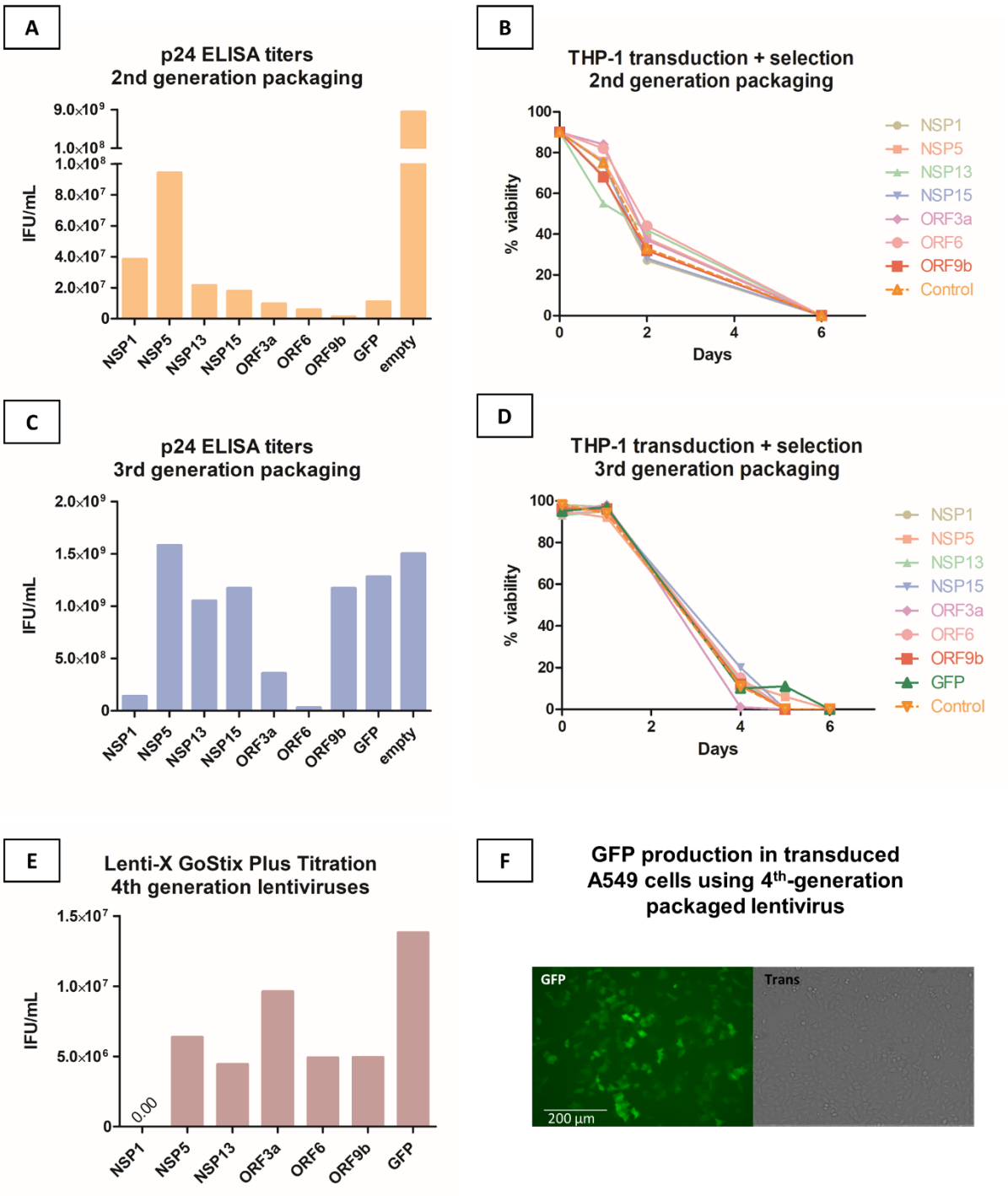

Figure 14) Optimization of lentivirus production and transduction. *2nd, 3rd and 4th generation LV packaging systems were used to produce recombinant LVs for the selected SARS-CoV-2 viral proteins. After co-transfection of packaging, envelope and transfer plasmids into HEK293T cells, LV-containing supernatants were harvested after 24 and 48 hours, pulled together, concentrated 1:10 and titrated using either p24 ELISA or Lenti-X GoStix Plus Titration (A, C, E). Transduction of either THP-1 or A549 cells was assessed by B), D) trypan blue exclusion for THP-1 cells approximately one week of selection with puromycin, and F) by fluorescence microscopy of A549-GFP cells, selected for one week, grown to 80% confluency and after incubation with doxycycline for 48 hours. All titrations were performed once and p24 ELISA was performed in technical duplicates. Transduction of THP-1 cells with 2nd and 3rd generation LVs was performed three times and one representative is shown.*

4.3.2. Puromycin kill curves for efficient antibiotic selection

To prepare lentiviral transduction of the target cell lines, the concentration of the selection antibiotic (in this case puromycin) was determined for each type of target cells. This was done by treating wildtype cells with a range of puromycin concentrations (0-7 µg/mL) for 3 days and determining the number of viable cells by trypan blue exclusion. The selection concentration was defined as the minimum concentration at which 100% of wildtype cells died (i.e. a viable cell number of 0). According to the puromycin kill curves for A549 and Calu-3 cells (***Figure 15***), the optimal puromycin concentration for A549 cells was 1 µg/mL and 2 µg/mL for Calu-3 cells. ***Suppl. Figure 2*** shows the puromycin kill curve for THP-1 cells.

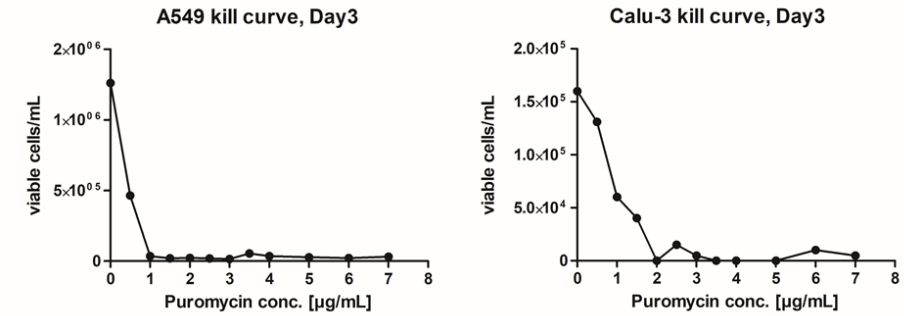

Figure 15) Puromycin killing curves for A549 and Calu-3 cells. *Cells were incubated in complete growth medium with a range of puromycin concentrations (0.5-7.0 µg/mL) for 72 hours, detached using 0.25% Trypsin/EDTA and cell viability assessed by trypan blue exclusion.*

4.3.3. Transduction of adherent cells works best by centrifugation

To determine which transduction method works best for adherent cells, the reverse transduction method was compared to transduction by centrifugation. The reverse transduction method was performed on HEK293T cells using GFP-LV and transduction efficiency assessed by fluorescence microscopy. In detail, GFP-LV was added to the well followed by addition of HEK293T cells in suspension. Following incubation at 37°C and 5% CO_2, this principle aimed to force high density cells to pass low density virus particles while cells sink to the well bottom and virus particles float to the liquid surface. Few cells were able to be infected using this method (***Figure 16***). Transduction by centrifugation (90 minutes at 1200 rpm and 37°C) was performed with A549 cells and GFP-LV and resulted in higher transduction efficiency compared to reverse transduction of HEK293T cells. The method was chosen for transduction of A549 and Calu-3 cells with all LVs.

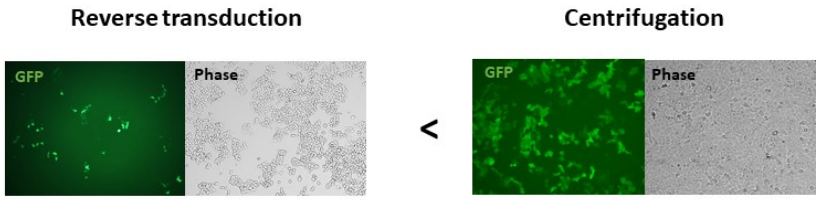

Figure 16) Reverse transduction vs. transduction by centrifugation of adherent cells. *Adherent cells were either infected with GFP-LV following the reverse transduction protocol or the centrifugation protocol. GFP fluorescence was assessed by fluorescence microscopy.*

4.3.4. Doxycycline titration of A549-GFP cells

A puromycin killing curve was performed previously because cell lines behave differently to puromycin treatment. Doxycycline was another antibiotic used in this study and was required to induce expression of pLVX-TetOne-Puro expression plasmids and transduced cell lines. Since doxycycline acts on the plasmid and not the cell, titration of doxycycline resulted in a concentration consistent for all cell lines used. To do so, a range of doxycycline concentrations was tested on the A549-GFP cell line. GFP expression was induced at all tested concentrations (***Figure 17***) with approximately same expression levels above 0.50 µg/mL. GFP expression was detected as soon as 24 hours post-treatment and stayed for up to 96 hours without addition of new Doxycycline (***Suppl. Figure 3***).

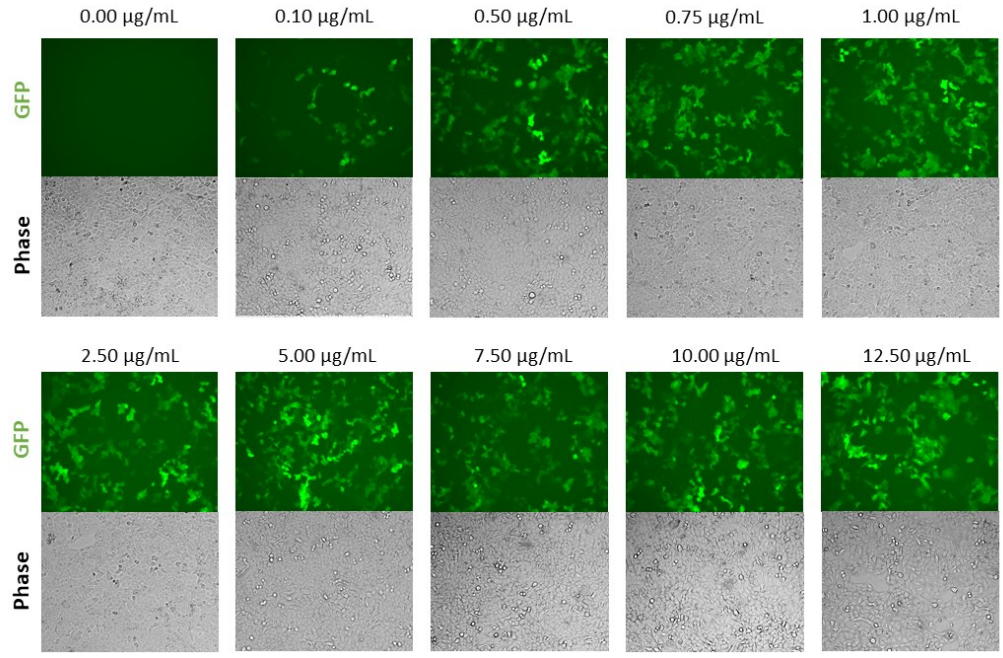

Figure 17) Doxycycline titration with A549-GFP cells. *Successfully selected A549-GFP cells were seeded in a 24-well plate and incubated with increasing concentrations of Doxycycline (0.10 – 12.50 µg/mL). After 52 hours, GFP expression was validated by fluorescence microscopy (EVOS™).*

4.3.5. Validation of successfully transduced cell lines

Transduction of A549 cells with lentiviral vectors for SARS-CoV-2 Orf3a, Orf6, Orf9b and the GFP control resulted in successful selection and expansion of polyclonal cell lines. Transduction of Calu-3 cells succeeded only with Orf6-LV. Protein expression for each cell line was validated by western blot analysis. GFP expression in A549-GFP cells was validated by fluorescence microscopy before (see ***Figure 14F***). Anti-Strep western blot analysis of successfully transduced cells identified expression of SARS-CoV-2 Orf3a, Orf6 and Orf9b in A549 cell lines, but not Nsp5 and Nsp13 (***Figure 18***).

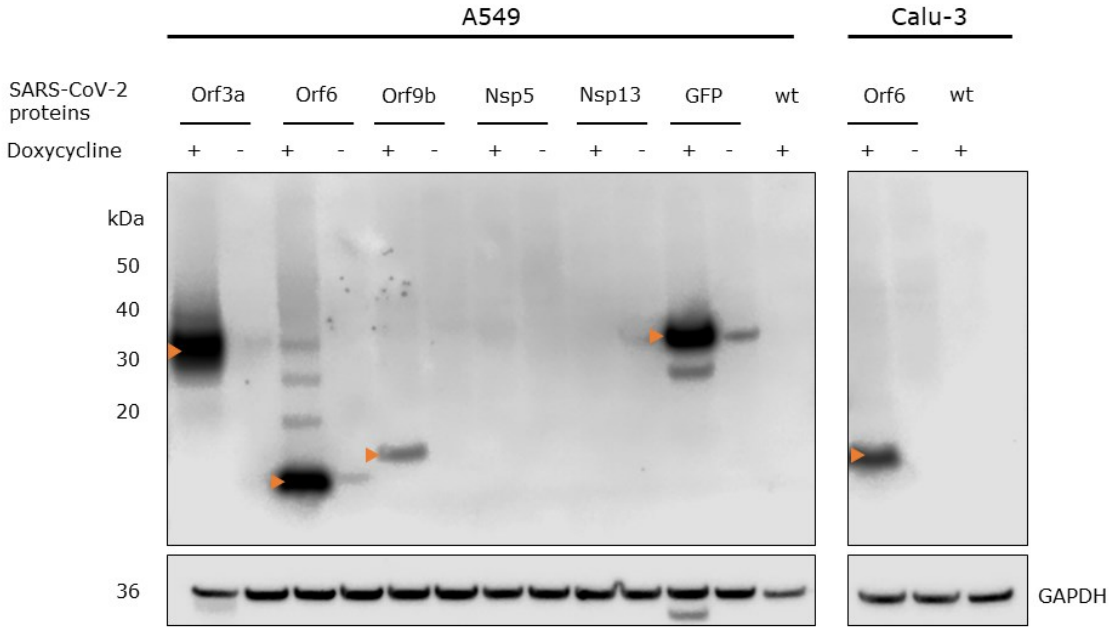

Figure 18) Expression verification of the individual SARS-CoV-2 viral proteins in A549 and Calu-3 cells. *Samples were collected from transduced A549 and Calu-3 lung epithelial cells stably expressing individual viral proteins after addition of 2.5 µg/mL Doxycycline. Controls included transduced cells and no addition of Doxycycline, as well as untransduced wildtype (wt) cells incubated with Doxycycline. Proteins were separated by SDS-PAGE and each SARS-CoV-2 viral protein detected by Western blotting using mouse anti-Strep II monoclonal antibody. As loading control, GAPDH was detected by mouse anti-human GAPDH monoclonal antibody.*

SARS-CoV-2 Orf6 could be detected in the respective Calu-3 cell lysate. Low signals of Orf6 and GFP were detected in A549 cells incubated in absence of doxycycline, indicating slight leakiness of the Tet-On promoter consistent to the previous findings from transiently transfected HEK293T cells (***Figure 13***). All cell lines expressed the loading control GAPDH. The presence of Nsp5 and Nsp13 in transduced A549 cells was further tested by incubating the cells with different concentrations of Doxycycline (2.5 – 7.5 µg/mL) and for 24 and 48 hours (see ***Suppl. Figure 4***). However, protein expression could not be detected.

4.4. Stimulation of wildtype A549 and Calu-3 cells with different synthetic viral ligands

PRR expression can vary between different cell types and therefore different viral ligands are more or less effective to study the pro-inflammatory cytokine and IFN response. In this study, a range of viral ligands was tested that were previously shown to activate TLR3, TLR7, TLR8 and RIG-I/MDA5, respectively.

4.4.1. Transfection of poly(I:C) stimulates secretion of IL-6 and IFN-λ2 from A549 and Calu-3 wildtype cells

The first stimulation experiment in this study aimed to test a range of viral ligands on their ability to induce IRF-mediated IFN-λ2 and NF-kB-mediated IL-6 production from human lung epithelial A549 and Calu-3 cells. The viral ligands included: poly(I:C) + pLA to activate TLR3; CL264 to activate TLR7; pU + pLA to activate TLR8 and transfected poly(I:C) to activate cytoplasmic RIG-I/MDA5. A549 and Calu-3 wildtype cells were treated with 5 µg/mL of each viral ligand for 4, 10, 24 and 48 hours, respectively. In detail, cells were stimulated at different timepoints and harvested at the same time. A 48-hour mock-control (only transfection reagent) was included during every stimulation experiment. Measurement of IL-6 and IFN-λ2 secretion after each indicated timepoint by ELISA revealed that only transfection of 5 µg/mL poly(I:C) induced sufficient secretion levels of both cytokines in A549 cells, peaking at 24 hours (***Figure 19A, C***). Similarly, Calu-3 cells only produced IFN-λ2 production upon transfection of poly(I:C) with highest concentration at 24 hours (***Figure 19D***). Of note, Calu-3 control cells produced about 1500 pg/mL IL-6 after 48-hour incubation under normal culture conditions and without viral ligand (***Figure 19B***). Furthermore, IL-6 could be detected in Calu-3 supernatant at each timepoint of each stimulation, but only RIG-I/MDA5 induced higher levels of IL-6 compared to the control. Of note, IL-6 secretion Calu-3 cells transfected with poly(I:C) and incubation for 24 hours could not be evaluated, because the absorbance measure was outside of the range of the standard curve. Higher dilution of the culture supernatant would have been required. However, since this experiment aimed to choose a ligand for further stimulation experiments, ELISA analysis was not further optimized.

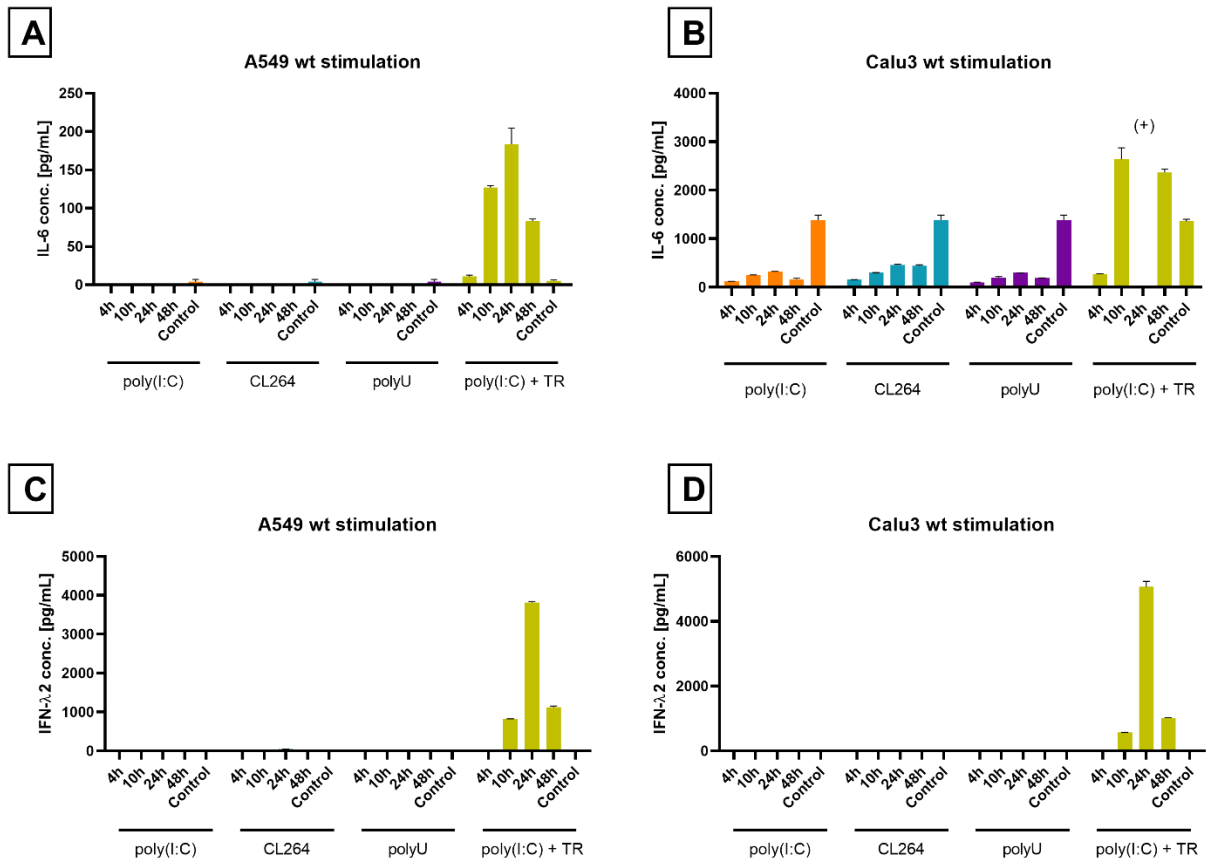

Figure 19) IL-6 and IFN-λ2 secretion upon stimulation of A549 (A&B) and Calu-3 (C&D) wildtype cells with a selection of synthetic viral ligands. *Cells were seeded the day before stimulation in a 24-well plate and stimulated with 5 µg/mL poly(I:C)+pLA, 5 µg/mL CL264, 5 µg/mL polyU+pLA or 5 µg/mL transfected poly(I:C) (+TR). After incubation for 4h, 10h, 24h or 48h, the supernatant was collected and IL-6 or IFN-λ2 production measured by ELISA (R&D). All samples were diluted 1:4 dilution in Reagent Diluent prior to analysis. Controls were incubated with complete growth medium alone (poly(I:C)+pLA, CL264, pU+pLA) or complete growth medium + Lipofectamine RNAiMAX (poly(I:C) + TR). Results show mean and standard deviation of technical duplicates and are representative of one experiment. (+) means the value was outside the range of the standard curve and could not be interpolated.*

4.4.2. A549 and Calu-3 cells respond differently to transfected poly(I:C)

Since A549 and Calu-3 cells secreted IL-6 and IFN-λ2 only after transfection of 5 µg/mL poly(I:C), following experiments were performed with this stimulation procedure. To determine if A549 and Calu-3 cells behaved differently to poly(I:C) treatment, the stimulation experiment was repeated and IL-8 and IFN-λ1/3 measured in addition to IL-6 and IFN-λ2 by ELISA. Of note, the stimulation procedure was performed slightly differently than before. The cells were incubated until 80% confluency with doxycycline, followed by simultaneous stimulation and harvesting supernatant after 4h, 10h, 24h or 48h, respectively. A 48-hour mock control (only RNAiMAX) was included.

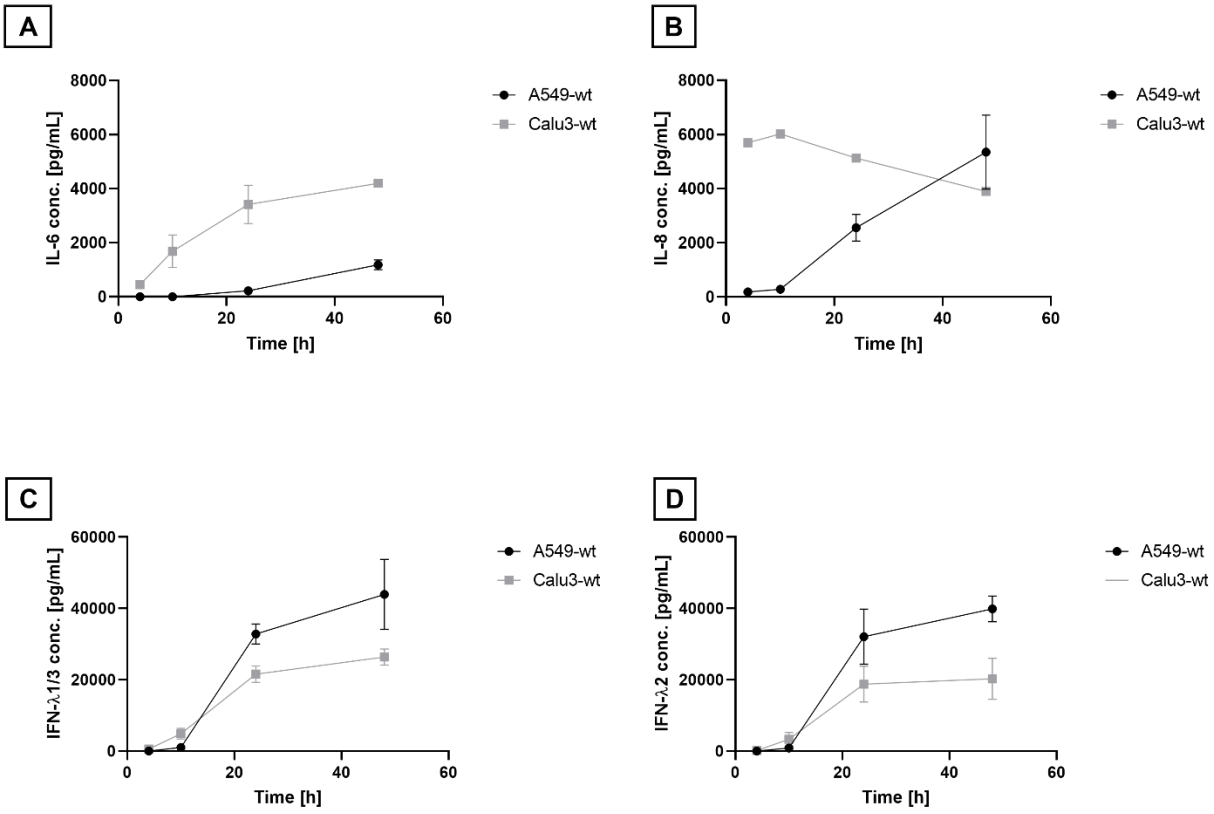

Figure 20) A549 and Calu-3 wildtype cells respond differently to transfected poly(I:C) (5 µg/mL). *Secretion of IL-6 (**A**), IL-8 (**B**), IFN-λ1/3 (**C**) and IFN-λ2 (**D**) from wildtype A549 and Calu-3 cells transfected with 5 µg/mL poly(I:C) for 4, 10, 24 and 48 hours. Secretion levels in culture supernatant were assessed by DuoSet ELISA (R&D) and duplicate absorbance measurements at 450nm. Values are shown in mean +/- SEM from three (IFNs) or two (IL-6, IL-8 A549; IL-6 Calu-3) or one (IL-8 Calu-3) independent experiments.*

Interestingly, in contrast to the screening assay, IL-6 and IFN-λ2 secretion levels increased continuously until 48 hours. This could have been due to the differences in stimulation procedure. In detail, IL-6 production by stimulated A549 wildtype cells increased after 24 hours and peaked at 48 hours with a maximum concentration of 1000 pg/mL. In contrast, IL-6 production by stimulated Calu-3 cells started earlier, after 4-10 hours of stimulation, and showed a 4-fold increase at 24 and 48 hours compared to A549 cells (***Figure 20A***). IL-8 secretion from stimulated Calu-3 cells could be detected at all timepoints (~6000 pg/mL) with a slight decrease over time (***Figure 20B***). In comparison, IL-8 production by stimulated A549 cells increased after 10 hours peaking at 48 hours at a level comparable to Calu-3 cells. Strikingly, mock-transfected Calu-3 cells and not A549 cells showed high IL-6 and IL-8 production (***Figure 21***), similar to what was observed for IL-6 during the ligand screening assay (***Figure 19A, B***). Both A549 and Calu-3 wildtype cells secreted type

III IFNs (IFN-λ2, IFN-λ1/3) as soon as 10 hours post-stimulation, peaking at 48 hours (***Figure 20C***, ***D***). A549 cells responded with almost double the type III IFN secretion levels after 24 and 48 hours when compared to Calu-3 cells. Mock transfected A549 and Calu-3 wildtype cells did not secrete IFN-λ2 nor IFN-λ1/3 (***Figure 21***).

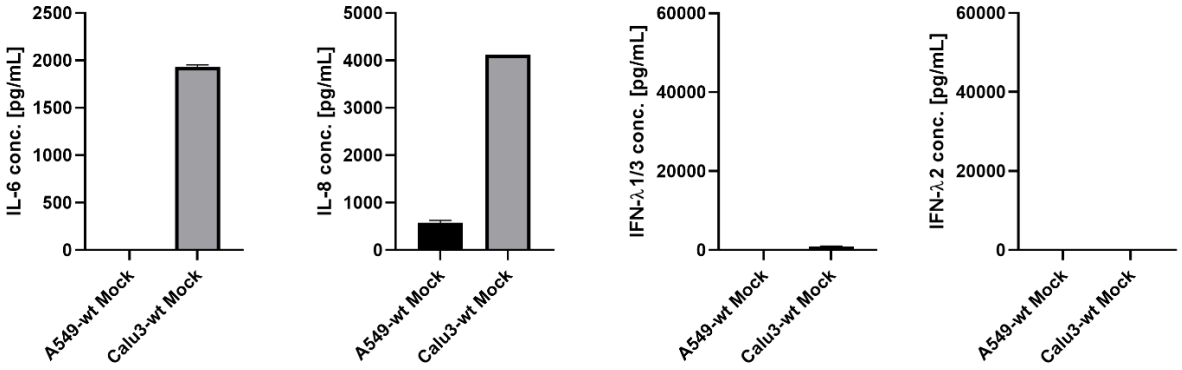

Figure 21) Mock-transfected Calu-3 wildtype cells produce IL-6 and IL-8. *A549 and Calu-3 wildtype cells were treated with transfection reagent only for 48 hours. IL-6, IL-8 and type III IFN secretion into culture supernatant was measured by DuoSet ELISA (R&D) from three (INFs), two (IL-6, IL-8 A549; IL-6 Calu-3) or one (IL-8 Calu-3) independent experiments. Measures are shown as mean +/- SEM.*

4.5. Type III IFN and inflammatory cytokine production from stimulated wildtype and viral protein expressing cells

4.5.1. Type III IFN production is differently altered by Orf3a, Orf6 and Orf9b in A549 and Calu-3 cells

To investigate the hypothesized type III IFN antagonism of SARS-CoV-2 Orf3a, Orf6 and Orf9b, secretion levels of type III IFNs (IFN-λ1/3, IFN-λ2) from viral protein-expressing A549 and Calu-3 cells were compared to wildtype cells. Like before, doxycycline-treated cells were transfected with 5 µg/mL poly(I:C) at the same time and supernatant harvested after 4, 10, 24 and 48 hours for ELISA, respectively. Interestingly, A549 cells expressing Orf3a, Orf6 and Orf9b showed a slight reduction in IFN-λ2 secretion compared to wildtype A549 cells at 24 and 48 hours post stimulation, albeit no statistical significance (***Figure 22C***). In contrast, none of the SARS-CoV-2 proteins significantly altered IFN-λ1/3 production compared to A549 wildtype cells (***Figure 22A***). In contrast, Orf6 expressing Calu-3 cells responded with higher type III IFN production compared to wildtype cells (***Figure 22B***, ***D***), albeit no statistical significance.

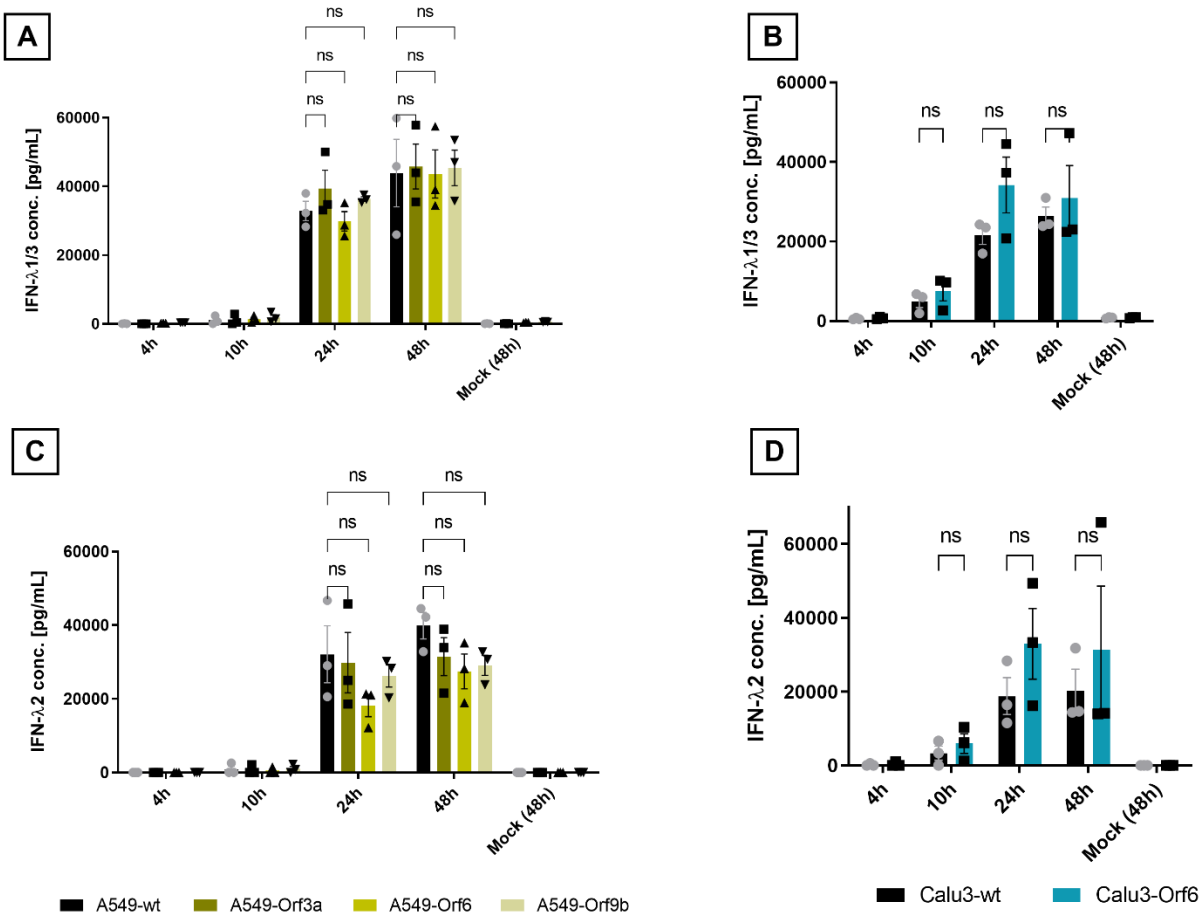

Figure 22) Secretion of type III IFNs from wildtype and SARS-CoV-2 viral protein expressing A549 and Calu-3 cell lines transfected with 5 µg/mL poly(I:C). *Analysis of type III IFN secretion levels were performed by DuoSet ELISA (R&D), quantification of absorbance (450nm) in technical duplicates.* ***A-B****) Secretion of IFN-λ1/3 by wildtype and transduced A549 (A) and Calu-3 cells (B) transfected with 5 µg/mL poly(I:C) for 4, 10, 24 and 48 hours. Mean +/- SEM from three independent experiments.* ***C-D****) Secretion of IFN-λ2 by wildtype and transduced A549 (C) and Calu-3 cells (D) transfected with 5 µg/mL poly(I:C) for the same timepoints. Mean +/- SEM from three independent experiments. Groups were compared in a two-way ANOVA and Bonferonni's multiple comparisons test (p = 0.05).*

4.5.2. IL-6, IL-8 production is not altered by Orf3a, Orf6 and Orf9b in A549 and Calu-3 cells

To further investigate if the viral proteins had an effect on inflammatory cytokine responses, the production of NF-κB-dependent inflammatory cytokine/chemokine (IL-6, IL-8) from transduced and wildtype A549 and Calu-3 cells were compared. No statistically significant difference was detected for IL-8 and IL-6 production from stimulated viral protein-expressing A549 cells compared to wildtype cells (***Figure 23A*** and ***C***). However, a slight induction of IL-8 from Orf9b expressing A549 cells could be detected, albeit no statistical significance (***Figure 23C***). IL-6 production from Calu-3 wildtype cells and Orf6 expressing cells did not significantly differ as well

(***Figure 23B***). IL-8 production stayed similar at all time points for both wildtype and Orf6-Calu-3 cells and including the mock control (***Figure 23D***). Furthermore, comparing IL-6 production from stimulated and mock-transfected Calu-3 cells showed no statistically significant induction in stimulated cells (***Figure 23B***). This suggests that poly(I:C) transfection of Calu-3 cells did not significantly induce secretion of IL-6 or IL-8.

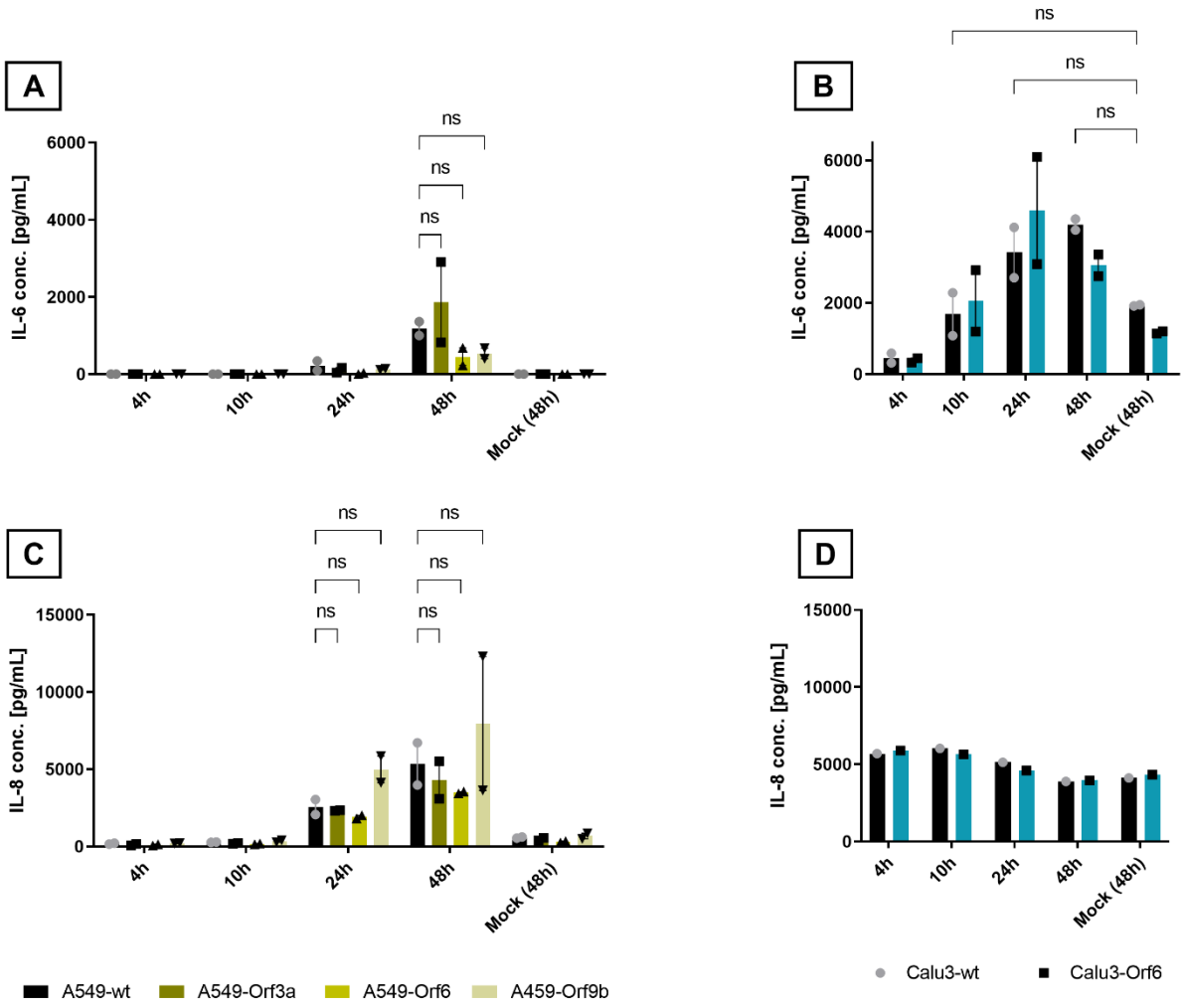

Figure 23) Secretion of pro-inflammatory cytokines from wildtype and SARS-CoV-2 viral protein expressing A549 and Calu-3 cell lines transfected with 5 µg/mL poly(I:C). *Analysis of pro-inflammatory cytokine secretion levels were performed by DuoSet ELISA (R&D), quantification of absorbance (450nm) in technical duplicates.* ***A-B****) Secretion of IL-6 by wildtype and transduced A549 (A) and Calu-3 cells (B) transfected with 5 µg/mL poly(I:C) for 4, 10, 24 and 48 hours. Mean +/- SEM from two independent experiments.* ***C-D****) Secretion of IL-8 by wildtype and transduced A549 (C) and Calu-3 cells (D) transfected with 5 µg/mL poly(I:C) for the same timepoints. Mean +/- SEM from two independent experiments (A549 cells) or one independent experiment (Calu-3 cells). Groups were compared in a two-way ANOVA and Bonferonni's or Dunnett's multiple comparisons test and comparisons were non-significant (p = 0.05).*

4.5.3. Transfection of poly(I:C) induces cell death in A549 and Calu-3 cells

During cell stimulation experiments, high cell death was observed for all cell lines after transfection with 5 µg/mL poly(I:C). To determine viability of all cell lines over time, an MTS assay was performed (***Figure 24***). A mock control was included to determine whether the transfection reagent had an influence on cell viability. Since mock transfection did not reduce cell viability (see ***Suppl. Figure 5***), absorbance measures from all treated samples were normalized to mock controls. The cell viability of wildtype and SARS-CoV-2 viral protein expressing A549 and Calu-3 cells decreased drastically after 24 hours and differed between wildtype and transduced cell lines with transduced cells showing higher reduction in cell viability than wildtype cells. In fact, compared to the mock control only 25% viable A549-Orf9b cells were present in culture after 48-hour incubation (***Figure 24A***). In comparison, A549-wt cells showed the lowest reduction with 50% viable cells after 48 hours compared to the mock control. Cell viability of Calu-3-Orf6 decreased by almost 73% after 48 hours of incubation compared to the mock control (***Figure 24B***). Calu-3-wt cells showed a lower decrease in cell viability, counting 60% of viable cells after 48 hours of incubation with transfected poly(I:C). Further analysis of the effect of transfected poly(I:C) revealed high release of lactate dehydrogenase (LDH) from A549 and Calu-3 cells at 48 hours post-stimulation, equal across all cell lines, indicating pro-inflammatory cell death (***Figure 24C***). Interestingly, mock controls of both Calu-3-wt and Calu-3-Orf6 cells showed high concentration of LDH in the culture supernatant. ***Figure 24D*** shows light microscopy images (10x magnification) of wildtype A549 and Calu-3 cells transfected with 5 µg/mL poly(I:C) where an increase in floating dead cells is visible >24 hours.

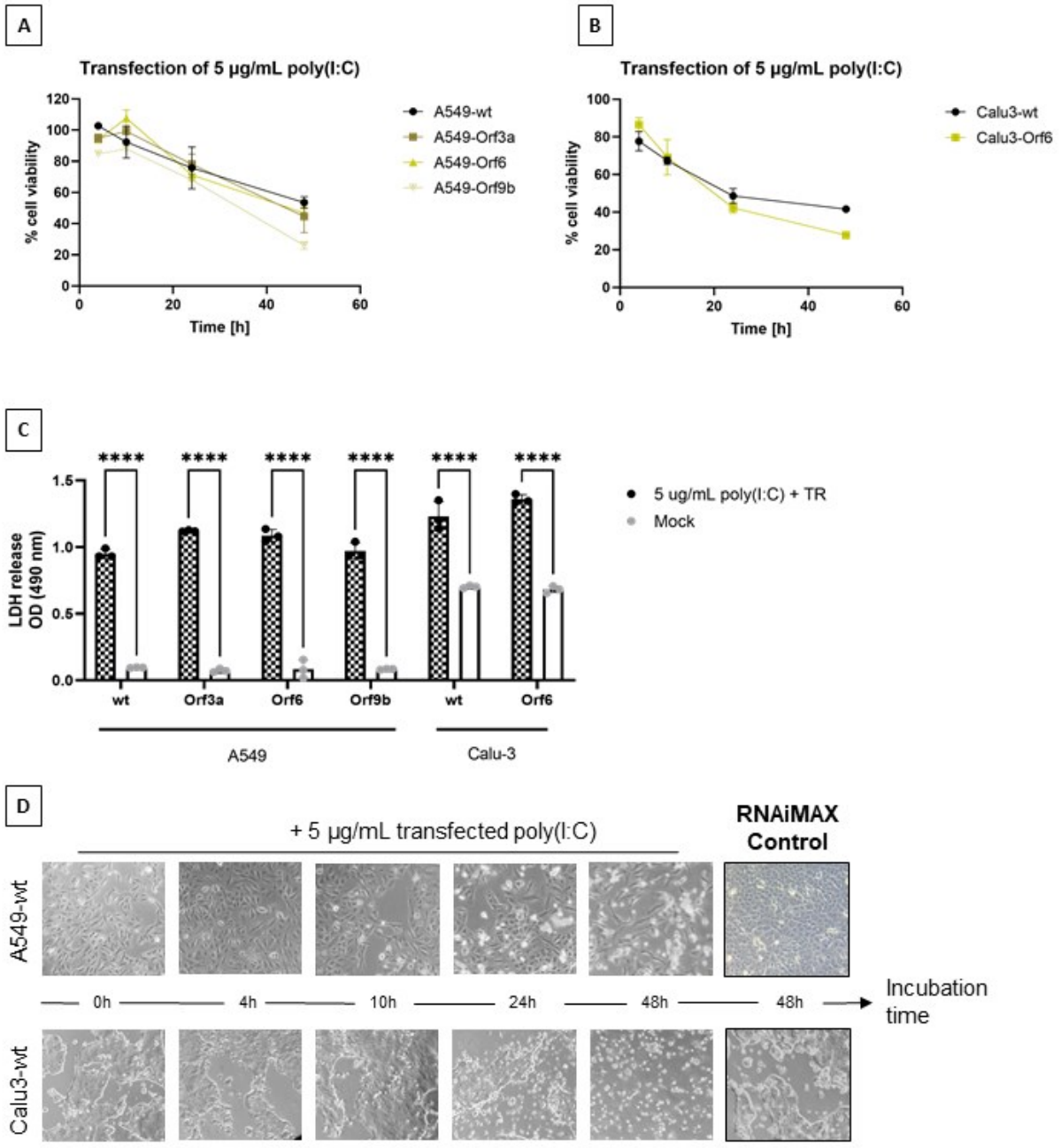

Figure 24) Transfection of 5 µg/mL poly(I:C) in A549 and Calu-3 wildtype and transduced cells reduces cell viability and induces cell death. *A) Cell viability (MTS) assay of A549 and Calu-3 cell lines transfected with 5 µg/mL poly(I:C) (TR) for 4h, 10h, 24h and 48h. Quantification of absorbance at 490 nm. Normalized measures (compared to mock controls) are given as mean +/- SEM, n=2. B) Lactate dehydrogenase (LDH) release into culture supernatants from mock treated and transfected cells with 5 µg/mL poly(I:C) (TR) by quantification of absorbance at 490 nm, means +/- SEM, n=3. Two-way ANOVA with Bonferroni post-test, **** (p<0.001). C) Light microscopy (10x magnification) images from wildtype A549 and Calu-3 cells transfected with 5 µg/mL poly(I:C) for the given timepoints.*

4.5.4. Transfection of 1 µg/mL poly(I:C) concentration increases cell viability

To determine if a decrease in poly(I:C) concentration could lower the amount of cell death, cell viability after transfection of 5 µg/mL poly(I:C) was compared to measures

from cell lines transfected with 1 µg/mL poly(I:C), incubated for 4, 10, 24 and 48 hours. Furthermore, to determine whether poly(I:C) alone or specifically transfected poly(I:C) induced cell death in A549 and Calu-3 cell lines, all cell lines were incubated with 5 and 1 µg/mL pure poly(I:C). ***Figure 25*** shows cell viability measures over time for all A549 and Calu-3 cell lines. In general, transfection of poly(I:C) showed a higher effect on cell viability compared to treatment with pure poly(I:C). Decreasing the concentration from 5 to 1 ug/mL poly(I:C) increased cell viability almost by 2-fold in all cell lines after 48-hour stimulation.

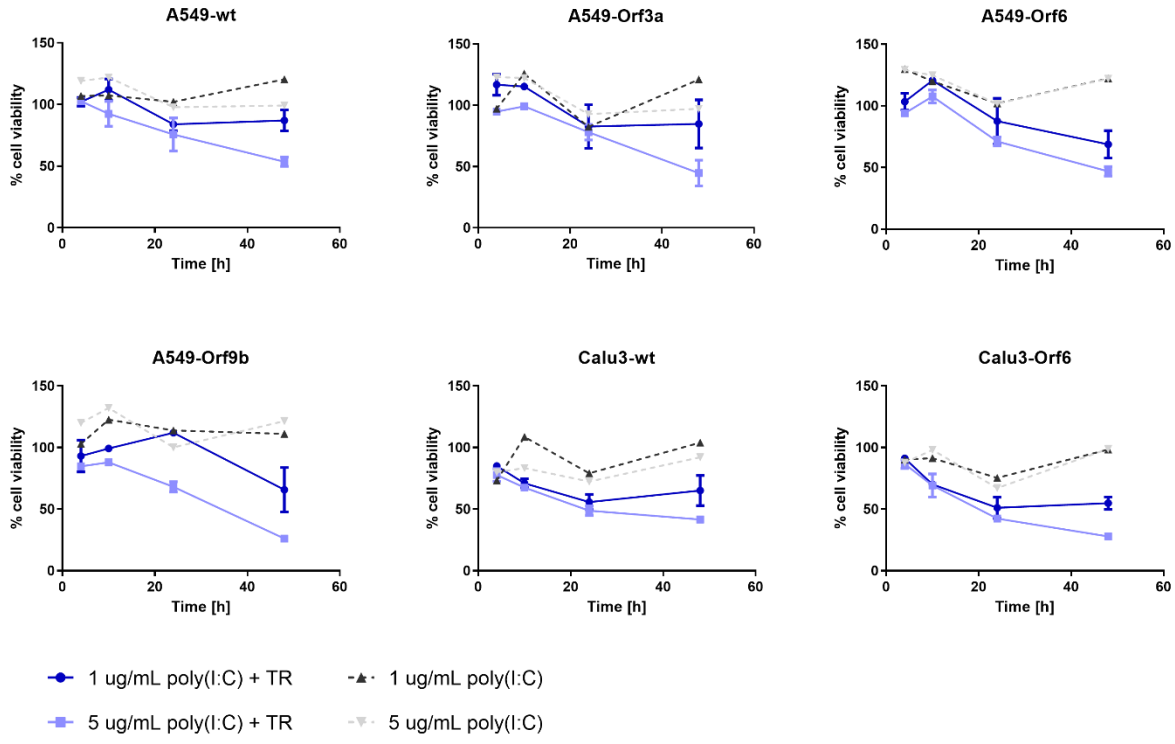

Figure 25) Cell viability decreases due to transfection of poly(I:C) and depends on the concentration of poly(I:C). *MTS assay of wt and transduced A549 and Calu-3 cells treated with different concentrations of pure and transfected poly(I:C) (+TR) for 4h, 10h, 24h and 48h. Mock controls were used to normalize measures. Measures are given as mean +/- SD from two biological replicates (transfected poly(I:C) treatment) or as single measures (pure poly(I:C) treatment).*

5. Discussion

5.1. Monocyte-derived macrophages are not permissive to SARS-CoV-2

At the beginning of this study, our knowledge about SARS-CoV-2 mainly depended on previous studies on the related SARS-CoV and MERS-CoV. Both SARS-CoV and SARS-CoV-2 primarily infect ACE2-expressing epithelial and endothelial cells[11, 113]. However, earlier studies on SARS-CoV reported that monocyte-derived macrophages (MDMs) are permissive to infection and that the virus can replicate in these cells, consequently allowing translation of viral proteins[114, 115]. Since macrophages were also found to be involved in promoting the hyper-inflammatory phenotype of severe COVID-19[76, 77, 116], with some studies even suggesting that macrophages can be infected by SARS-CoV-2[74, 77, 117], we first sought to study immunomodulatory effects of SARS-CoV-2 viral proteins in human THP-1 monocytic cells. However, SARS-CoV-2 infection studies performed by Markus Haug later revealed that both primary MDMs and THP-1 cells are not infected by SARS-CoV-2 (***Figure 12***) and we conclude that viral proteins can thus not be expressed in THP-1 cells. Instead we found that Calu-3 human lung epithelial cells and VeroE6 monkey epithelial cells were productively infected and showed an increase in intracellular viral RNA (***Figure 12***), consistent to previous studies[30, 32, 55]. Infected lung epithelial cells directly influence innate immune responses by recruiting, activating, and inducing antiviral immune programs in innate immune cells via chemokine, cytokine, and type I and III IFN production[30, 76]. Since no functional studies have yet been published on SARS-CoV-2 viral proteins in lung epithelial cell lines nor with major focus on type III IFN responses, we continued by investigating the effects of SARS-CoV-2 viral proteins in lung epithelial cell lines in regard to the production type III IFNs and inflammatory cytokines and chemokines.

5.2. Successful lentiviral transduction relies on several parameters

We obtained lentiviral expression plasmids for 26 out of 29 SARS-CoV-2 viral proteins as a gift from Krogan's lab[69]. He and his team codon optimized and cloned all mature Nsps and predicted Orfs into pLVX-TetOne-Puro and pLVX-Puro plasmid backbones. His team used the plasmid to generate the first host interaction maps for SARS-CoV-2 and made them available to research labs all over the world. In our lab, we used

pLVX-TetOne-Puro plasmids for the selected SARS-CoV-2 viral proteins to stably transduce A549 and Calu-3 human lung epithelial cells. The use of pLVX-TetOne-Puro plasmids further allowed controlled gene expression in the presence of doxycycline. Selection of successful clones was performed by puromycin treatment. Several steps of optimization and troubleshooting were required to achieve high-titer LV production, efficient transduction, precise selection, and doxycycline-inducible gene expression.

5.2.1. Optimization of lentivirus production

To efficiently transduce target cells, it was necessary to obtain high viral titers ($>10^7$/mL) of correctly packaged LVs. Three different factors can affect LV production: 1) the packaging cells and culture conditions, 2) the choice of LV packaging system and transfection efficiency and 3) concentration of the virus stock and storage.

At first, high cell viability and low passage numbers of packaging cells (here HEK293T cells) is crucial to obtain high LV titers and correctly packaged LVs, because these factors affect the productivity and functionality of the cells. Furthermore, the quality of serum in complete growth medium can affect the efficiency of LV production when using tetracycline-dependent transactivation systems. In fact, 4th-generation LV packaging using 4th-generation packaging plasmids includes an additional regulatory plasmid that expresses the transactivator protein tTA only in absence of tetracycline which, in turn, activates the expression of viral packaging proteins, thus mediating LV packaging. Importantly, standard FCS can contain traces of tetracyclines and the use of tetracycline-free FCS is recommended for efficient production of 4th-generation LVs[108]. Since we used standard FCS in this study, this could explain the relatively low viral titers obtained ($<10^7$) (***Figure 14E***) compared to the expectations suggested by the manufacturer[108].

Furthermore, the choice of LV packaging system is crucial to ensure correct LV packaging and high efficiency of LV production. In this study, 2nd-, 3rd- and 4th-generation lentiviral packaging systems were tested, and only 4th-generation LVs were able to successfully transduce target cells (***Figure 14***). This was due to the main difference between the different packaging systems, namely the presence or

absence of the HIV-1 Tat protein and chimeric or standard HIV-1 LTRs on the transfer plasmid, respectively. In fact, pLVX-TetOne-Puro expression plasmids belong to the 4th generation of lentiviral expression plasmids that require the presence of Tat. In line with this, the use of 3rd generation packaging plasmids – which do not express Tat – did not result in functional LVs as evidenced by unsuccessful transduction of THP-1 cells (***Figure 14***). High concentration of p24 measured in supernatant of HEK293T cells transfected with 3rd-generation packaging, envelope and 4th-generation transfer plasmids or 3rd-generation packaging and envelope plasmids alone (***Figure 14***) suggested that LVs were not successfully produced. Both 2nd and 4th generation packaging plasmids express Tat and should thus have been successful in making LV with pLVX-TetOne-Puro plasmids. However, target cells were not successfully transduced with 2nd-generation LVs albeit high viral titers measured (***Figure 14***). An explanation could be the cumbersome process of co-transfection of packaging, envelope and transfer plasmids into HEK293T cells, as well as the viability and phenotype of the HEK293T cells at that time. In fact, we observed high cell death of HEK293T cells early during LV production following the 2nd generation protocol. This could have led to an increase of p24 capsid protein in the supernatant due to cell rupture before LVs could be produced, as evidenced by high titers for empty LV particles (***Figure 14B***). In contrast, the protocol for 4th-generation LV packaging avoided complex preparation of co-transfection by the use of pre-made "Single Shots" containing the transfection reagent lyophilized with all required packaging, regulatory and envelope plasmids at optimized ratios. However, the manufacturer stated that their optimized system produces very high titers (>10^7) which could not be obtained in this study (***Figure 14***). As mentioned, this was probably due to the use of standard FCS in the HEK293T cell culture medium.

Finally, viral titers can be increased by an additional concentration step, e.g. by poly-ethylene glycol (PEG)-based virus precipitation and concentration, ultra-centrifugation, ultrafiltration, or column purification via biotinylated VSV-G[118]. Here, we used PEG-based concentration. When carefully executed, PEG-based concentration was simple to perform and resulted in higher viral titers compared to titers of unconcentrated LVs. This was tested one time with SARS-CoV-2 Orf9b LV where viral titers were measured before and after concentration by 1:10 (***Suppl.***

Figure 1). However, concentration resulted in a titer increase of only 1:2, suggesting that concentration was not as efficient as the protocol stated. This could have been due to multiple freeze-thaw cycles prior to concentration of the virus. In fact, multiple freeze-thaw cycles should be generally avoided because this could drastically lower viral titers.

5.2.2. Optimization of lentiviral transduction

Once intact LV particles are harvested from the packaging cells, the target cells can be transduced by adding the LV-containing supernatant. However, successful transduction is dependent on several factors: 1) the cell viability of the target cells, 2) the use of polybrene to enhance viral uptake, 3) the transduction method, 4) the right concentration of virus (MOI) and 5) the optimal concentration of puromycin to select for transduced cells.

As for LV-producing cells, high cell viability before and during transduction was required. The transduction procedure as well as the use of transduction enhancers like polybrene can affect the cell viability of cell lines[119]. Visual inspection of A549 and Calu-3 cells after transduction by centrifugation and incubation with polybrene showed cell death among Calu-3 cells but not A549 cells. This is also the reason why A549 cells were successfully transduced with several different viral proteins and Calu-3 cells only survived transduction with Orf6-LV (***Figure 18***). To reduce cell death resulting from the transduction procedure, other transduction methods could be used that will be mentioned later.

Lentiviral transduction can be enhanced by adding positively charged polycations like polybrene, DEAE-dextran, protamine sulfate or poly-L-lysine[119, 120]. These reagents have been suggested to enhance viral uptake by reducing the repulsion forces between the opposite charges of the viral particle and the cell[119, 120]. In this study, polybrene was used at a concentration that was previously optimized for an in-house protocol (8 µg/mL) and should generally be between 2-12 µg/mL[119]. However, the incubation period with polybrene was kept as short as possible, because polybrene can be cytotoxic to many types of cells[119], consequently reducing cell viability and the number of efficiently transduced cells.

As already mentioned, the transduction procedure also has an influence on transduction efficiency. Comparing the efficiency of centrifugation vs. reverse transduction showed high transduction efficiency of A549 cells by centrifugation compared to low transduction efficiency of HEK293T cells by reverse transduction (***Figure 16***). However, the differences could have been additionally caused by the use of different cell types, although both cell types are highly permissive to VSV-G coated LVs due to the ubiquitous expression of phosphatidylserine on all mammalian cells which is required for viral entry[106, 121]. Despite the lower transduction efficiency, reverse transduction constitutes a less harsh method for transduction and thus could be more suitable for sensitive adherent cells, e.g. Calu-3. Another option could also be to detach the cells and transduce them in suspension by spinofection, the method-of-choice for suspension cells[122].

Next, the MOI can affect transduction efficiency and the occurrence of multiple insertion events. An MOI > 1, for example, could lead to a number of cells with >1 copies of transgenes in their genome. However, transducing with MOI < 1 would greatly affect transduction efficiency. Empirical studies evaluated the optimal MOI for different cell lines[123] and suggested an MOI = 5 for A549 and HEK293T cells, since these cells are generally easier to transduce compared to other cell lines (e.g. HMVEC). The MOI of 5 worked well for both A549 and Calu-3 cells, as reflected by successful transduction for most LVs used (***Figure 18***).

Lastly, cell lines showed different sensitivities to puromycin, the reagent to select for successfully transduced cells (***Figure 15***). Since cell lines behave differently to antibiotics, a kill curve is a standard optimization procedure for successful selection, and expansion of cellular clones after lentiviral transduction.

5.2.3. Optimization of doxycycline-inducible gene expression

The ability to regulate expression of the GOI is ideal for genes that might cause adverse side effects, e.g. cytotoxicity. For example, SARS-CoV-2 Orf3a has been suggested to induce apoptosis in cell lines[124]. The Tet-On 3G expression system of the GOI involves the presence of a transactivator protein (Tet-On 3G) and a Tet-On 3G-dependent promoter of the GOI (pTRE3G). Upon presence of doxycycline, Tet-On 3G binds to pTRE3G and activates the expression of the GOI[110, 125]. We demonstrated

that the doxycycline-inducible expression system is highly sensitive towards doxycycline with minimal concentrations required and long-lasting gene expression if doxycycline was not removed (***Figure 17, Suppl. Figure 3***). This could also explain the leaky expression of Orf3a, Orf6 and GFP in transduced A549 cells and Nsp1, Nsp5 and Orf3a in transiently transfected HEK293T cells incubated without doxycycline, since the cell culture medium contained standard FCS that can contain traces of tetracyclines (***Figure 13, Figure 18***). Strikingly, some viral proteins (Nsp5, Nsp13) were not found to be expressed after transduction and successful puromycin selection of A549 cells for >1 week (***Figure 18***), even after incubation with different concentrations of doxy and incubation for different timepoints (24, 48 hours) (***Suppl. Figure 4***). A possible explanation could be that *Nsp5* and *Nsp13* were epigenetically silenced, a side-effect that can occur during lentiviral transduction[126]. Furthermore, since Nsp5 and Nsp13 are exogenous proteins, they could have been targeted for degradation by the host after expression in the cytoplasm. However, Nsp5 and Nsp13 were detected in HEK293T cells after transient transfection, suggesting that they can be expressed in the cytosol of cancer cell lines. Further optimization and troubleshooting will be required to identify the reason for undetectable Nsp5 and Nsp13 expression in A549 cells.

In general, recombinant protein expression by lentiviral transduction has several advantages over transient transfection. Transient transfection allows protein expression only for a limited time-frame (ca. 12-72 hrs) followed by rapid decline of expression[94]. Lentiviral transduction, in contrast, allows long-term protein expression which can be turned on or off if an inducible expression system is incorporated[94]. However, lentiviral transduction is a time-consuming process and takes several weeks from plasmid cloning to rigorous selection and expansion of polyclonal cell lines. Additionally, several steps require optimization, as explained before, further increasing the time needed to establish protocols. Lastly, since the site of DNA integration is not targetable with currently existing protocols, lentiviral transduction may affect the cytogenetic and phenotypic characteristics of the target cells, e.g. by insertional mutagenesis or alterations in host DNA methylation patterns[126]. Thus, experiments based on genetically manipulated cell lines should be analyzed with

caution. In the future, more precise lentiviral transduction technologies should be investigated, e.g. including strategies to control the site of insertion.

5.3. The suitability of A549 and Calu-3 epithelial cells to study SARS-CoV-2 viral proteins

To date, most functional studies of individual SARS-CoV-2 viral proteins were conducted in human embryonic kidney HEK293T cells[17-19, 82] and not in lung epithelial cell lines which present the primary target cell type of SARS-CoV-2. We therefore sought to investigate immunomodulatory effects of SARS-CoV-2 Orf3a, Orf6 and Orf9b in Calu-3 and A549 lung epithelial cells which mimic the phenotypes of primary airway epithelial cells (ACEs)[127, 128] or type II alveolar cells[129], respectively, and have previously been used to study SARS-CoV-2 infection[30, 32, 55]. In contrast to A549 wildtype cells, Calu-3 cells express high levels of hACE2[128] rendering them as the most suitable model to study SARS-CoV-2 lung infection. This is also the reason why A549 cells are often transduced with hACE2 to study SARS-CoV-2 infection of this cell type[31, 32].

Here, we demonstrated that A549 cells exhibited more suitable inflammatory and antiviral responses upon poly(I:C) stimulation to study viral interference with innate immune pathways compared to Calu-3 cells. In detail, we observed that Calu-3 cells secreted inflammatory markers (IL-6, IL-8, LDH) in absence of poly(I:C) (***Figure 21, Figure 24C***) and that transfection of poly(I:C) did not result in statistically significant induction of IL-6 and IL-8 production (***Figure 23***), only a significant increase in secreted LDH (***Figure 24C***). LDH secretion from mock-infected Calu-3 cells was also measured by another study, with OD(492nm) values consistent to our findings[30]. However, in contrast to our data, the same study showed that Calu-3 cells strongly induced IL-6 and IL-8 mRNA expression after 24 hours followed by IL-6 cytokine secretion after 48 hours upon poly(I:C) transfection as well as SARS-CoV-2 infection, respectively[30]. Of note, their Calu-3 mock controls did not secrete IL-6 at any timepoint[30], in contrast to our findings. Our findings, thus, raise concerns about the suitability of the herein presented Calu-3 cell model to study the antagonistic functions of SARS-CoV-2 viral proteins on innate immune pathways. Several factors could explain the variations of inflammatory responses by Calu-3 cells in this study.

At first, Calu-3 cells are able to form polarized monolayers by forming tight junctions and developing transepithelial electrical resistance (TEER)[127]. Disruption of the epithelial monolayer can alter the normal function of epithelial cells by modulating signaling pathways involved in repair and differentiation as well as pro-inflammatory responses[130]. In this study, intact monolayers were difficult to ensure due to a) the high cell death observed >24 hours upon poly(I:C) transfection (***Figure 24***) and b) cell culture difficulties and possible pre-existing phenotypic alterations. In fact, Calu-3 cells were obtained as a gift from Denis Kainov's lab without information about passage numbers or freeze-thaw cycles. According to the experiences with Calu-3 cell culturing from the Lucy Thorne (information upon request), the author of a previously mentioned study that used Calu-3 cells to study SARS-CoV-2 infection[30], Calu-3 cells are very susceptible to high passage numbers (>12) which can result in altered phenotypes. Calu-3 cells used in this study likely reached passage numbers above 12. Furthermore, we observed high cell death when detaching and seeding Calu-3 cells, possibly due to the long trypsin/EDTA treatment that was required to detach cells (>15 min), resulting in death of early detached cells. This could have then affected the culture environment of freshly seeded, viable cells since cell debris and release of stress-released damage associated molecular patterns (DAMPs) from dying cells could have triggered innate immune pathways inducing inflammatory responses prior and/or in addition to stimulation by poly(I:C) transfection[131]. In contrast, A549 cells did not produce inflammatory cytokines prior to stimulation, possibly because their phenotype is not dependent on the formation of tight junctions and TEER[129]. In general, they were less susceptible to phenotypic changes with increasing passage numbers and were easier to maintain in culture compared to Calu-3 cells. Upon poly(I:C) transfection, A549 cells significantly produced inflammatory IL-6, IL-8 and antiviral type III IFNs as soon as 10 hours post-stimulation and peaking at 48 hours (***Figure 20***). Furthermore, no LDH release was detected in mock-infected cells, only upon transfection of poly(I:C) and cell viability was slightly higher compared to Calu-3 at all timepoints during stimulation experiments (***Figure 24***).

To summarize, A549 cells showed more suitable inflammatory responses upon poly(I:C) transfection compared to Calu-3 cells. Additional factors complicated the

use and applicability of Calu-3 cells. However, since Calu-3 cells present a highly valuable cell model for studying SARS-CoV-2 biology, further characterization of new batches of Calu-3 cells and culturing under optimized culture conditions will be necessary. In addition to that, even further cell model optimizations could be addressed by considering the use of induced pluripotent stem cell (iPSC) derived cell models instead of cancer cell lines. Importantly, iPSC-derived cell models are suggested to have several advantages over cancer cell lines to study disease and evaluate drugs[132-134]. iPSCs are derived from primary cells of non-cancerous origin (e.g. fibroblasts) by highly controlled genetic manipulation and hence do not carry tumor-associated mutations like cancer cell lines do. Because of their origin, cancer cell lines harbor many mutations, including loss-of-function mutations in genes that could be important for responses in primary cells. For example, mutations of p53 were found in 20-25% of human cancer cell lines[135] and intact p53 was shown to down-regulate SARS-CoV infection in p53-expressing HCT116 cells[136]. Moreover, cancer cells have mutations in tumor-suppressor genes and oncogenes making them highly proliferative and undifferentiated which could additionally have an impact on their ability to model viral infection of primary cells[134]. Interestingly, a protocol for iPSC-derived type II alveolar epithelial cells has recently been published[137] and another study demonstrates the potential of an iPSC-based platform to study SARS-CoV-2 infection in human primary cells and organoids[134]. These are some examples of the possibilities and ongoing efforts for advanced iPSC-based *in vitro* cell models to study SARS-CoV-2 biology.

5.4. Inflammatory cytokines, chemokines, and type III IFNs are secreted in a RIG-I/MDA5-dependent manner from human lung epithelial cells

Both ssRNA and dsRNA intermediates of coronaviruses can be sensed by cytosolic RLRs (dsRNA)[35, 138] and endosomal TLR3 (dsRNA)[28], TLR7 (ssRNA)[139, 140] and TLR8 (ssRNA)[139, 140] which subsequently drive innate immune responses to restrict viral replication and dampen the infection. So far, research on SARS-CoV-2 has found that human lung epithelial cells produce inflammatory cytokines and type I and III IFNs in a RIG-I/MDA5-dependent manner[30, 32]. The role of TLR3, 7 and 8 in lung epithelial cells during SARS-CoV-2 infection has not yet been revealed and further research will

be required. Interestingly, a very recent study demonstrated that TLR2 senses the SARS-CoV-2 envelope (E) protein on the plasma membrane of human bone marrow derived macrophages (BMDMs) and human PBMCs resulting in the production of inflammatory cytokines[34]. To what extent TLR2 can sense the E protein on human lung epithelial cells has not yet been studied. Since previous studies showed that human airway epithelial cells express TLR2 and respond to inflammatory stimuli in a TLR2-dependent manner[141, 142], it would be interesting to find out if TLR2 can sense SARS-CoV-2 on lung epithelial cells as well.

In this study, we found that solely transfection of poly(I:C), a dsRNA mimic, induced inflammatory and type III IFN responses in A549 and Calu-3 lung epithelial cells (***Figure 19***, ***Figure 20***). Transfection of poly(I:C) has previously been shown to induce RIG-I/MDA5 signaling pathways[143-145], suggesting that inflammatory and type III IFN responses measured in this study were driven in a RIG-I/MDA5 dependent manner. Strikingly, previous SARS-CoV-2 infection studies demonstrated that inflammatory cytokine and type III IFN responses from infected Calu-3 and hACE2-A549 cells were driven in a RIG-I/MDA5-dependent manner[30, 32]. This, furthermore, suggests that transfection of poly(I:C) could mimic PRR stimulation by SARS-CoV-2 and that subsequent investigations of the antagonistic effects of SARS-CoV-2 viral proteins can be discussed in relation to RIG-I/MDA5-dependent pathways. However, further studies will be required to validate the role of RIG-I/MDA5 in our setup. This could be done by knocking out genes that are essential for RIG-I/MDA5-mediated signaling (e.g. *RIG-I, MDA5* or *MAVS*).

Although previous studies showed that A549 and Calu-3 cells express endogenous TLR3[146-149], IL-6 and IFN-λ2 were not detected in the culture supernatant from A549 and Calu-3 cells stimulated with pure poly(I:C) (***Figure 19***), a dsRNA mimic and commonly used TLR3 agonist when untransfected[146, 149]. One factor could have been the concentration of poly(I:C) used in this study which should be optimized by poly(I:C) titration. In fact, previous studies showed that A549 cells only responded to high concentrations of poly(I:C) (>10 µg/mL), as detected by IL-6 and/or IL-8 production after 10 hours, albeit low concentrations (IL-6 < 100 pg/mL; IL-8 < 800 pg/mL)[150]. In addition, other studies found that TLR3 expression in A549 cells and poly(I:C)-induced downstream inflammatory activity was enhanced by pre-

treatment with IFN-a[149] or pre-infection with respiratory syncytial virus (RSV)[149], respectively. This suggests that basal TLR3 expression levels could have been too low to induce detectable cytokine responses. Expression of TLR3 should be validated and quantified by western blot and/or RT-qPCR.

Finally, no IL-6 nor IFN-λ2 production was detected from A549 and Calu-3 cells treated with the TLR7 agonist CL264[151] and TLR8 agonist polyU[152], respectively (***Figure 19***). Previous studies reported contradicting findings for the expression and activity of both receptors in human lung epithelial cells. One study reported no expression of TLR7 and 8 nor inflammatory cytokine responses to treatment with respective synthetic ligands in A549 cells[150] while another study reported expression of TLR7 and 8 in A549 cells as well as NF-kB activation induced by polyU and Loxoribine, another TLR7 agonist[153]. Our findings suggest that TLR7 and 8 are not activated in A549 and Calu-3 human lung epithelial cells, but again, this finding would require validation by western blot analysis and/or RT-qPCR as well as titration of both ligands.

To summarize, transfection of poly(I:C) could mimic sensing of SARS-CoV-2 dsRNA by RIG-I/MDA5 in A549 and Calu-3 lung epithelial cells in regard to inflammatory and antiviral immune responses. Furthermore, additional research will be required to investigate the role of TLR3, 7 and 8 in human lung epithelial cells during SARS-CoV-2 infection. Although this study suggests that A549 and Calu-3 lung epithelial cells do not respond to TLR3, 7 or 8 stimulation, respectively, this has to be validated by more detailed studies. Since previous studies suggest important roles of TLR3, 7 and 8 during viral infections of lung epithelial cells, it would be interesting to see if these TLRs play a role in sensing SARS-CoV-2 viral PAMPs and if they are associated with COVID-19 severity.

5.5. Do SARS-CoV-2 Orf3a, Orf6 and Orf9b inhibit type III IFN production?

To this date, our understanding of SARS-CoV-2 and antiviral IFN responses is far from being complete. Several clinical observations and data from *in vitro* and *in vivo* studies have demonstrated missing antiviral IFN production upon SARS-CoV-2 infection[17, 18, 54-56]. Furthermore, several studies have demonstrated that at least 13

SARS-CoV-2 viral proteins, including Orf3a, Orf6 and Orf9b, potently suppress type I IFN responses when transiently transfected in HEK293T cells[17, 18, 66]. However, emerging data from more recent studies show contradicting findings in human lung epithelial cells (primary human air-liquid airway epithelial cells (HAECs), hACE2-A549, Calu-3) where SARS-CoV-2 *does* induce type I and III IFN responses, but that IFNs were not capable of limiting viral replication, suggesting that rather the timing of antiviral IFN responses could influence disease severity[30, 32, 154]. In fact, our data demonstrates that SARS-CoV-2 Orf3a, Orf6 and Orf9b – previously shown to suppress type I IFN induction in HEK293T cells[17, 18, 66] – does not significantly antagonize type III IFN production in A549 and Calu-3 lung epithelial cells (***Figure 22***). Notably, slight reduction of IFN-λ2 secretion by A549 cells expressing all three viral proteins could be detected, with highest effect by Orf6 (***Figure 22C***). Based on our findings, we suggest that either 1) SARS-CoV-2 Orf3a, Orf6 and Orf9b antagonize type III IFN responses only at low viral loads early during infection in lung epithelial cells, as proposed by the previously mentioned studies[17, 18, 54-56], 2) SARS-CoV-2 antagonizes type I IFN more potently than type III IFN induction, as proposed by a recent study[66] and in line with the viral protein studies focusing on type I IFNs[17, 18], or 3) that studying type III IFN antagonism by SARS-CoV-2 Orf3a, Orf6 or Orf9b expressed individually in lung epithelial cells or upon infection with the whole virus differs due to synergistic functions of the viral proteins.

A very recent study on BioRxiv[30] gives a possible explanation for how viral load and the timing of antiviral IFN responses could be associated with clinical manifestations of severe COVID-19 (***Figure 26***). The study showed that viral replication in infected lung epithelial cells (Calu-3) had a decisive lead compared to type I and III IFN secretion and suggested that IFN antagonism occurs early during infection associated with low viral titers and diminishes once viral titers reach a certain "threshold"[30]. In fact, their hypothesis is supported by another study that reported reduced IFN-I and -III responses only at low MOI and not high-MOI infection in hACE2-A549 and Calu-3 cells[55]. In this study, we report results that could fit to the late inflammatory state at high viral load. In fact, we used quite strong inflammatory stimulus by transfecting 5 µg/mL poly(I:C), accompanied with high levels of inflammatory cell death (***Figure 24***), which could have mimicked the late stage during viral infection with high viral

titers. While inflammatory cell death could have induced more inflammation by release of DAMPs and subsequent activation of other PRRs than RIG-I/MDA5 in remaining cells, the cell death observed during stimulation experiments also complicated our analysis of ELISA data. In fact, we saw a decrease in cell viability at the same time as we saw an increase in cytokine production (>24 hrs), making it difficult to conclude how strong the cytokine response actually was, since number of viable cells differed greatly between the different timepoints. We showed that lowering the concentration of poly(I:C) to 1 µg/mL significantly increased cell viability (***Figure 25***). Thus, titrating poly(I:C) could help to reduce cell death-associated variations as well as potentially simulate an environment more similar to low viral loads and early stage of SARS-CoV-2 infection. In a next step, it would be interesting to find out if the concentration of poly(I:C) makes a difference on type III IFN antagonism by the respective viral proteins.

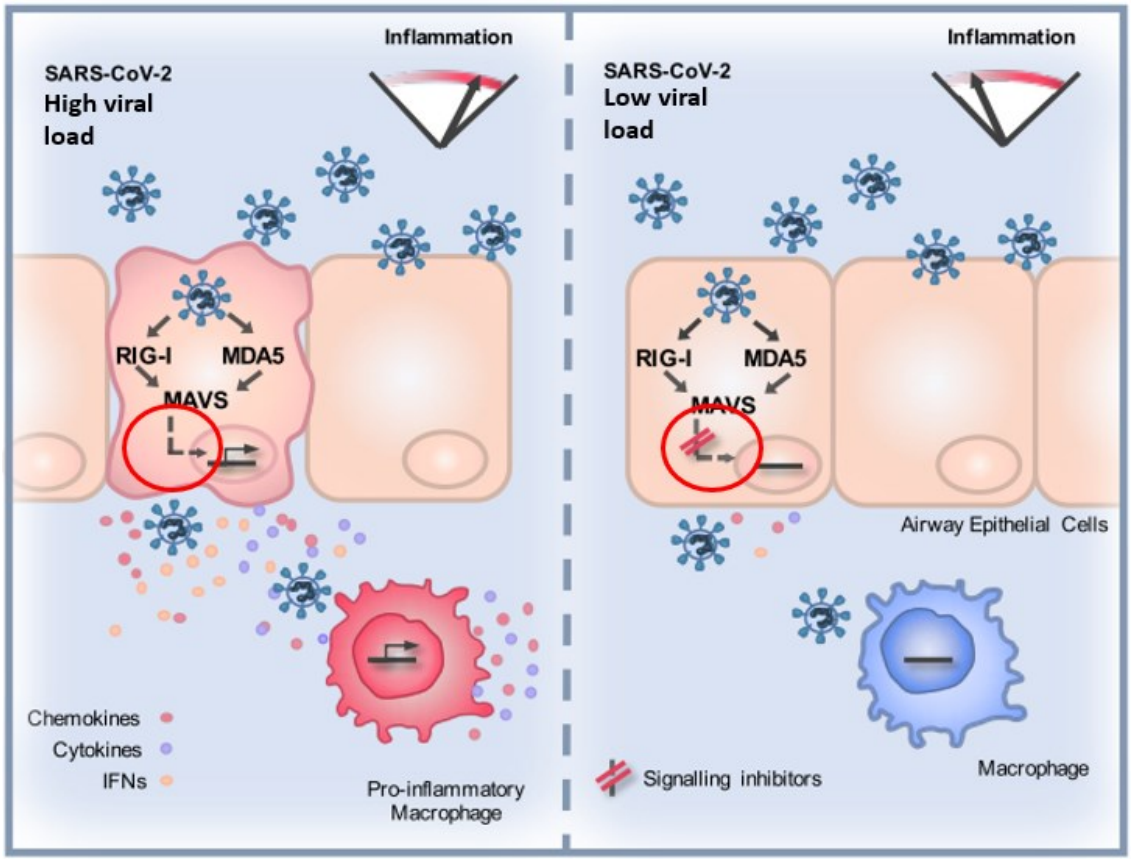

Figure 26) RLR-mediated inflammatory cytokine, chemokine and IFN production could be dependent on the stage and extent of SARS-CoV-2. *SARS-CoV-2 activates RIG-I/MDA5 sensors and consequent inflammatory responses in lung epithelial cells. The inflammatory environment and viral load reduce antagonistic effects of SARS-CoV-2 on RLR-signaling, leading to an increase in cytokine production and activation of macrophages. The figure was adapted from Thorne et al., BioRxiv, 2021*[30].

As mentioned, SARS-CoV-2 Orf3a, Orf6 and Orf9b were previously shown to reduce type I IFN expression when transiently expressed in HEK293T cells[17, 18]. Since our data demonstrate contradicting findings, another suggestion could be that gene expression of type I and III IFNs could be differently antagonized by SARS-CoV-2 viral proteins. In fact, emerging research reports that type I and III IFNs are induced under different circumstances from epithelial cells[51, 53, 155, 156]. For example, it was shown that the localization of MAVS on peroxisomes selectively expresses type III IFNs while mitochondria-localized MAVS induce type I IFNs[52, 53]. Interestingly, the abundance of peroxisomes in epithelial cells and a consequent increase in type III IFNs was found to correlate with cell differentiation and polarization[53]. This might raise concerns about the use of immortalized epithelial cell lines to study type III IFNs in this study and in general, since these are associated with an undifferentiated phenotype[157]. Additionally, research on regulation of gene expression of type I and III IFNs has found that they exhibit different promoter regions with different transcription factor binding sites. Data from type III IFN studies has found that IRF1 is a distinct transcription factor which does not induce type I IFN expression[53]. Furthermore, in contrast to expression of type I IFNs which requires promoter activation by both IRFs and NF-kB, gene expression of type III IFNs appears to be controlled through independent actions of IRFs and NF-kB[53, 155, 156]. SARS-CoV-2 is proposed to specifically target the IRF3-mediated IFN induction pathway and not NF-kB-mediated pathways in human lung epithelial cells[158]. Thus, the fact that NF-kB could suffice to induce expression of type III IFNs could explain our observations compared to the strong type I IFN antagonism found in other studies[19, 78, 82, 83]. However, differential regulation of type I and III IFNs still remains largely undefined and represents a fundamental gap in our knowledge about viral infections of epithelial cells. Further knowledge will be necessary to draw reliable conclusions on the differences observed between the different type III IFN subtypes in this study.

Finally, we propose that studying single viral proteins in lung epithelial cells mismatches the effects seen from viral infection studies, naturally resulting in translation of all SARS-CoV-2 viral proteins. At least 13 viral proteins are suggested to be involved in antagonizing IFN responses by interacting with one or more mediators of the RLR-mediated innate immune pathway[66, 69, 78]. Thus, measuring type

III IFN production from cells infected with the whole virus surely will differ from cells expressing only one viral protein at a time.

To summarize, more experiments will be required to conclude the findings from this study. More experimental replicates will reveal if the slight antagonism seen in this study is statistically significant. Furthermore, reducing cytosolic poly(I:C)-mediated cell death will help to lower cell death and decrease discrepancies in ELISA data. Also, it would be necessary to supplement the findings by RT-qPCR analysis of cell lysates to validate the findings at mRNA level. Additionally, since gene induction is often given as fold change compared to a housekeeping gene, this would give information about data normalized to viable cells. Furthermore, gene induction generally precedes protein secretion and thus will be detected earlier. This could help to investigate changes in cytokine gene expression before cell death occurs (>24 hours).

5.6. Hyperinflammation in COVID-19 is not due to viral proteins but other factors

Finally, we determined IL-6 and IL-8 production from wildtype and viral protein expressing lung epithelial cells to investigate the effect of SARS-CoV-2 Orf3a, Orf6 or Orf9b on interfering with NF-kB-mediated inflammatory cytokine pathways. We found that none of the proteins significantly interfered with IL-6 or IL-8 production from A549 and Calu-3 cells (***Figure 23***). Notably, Calu-3 cells did not significantly induce production of IL-6 or IL-8 upon poly(I:C) transfection (***Figure 23B, D***) and will not be discussed further. A slight inducing effect of SARS-CoV-2 Orf9b on IL-8 production could be observed 48 hours post-stimulation of A549 cells. However, further experiments will be required to see if this difference is statistically significant. SARS-CoV-2 induces high IL-6 and IL-8 production upon infection of lung epithelial cells[30, 158] and high concentrations of IL-6 and IL-8 were detected in serum samples from severe COVID-19 patients[55, 73], consistent to our findings from poly(I:C) stimulated A549 cells. Furthermore, in contrast to the modulation of the antiviral IFN responses by several viral proteins including Orf3a, Orf6 and Orf9b, SARS-CoV-2 infection was not shown to affect NF-kB mediated inflammatory pathways. In fact, a previous study showed that only IRF3 and not NF-kB translocation was blocked in

hACE2-A549 cells infected with SARS-CoV-2, suggesting exclusive anti-IFN activity of SARS-CoV-2 viral proteins[158] that fits to our findings.

In summary, we propose the following model to explain the clinical manifestations observed in severe COVID-19. Early during infection, SARS-CoV-2 inhibits type I and III IFN responses allowing the virus to replicate and travel to the lower respiratory tract. With the increase of viral titers in the lung, the type I and III IFN responses increase, but are unable to defeat the virus and continue to allow further viral replication and spread. This leads to increasing amounts of infected cells that consequently produce high amounts of inflammatory cytokines and chemokines like IL-6, IL-8, CCL2 and CCL5. Consequently, monocytes/macrophages, neutrophils and T lymphocytes are recruited to the lung where they become activated and further amplify inflammation in feedforward loops. In addition, both the virus and cytotoxic T cells induce death of infected epithelial cells, while other infected epithelial cells produce fibrinogen that also damages the epithelial barrier. Leakage of the epithelial barriers eventually causes the release of the high amounts of cytokines and chemokines into the blood, leading to CRS, widespread inflammation, multi-organ damage and eventually death. In addition, infection of endothelial cells weakens blood vessels, allowing fluid to enter the lung cavities leading to respiratory failure.

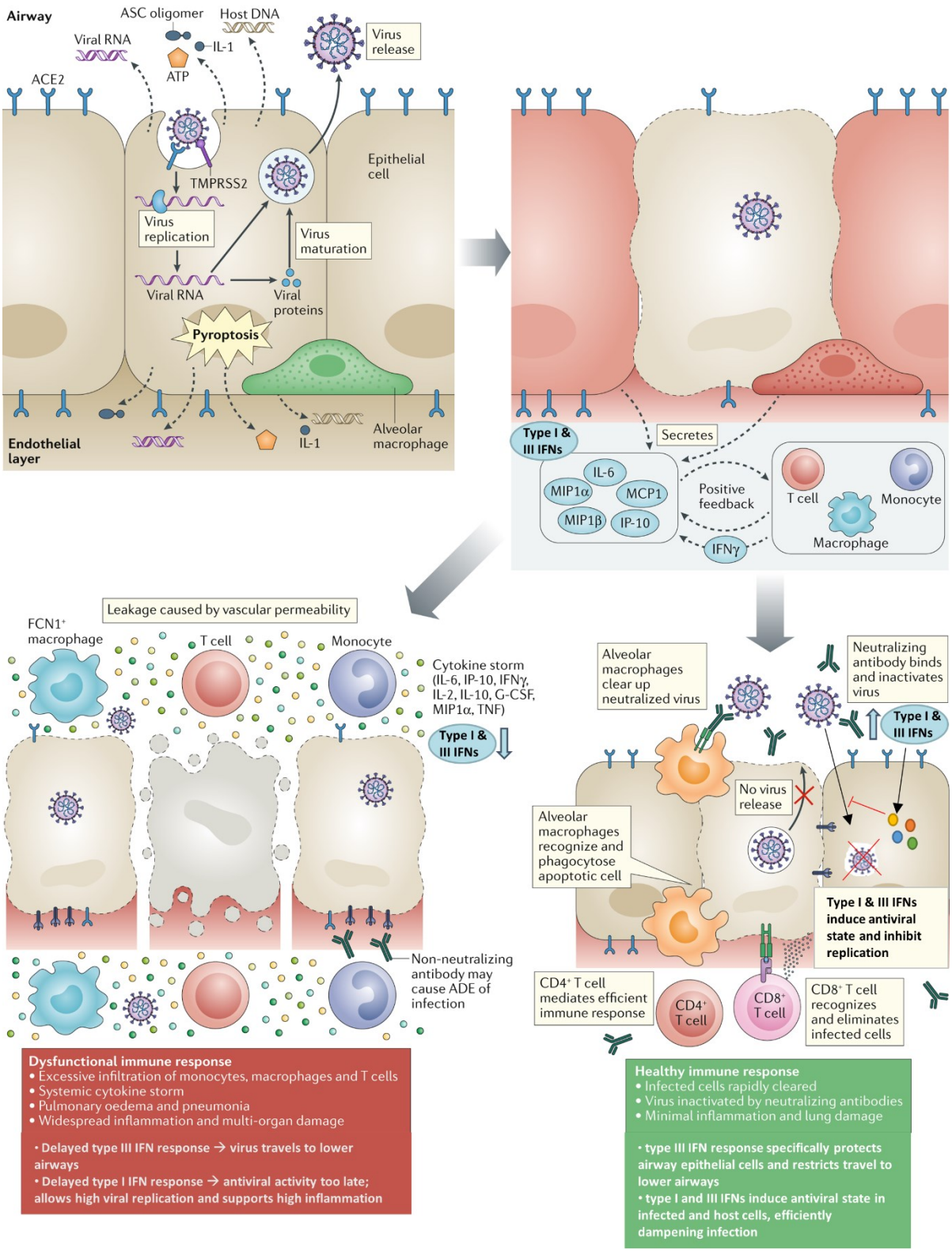

Figure 27) Proposed model for the chronology of events during SARS-CoV-2 infection that either lead to dysfunctional or healthy immune responses. *The figure was modified from Tay et al., Nature Reviews, 2020[4].*

6. Conclusion and Future Perspectives

Since COVID-19 severity correlates with dysregulated immune responses, a better understanding of the underlying mechanisms is crucial to find targets to develop more efficient antiviral treatments. Current knowledge on immunomodulation of the antiviral IFN responses by SARS-CoV-2 is mostly based on type I IFNs and in less relevant cell types, with only few mechanisms being characterized.

This study provides an optimized lentiviral transduction protocol to generate A549 and Calu-3 human lung epithelial cell lines stably expressing SARS-CoV-2 Orf3a, Orf6 and Orf9b upon doxycycline treatment. They can be used to study the viral protein interactions with host immune responses, specifically RIG-I/MDA5-mediated induction of inflammatory cytokines, chemokines and type III IFNs. Interestingly, our results suggest that expression of Orf3a, Orf6 and Orf9b in A549 cells almost exclusively inhibited type III IFN, but not inflammatory cytokine or chemokine production. We thus propose that type III IFNs are differentially regulated than type I IFNs, as also indicated by the emerging type III IFN research field. However, further studies will be required to validate our findings. Investigating mRNA expression levels of cytokines, type III IFNs as well as type I IFNs by RT-qPCR will complement our data from ELISA with more precise data. Furthermore, poly(I:C) titration will be necessary to fine-tune the analysis by decreasing the amount of cell death which correlates with the concentration of transfected poly(I:C).

Since the beginning of this study, Orf6 and Or9b have been well studied by others and have been shown to inhibit IRF3 translocation or IRF3 activation, respectively. Future studies on proteins that are less explored, such as Orf3a, Nsp13 and Nsp15 will reveal novel insight into immunomodulation by SARS-CoV-2. The A549-Orf3a cell line created in this study would be of great value for that. To mimic immunomodulation of human primary lung epithelial cells, which are difficult to obtain from the healthy human lung and unable to gene edit, a model system using iPSC-derived alveolar epithelial cells could be considered. To investigate host interactions and identify new targets for antiviral treatment, viral-host protein interaction complexes could be extracted from the cell using Strep-Tactin magnetic beads and analyzed by mass spectrometry. Based on these findings, siRNA or CRISPR/Cas9 knock-out studies of host interaction partners as well as important

mediators of IFN induction and signaling pathways could validate the findings and reveal underlying mechanisms of immunomodulation. Finally, to study the effect of SARS-CoV-2 immunomodulation on innate immune cells, co-culture systems would allow to investigate cellular crosstalk on inflammatory responses and infection outcome. In fact, another master student of our group has just recently found from RNAseq data that alveolar macrophages express the IFNLR1, suggesting that type III IFNs play an important role in mediating immune responses in alveolar macrophages. In conclusion, there is still a lot we do not know about SARS-CoV-2 infection, albeit the unprecedented speed of research focused on COVID-19. Especially in the field of host-pathogen interactions, there are still knowledge gaps as we lack conclusive studies from relevant cell models. Filling these gaps might provide us with knowledge to develop new and more effective COVID-19 treatments. Once research has succeeded in finding a cure against COVID-19, we will not only be able to save the lives of many more people and put an end to this pandemic but may also be prepared for future outbreaks of coronavirus with pandemic potential.

References

1. WorldHealthOrganization. WHO Coronavirus Disease (COVID-19) Dashboard. 2021.
2. Fauci AS, Lane HC and Redfield RR. Covid-19 - Navigating the Uncharted. *N Engl J Med*. 2020; 382: 1268-9.
3. Wu Z and McGoogan JM. Characteristics of and Important Lessons From the Coronavirus Disease 2019 (COVID-19) Outbreak in China: Summary of a Report of 72314 Cases From the Chinese Center for Disease Control and Prevention. *JAMA*. 2020; 323: 1239-42.
4. Tay MZ, Poh CM, Renia L, MacAry PA and Ng LFP. The trinity of COVID-19: immunity, inflammation and intervention. *Nat Rev Immunol*. 2020; 20: 363-74.
5. Skowronski DM, Astell C, Brunham RC, et al. Severe Acute Respiratory Syndrome (SARS): A Year in Review. *Annual Review of Medicine*. 2005; 56: 357-81.
6. Drosten C, Seilmaier M, Corman VM, et al. Clinical features and virological analysis of a case of Middle East respiratory syndrome coronavirus infection. *The Lancet Infectious Diseases*. 2013; 13: 745-51.
7. Drosten C, Gunther S, Preiser W, et al. Identification of a novel coronavirus in patients with severe acute respiratory syndrome. *N Engl J Med*. 2003; 348: 1967-76.
8. Zhou P, Yang XL, Wang XG, et al. A pneumonia outbreak associated with a new coronavirus of probable bat origin. *Nature*. 2020; 579: 270-3.
9. Cevik M, Kuppalli K, Kindrachuk J and Peiris M. Virology, transmission, and pathogenesis of SARS-CoV-2. *BMJ*. 2020; 371: m3862.
10. Letko M, Marzi A and Munster V. Functional assessment of cell entry and receptor usage for SARS-CoV-2 and other lineage B betacoronaviruses. *Nat Microbiol*. 2020; 5: 562-9.
11. Hoffmann M, Kleine-Weber H, Schroeder S, et al. SARS-CoV-2 Cell Entry Depends on ACE2 and TMPRSS2 and Is Blocked by a Clinically Proven Protease Inhibitor. *Cell*. 2020; 181: 271-80 e8.
12. Vabret N, Britton GJ, Gruber C, et al. Immunology of COVID-19: Current State of the Science. *Immunity*. 2020; 52: 910-41.
13. Ziegler CGK, Allon SJ, Nyquist SK, et al. SARS-CoV-2 Receptor ACE2 Is an Interferon-Stimulated Gene in Human Airway Epithelial Cells and Is Detected in Specific Cell Subsets across Tissues. *Cell*. 2020; 181: 1016-35 e19.
14. McBride R, van Zyl M and Fielding BC. The coronavirus nucleocapsid is a multifunctional protein. *Viruses*. 2014; 6: 2991-3018.
15. Mishra T, Sreepadmanabh M, Ramdas P, Sahu AK, Kumar A and Chande A. SARS CoV-2 Nucleoprotein Enhances the Infectivity of Lentiviral Spike Particles. *Front Cell Infect Microbiol*. 2021; 11: 663688.
16. Harrison AG, Lin T and Wang P. Mechanisms of SARS-CoV-2 Transmission and Pathogenesis. *Trends Immunol*. 2020; 41: 1100-15.

17. Lei X, Dong X, Ma R, et al. Activation and evasion of type I interferon responses by SARS-CoV-2. *Nat Commun*. 2020; 11: 3810.
18. Xia H, Cao Z, Xie X, et al. Evasion of Type I Interferon by SARS-CoV-2. *Cell Rep*. 2020; 33: 108234.
19. Yuen CK, Lam JY, Wong WM, et al. SARS-CoV-2 nsp13, nsp14, nsp15 and orf6 function as potent interferon antagonists. *Emerg Microbes Infect*. 2020; 9: 1418-28.
20. V'Kovski P, Kratzel A, Steiner S, Stalder H and Thiel V. Coronavirus biology and replication: implications for SARS-CoV-2. *Nat Rev Microbiol*. 2020.
21. Akira S, Uematsu S and Takeuchi O. Pathogen recognition and innate immunity. *Cell*. 2006; 124: 783-801.
22. Alexopoulou L, Holt AC, Medzhitov R and Flavell RA. Recognition of double-stranded RNA and activation of NF-kappaB by Toll-like receptor 3. *Nature*. 2001; 413: 732-8.
23. Ryu JH, Kim CH and Yoon JH. Innate immune responses of the airway epithelium. *Mol Cells*. 2010; 30: 173-83.
24. Schoggins JW and Rice CM. Interferon-stimulated genes and their antiviral effector functions. *Curr Opin Virol*. 2011; 1: 519-25.
25. Lazear HM, Schoggins JW and Diamond MS. Shared and Distinct Functions of Type I and Type III Interferons. *Immunity*. 2019; 50: 907-23.
26. Palm NW and Medzhitov R. Pattern recognition receptors and control of adaptive immunity. *Immunol Rev*. 2009; 227: 221-33.
27. Le Bon A and Tough DF. Links between innate and adaptive immunity via type I interferon. *Current Opinion in Immunology*. 2002; 14: 432-6.
28. Totura AL, Whitmore A, Agnihothram S, et al. Toll-Like Receptor 3 Signaling via TRIF Contributes to a Protective Innate Immune Response to Severe Acute Respiratory Syndrome Coronavirus Infection. *mBio*. 2015; 6: e00638-15.
29. Mazaleuskaya L, Veltrop R, Ikpeze N, Martin-Garcia J and Navas-Martin S. Protective role of Toll-like Receptor 3-induced type I interferon in murine coronavirus infection of macrophages. *Viruses*. 2012; 4: 901-23.
30. Thorne LG, Reuschl A-K, Zuliani-Alvarez L, et al. SARS-CoV-2 sensing by RIG-I and MDA5 links epithelial infection to macrophage inflammation. *bioRxiv*. 2020: 2020.12.23.424169.
31. Li Y, Renner DM, Comar CE, et al. SARS-CoV-2 induces double-stranded RNA-mediated innate immune responses in respiratory epithelial derived cells and cardiomyocytes. *bioRxiv*. 2020.
32. Rebendenne A, Valadao ALC, Tauziet M, et al. SARS-CoV-2 triggers an MDA-5-dependent interferon response which is unable to control replication in lung epithelial cells. *J Virol*. 2021.
33. Goubau D, Deddouche S and Reis e Sousa C. Cytosolic sensing of viruses. *Immunity*. 2013; 38: 855-69.

34. Zheng M, Karki R, Williams EP, et al. TLR2 senses the SARS-CoV-2 envelope protein to produce inflammatory cytokines. *Nature Immunology*. 2021.
35. Zalinger ZB, Elliott R, Rose KM and Weiss SR. MDA5 Is Critical to Host Defense during Infection with Murine Coronavirus. *J Virol*. 2015; 89: 12330-40.
36. Seth RB, Sun L, Ea CK and Chen ZJ. Identification and characterization of MAVS, a mitochondrial antiviral signaling protein that activates NF-kappaB and IRF 3. *Cell*. 2005; 122: 669-82.
37. Kawai T, Takahashi K, Sato S, et al. IPS-1, an adaptor triggering RIG-I- and Mda5-mediated type I interferon induction. *Nat Immunol*. 2005; 6: 981-8.
38. Fitzgerald KA, McWhirter SM, Faia KL, et al. IKKepsilon and TBK1 are essential components of the IRF3 signaling pathway. *Nat Immunol*. 2003; 4: 491-6.
39. Honda K, Takaoka A and Taniguchi T. Type I interferon [corrected] gene induction by the interferon regulatory factor family of transcription factors. *Immunity*. 2006; 25: 349-60.
40. Akira S and Hoshino K. Myeloid differentiation factor 88-dependent and -independent pathways in toll-like receptor signaling. *J Infect Dis*. 2003; 187 Suppl 2: S356-63.
41. Fitzgerald KA and Kagan JC. Toll-like Receptors and the Control of Immunity. *Cell*. 2020; 180: 1044-66.
42. Wack A, Terczynska-Dyla E and Hartmann R. Guarding the frontiers: the biology of type III interferons. *Nat Immunol*. 2015; 16: 802-9.
43. Domanski P and Colamonici OR. The type-I interferon receptor. The long and short of it. *Cytokine & Growth Factor Reviews*. 1996; 7: 143-51.
44. Sheppard P, Kindsvogel W, Xu W, et al. IL-28, IL-29 and their class II cytokine receptor IL-28R. *Nat Immunol*. 2003; 4: 63-8.
45. Kotenko SV, Gallagher G, Baurin VV, et al. IFN-lambdas mediate antiviral protection through a distinct class II cytokine receptor complex. *Nat Immunol*. 2003; 4: 69-77.
46. Durbin RK, Kotenko SV and Durbin JE. Interferon induction and function at the mucosal surface. *Immunol Rev*. 2013; 255: 25-39.
47. Galani IE, Triantafyllia V, Eleminiadou EE, et al. Interferon-lambda Mediates Non-redundant Front-Line Antiviral Protection against Influenza Virus Infection without Compromising Host Fitness. *Immunity*. 2017; 46: 875-90 e6.
48. Klinkhammer J, Schnepf D, Ye L, et al. IFN-lambda prevents influenza virus spread from the upper airways to the lungs and limits virus transmission. *Elife*. 2018; 7.
49. Blazek K, Eames HL, Weiss M, et al. IFN-λ resolves inflammation via suppression of neutrophil infiltration and IL-1β production. *Journal of Experimental Medicine*. 2015; 212: 845-53.
50. Broggi A, Tan Y, Granucci F and Zanoni I. IFN-λ suppresses intestinal inflammation by non-translational regulation of neutrophil function. *Nature Immunology*. 2017; 18: 1084-93.

51. Odendall C and Kagan JC. The unique regulation and functions of type III interferons in antiviral immunity. *Current Opinion in Virology*. 2015; 12: 47-52.
52. Dixit E, Boulant S, Zhang Y, et al. Peroxisomes are signaling platforms for antiviral innate immunity. *Cell*. 2010; 141: 668-81.
53. Odendall C, Dixit E, Stavru F, et al. Diverse intracellular pathogens activate type III interferon expression from peroxisomes. *Nat Immunol*. 2014; 15: 717-26.
54. Hadjadj J, Yatim N, Barnabei L, et al. Impaired type I interferon activity and inflammatory responses in severe COVID-19 patients. *Science*. 2020; 369: 718-24.
55. Blanco-Melo D, Nilsson-Payant BE, Liu WC, et al. Imbalanced Host Response to SARS-CoV-2 Drives Development of COVID-19. *Cell*. 2020; 181: 1036-45 e9.
56. Vanderheiden A, Ralfs P, Chirkova T, et al. Type I and Type III Interferons Restrict SARS-CoV-2 Infection of Human Airway Epithelial Cultures. *J Virol*. 2020; 94.
57. Garcia LF. Immune Response, Inflammation, and the Clinical Spectrum of COVID-19. *Front Immunol*. 2020; 11: 1441.
58. Zhou F, Yu T, Du R, et al. Clinical course and risk factors for mortality of adult inpatients with COVID-19 in Wuhan, China: a retrospective cohort study. *Lancet*. 2020; 395: 1054-62.
59. Ruan Q, Yang K, Wang W, Jiang L and Song J. Clinical predictors of mortality due to COVID-19 based on an analysis of data of 150 patients from Wuhan, China. *Intensive Care Medicine*. 2020; 46: 846-8.
60. Merad M and Martin JC. Pathological inflammation in patients with COVID-19: a key role for monocytes and macrophages. *Nat Rev Immunol*. 2020; 20: 355-62.
61. Wang P, Luo R, Zhang M, et al. A cross-talk between epithelium and endothelium mediates human alveolar-capillary injury during SARS-CoV-2 infection. *Cell Death Dis*. 2020; 11: 1042.
62. Lee I-C, Huo T-I and Huang Y-H. Gastrointestinal and liver manifestations in patients with COVID-19. *Journal of the Chinese Medical Association*. 2020; 83: 521-3.
63. Yachou Y, El Idrissi A, Belapasov V and Ait Benali S. Neuroinvasion, neurotropic, and neuroinflammatory events of SARS-CoV-2: understanding the neurological manifestations in COVID-19 patients. *Neurol Sci*. 2020; 41: 2657-69.
64. Ramlall V, Thangaraj PM, Meydan C, et al. Immune complement and coagulation dysfunction in adverse outcomes of SARS-CoV-2 infection. *Nat Med*. 2020; 26: 1609-15.
65. Bernard I, Limonta D, Mahal LK and Hobman TC. Endothelium Infection and Dysregulation by SARS-CoV-2: Evidence and Caveats in COVID-19. *Viruses*. 2020; 13.
66. Hayn M, Hirschenberger M, Koepke L, et al. Systematic functional analysis of SARS-CoV-2 proteins uncovers viral innate immune antagonists and remaining vulnerabilities. *Cell Reports*. 2021; 35: 109126.
67. Miorin L, Kehrer T, Sanchez-Aparicio MT, et al. SARS-CoV-2 Orf6 hijacks Nup98 to block STAT nuclear import and antagonize interferon signaling. *Proc Natl Acad Sci U S A*. 2020; 117: 28344-54.

68. Felgenhauer U, Schoen A, Gad HH, et al. Inhibition of SARS-CoV-2 by type I and type III interferons. *J Biol Chem*. 2020; 295: 13958-64.
69. Gordon DE, Jang GM, Bouhaddou M, et al. A SARS-CoV-2 protein interaction map reveals targets for drug repurposing. *Nature*. 2020; 583: 459-68.
70. Zhang Q, Bastard P, Liu Z, et al. Inborn errors of type I IFN immunity in patients with life-threatening COVID-19. *Science*. 2020.
71. Bastard P, Rosen LB, Zhang Q, et al. Auto-antibodies against type I IFNs in patients with life-threatening COVID-19. *Science*. 2020.
72. Turner MD, Nedjai B, Hurst T and Pennington DJ. Cytokines and chemokines: At the crossroads of cell signalling and inflammatory disease. *Biochimica et Biophysica Acta (BBA) - Molecular Cell Research*. 2014; 1843: 2563-82.
73. Huang C, Wang Y, Li X, et al. Clinical features of patients infected with 2019 novel coronavirus in Wuhan, China. *Lancet*. 2020; 395: 497-506.
74. Wang C, Xie J, Zhao L, et al. Alveolar macrophage dysfunction and cytokine storm in the pathogenesis of two severe COVID-19 patients. *EBioMedicine*. 2020; 57: 102833.
75. Qin C, Zhou L, Hu Z, et al. Dysregulation of Immune Response in Patients With Coronavirus 2019 (COVID-19) in Wuhan, China. *Clin Infect Dis*. 2020; 71: 762-8.
76. Chua RL, Lukassen S, Trump S, et al. COVID-19 severity correlates with airway epithelium-immune cell interactions identified by single-cell analysis. *Nat Biotechnol*. 2020; 38: 970-9.
77. Grant RA, Morales-Nebreda L, Markov NS, et al. Circuits between infected macrophages and T cells in SARS-CoV-2 pneumonia. *Nature*. 2021.
78. Meyers JM, Ramanathan M, Shanderson RL, et al. The proximal proteome of 17 SARS-CoV-2 proteins links to disrupted antiviral signaling and host translation. *bioRxiv*. 2021.
79. Gordon DE, Hiatt J, Bouhaddou M, et al. Comparative host-coronavirus protein interaction networks reveal pan-viral disease mechanisms. *Science*. 2020; 370.
80. Banerjee AK, Blanco MR, Bruce EA, et al. SARS-CoV-2 Disrupts Splicing, Translation, and Protein Trafficking to Suppress Host Defenses. *Cell*. 2020.
81. Thoms M, Buschauer R, Ameismeier M, et al. Structural basis for translational shutdown and immune evasion by the Nsp1 protein of SARS-CoV-2. *Science*. 2020; 369: 1249-55.
82. Jiang HW, Zhang HN, Meng QF, et al. SARS-CoV-2 Orf9b suppresses type I interferon responses by targeting TOM70. *Cell Mol Immunol*. 2020; 17: 998-1000.
83. Li JY, Liao CH, Wang Q, et al. The ORF6, ORF8 and nucleocapsid proteins of SARS-CoV-2 inhibit type I interferon signaling pathway. *Virus Res*. 2020; 286: 198074.
84. Liu XY, Wei B, Shi HX, Shan YF and Wang C. Tom70 mediates activation of interferon regulatory factor 3 on mitochondria. *Cell Res*. 2010; 20: 994-1011.

85. Miao G, Zhao H, Li Y, et al. ORF3a of the COVID-19 virus SARS-CoV-2 blocks HOPS complex-mediated assembly of the SNARE complex required for autolysosome formation. *Dev Cell*. 2020.
86. Siu KL, Yuen KS, Castano-Rodriguez C, et al. Severe acute respiratory syndrome coronavirus ORF3a protein activates the NLRP3 inflammasome by promoting TRAF3-dependent ubiquitination of ASC. *FASEB J*. 2019; 33: 8865-77.
87. Minakshi R, Padhan K, Rani M, Khan N, Ahmad F and Jameel S. The SARS Coronavirus 3a protein causes endoplasmic reticulum stress and induces ligand-independent downregulation of the type 1 interferon receptor. *PLoS One*. 2009; 4: e8342.
88. Tan YJ, Tham PY, Chan DZ, et al. The severe acute respiratory syndrome coronavirus 3a protein up-regulates expression of fibrinogen in lung epithelial cells. *J Virol*. 2005; 79: 10083-7.
89. Davalos D and Akassoglou K. Fibrinogen as a key regulator of inflammation in disease. *Semin Immunopathol*. 2012; 34: 43-62.
90. Fuss C, Palmaz JC and Sprague EA. Fibrinogen: structure, function, and surface interactions. *J Vasc Interv Radiol*. 2001; 12: 677-82.
91. Stepanenko AA and Dmitrenko VV. HEK293 in cell biology and cancer research: phenotype, karyotype, tumorigenicity, and stress-induced genome-phenotype evolution. *Gene*. 2015; 569: 182-90.
92. de Bouteiller O, Merck E, Hasan UA, et al. Recognition of double-stranded RNA by human toll-like receptor 3 and downstream receptor signaling requires multimerization and an acidic pH. *J Biol Chem*. 2005; 280: 38133-45.
93. Fitzgerald ME, Rawling DC, Potapova O, Ren X, Kohlway A and Pyle AM. Selective RNA targeting and regulated signaling by RIG-I is controlled by coordination of RNA and ATP binding. *Nucleic Acids Research*. 2016; 45: 1442-54.
94. Elegheert J, Behiels E, Bishop B, et al. Lentiviral transduction of mammalian cells for fast, scalable and high-level production of soluble and membrane proteins. *Nat Protoc*. 2018; 13: 2991-3017.
95. Durand S and Cimarelli A. The inside out of lentiviral vectors. *Viruses*. 2011; 3: 132-59.
96. Naldini L, Blomer U, Gallay P, et al. In vivo gene delivery and stable transduction of nondividing cells by a lentiviral vector. *Science*. 1996; 272: 263-7.
97. Li M, Husic N, Lin Y and Snider BJ. Production of lentiviral vectors for transducing cells from the central nervous system. *J Vis Exp*. 2012: e4031.
98. Coffin JM. Retrovirus restriction revealed. *Nature*. 1996; 382: 762-3.
99. Miyoshi H, Blomer U, Takahashi M, Gage FH and Verma IM. Development of a self-inactivating lentivirus vector. *J Virol*. 1998; 72: 8150-7.
100. Dull T, Zufferey R, Kelly M, et al. A third-generation lentivirus vector with a conditional packaging system. *J Virol*. 1998; 72: 8463-71.

101. Akkina RK, Walton RM, Chen ML, Li QX, Planelles V and Chen IS. High-efficiency gene transfer into CD34+ cells with a human immunodeficiency virus type 1-based retroviral vector pseudotyped with vesicular stomatitis virus envelope glycoprotein G. *J Virol*. 1996; 70: 2581-5.
102. Sharma S, Miyanohara A and Friedmann T. Separable mechanisms of attachment and cell uptake during retrovirus infection. *J Virol*. 2000; 74: 10790-5.
103. Zufferey R, Nagy D, Mandel RJ, Naldini L and Trono D. Multiply attenuated lentiviral vector achieves efficient gene delivery in vivo. *Nat Biotechnol*. 1997; 15: 871-5.
104. Fouchier RA, Simon JH, Jaffe AB and Malim MH. Human immunodeficiency virus type 1 Vif does not influence expression or virion incorporation of gag-, pol-, and env-encoded proteins. *J Virol*. 1996; 70: 8263-9.
105. Mastromarino P, Conti C, Goldoni P, Hauttecoeur B and Orsi N. Characterization of membrane components of the erythrocyte involved in vesicular stomatitis virus attachment and fusion at acidic pH. *J Gen Virol*. 1987; 68 (Pt 9): 2359-69.
106. Burns JC, Friedmann T, Driever W, Burrascano M and Yee JK. Vesicular stomatitis virus G glycoprotein pseudotyped retroviral vectors: concentration to very high titer and efficient gene transfer into mammalian and nonmammalian cells. *Proceedings of the National Academy of Sciences*. 1993; 90: 8033-7.
107. Engelman A and Cherepanov P. The structural biology of HIV-1: mechanistic and therapeutic insights. *Nature Reviews Microbiology*. 2012; 10: 279-90.
108. Takara Bio USA I. Lenti-X™ Lentiviral Expression System User Manual. 2015.
109. Wu X, Wakefield JK, Liu H, et al. Development of a novel trans-lentiviral vector that affords predictable safety. *Mol Ther*. 2000; 2: 47-55.
110. Gossen M and Bujard H. Tight control of gene expression in mammalian cells by tetracycline-responsive promoters. *Proc Natl Acad Sci U S A*. 1992; 89: 5547-51.
111. Das AT, Tenenbaum L and Berkhout B. Tet-On Systems For Doxycycline-inducible Gene Expression. *Curr Gene Ther*. 2016; 16: 156-67.
112. Millipore M. Lentiviral Titer via p24 (viral coat protein) ELISA Assay. https://www.sigmaaldrich.com/technical-documents/protocols/biology/lentiviral-titer-p24-assay.html: Merck Millipore 2021.
113. Li W, Moore MJ, Vasilieva N, et al. Angiotensin-converting enzyme 2 is a functional receptor for the SARS coronavirus. *Nature*. 2003; 426: 450-4.
114. Cheung CY, Poon LL, Ng IH, et al. Cytokine responses in severe acute respiratory syndrome coronavirus-infected macrophages in vitro: possible relevance to pathogenesis. *J Virol*. 2005; 79: 7819-26.
115. Yilla M, Harcourt BH, Hickman CJ, et al. SARS-coronavirus replication in human peripheral monocytes/macrophages. *Virus Research*. 2005; 107: 93-101.
116. Liao M, Liu Y, Yuan J, et al. Single-cell landscape of bronchoalveolar immune cells in patients with COVID-19. *Nature Medicine*. 2020; 26: 842-4.

117. Chu H, Chan JF, Wang Y, et al. Comparative Replication and Immune Activation Profiles of SARS-CoV-2 and SARS-CoV in Human Lungs: An Ex Vivo Study With Implications for the Pathogenesis of COVID-19. *Clin Infect Dis*. 2020; 71: 1400-9.
118. al Yacoub N, Romanowska M, Haritonova N and Foerster J. Optimized production and concentration of lentiviral vectors containing large inserts. *J Gene Med*. 2007; 9: 579-84.
119. Denning W, Das S, Guo S, Xu J, Kappes JC and Hel Z. Optimization of the transductional efficiency of lentiviral vectors: effect of sera and polycations. *Mol Biotechnol*. 2013; 53: 308-14.
120. Cornetta K and Anderson WF. Protamine sulfate as an effective alternative to polybrene in retroviral-mediated gene-transfer: implications for human gene therapy. *Journal of Virological Methods*. 1989; 23: 187-94.
121. Morita S-y, Shirakawa S, Kobayashi Y, et al. Enzymatic measurement of phosphatidylserine in cultured cells. *Journal of Lipid Research*. 2012; 53: 325-30.
122. Berggren WT, Lutz M and Modesto V. General Spinfection Protocol. *StemBook*. Cambridge (MA): Harvard Stem Cell Institute
Copyright: © 2012 W. Travis Berggren, Margaret Lutz and Veronica Modesto., 2008.
123. Davis E. Lentivirus: That's My MOI, and I'm Sticking To It. www.genecopoeia.com: GeneCopoeia, Inc. , 2014.
124. Ren Y, Shu T, Wu D, et al. The ORF3a protein of SARS-CoV-2 induces apoptosis in cells. *Cell Mol Immunol*. 2020; 17: 881-3.
125. Moonmuang S, Saoin S, Chupradit K, et al. Modulated expression of the HIV-1 2LTR zinc finger efficiently interferes with the HIV integration process. *Biosci Rep*. 2018; 38.
126. Stepanenko AA and Heng HH. Transient and stable vector transfection: Pitfalls, off-target effects, artifacts. *Mutat Res*. 2017; 773: 91-103.
127. Stewart CE, Torr EE, Mohd Jamili NH, Bosquillon C and Sayers I. Evaluation of differentiated human bronchial epithelial cell culture systems for asthma research. *J Allergy (Cairo)*. 2012; 2012: 943982.
128. Tseng C-TK, Tseng J, Perrone L, Worthy M, Popov V and Peters CJ. Apical Entry and Release of Severe Acute Respiratory Syndrome-Associated Coronavirus in Polarized Calu-3 Lung Epithelial Cells. *Journal of Virology*. 2005; 79: 9470-9.
129. Foster KA, Oster CG, Mayer MM, Avery ML and Audus KL. Characterization of the A549 cell line as a type II pulmonary epithelial cell model for drug metabolism. *Exp Cell Res*. 1998; 243: 359-66.
130. Aghapour M, Raee P, Moghaddam SJ, Hiemstra PS and Heijink IH. Airway Epithelial Barrier Dysfunction in Chronic Obstructive Pulmonary Disease: Role of Cigarette Smoke Exposure. *American Journal of Respiratory Cell and Molecular Biology*. 2018; 58: 157-69.
131. Vénéreau E, Ceriotti C and Bianchi ME. DAMPs from Cell Death to New Life. *Front Immunol*. 2015; 6: 422.

132. Rowe RG and Daley GQ. Induced pluripotent stem cells in disease modelling and drug discovery. *Nat Rev Genet*. 2019; 20: 377-88.
133. Robinton DA and Daley GQ. The promise of induced pluripotent stem cells in research and therapy. *Nature*. 2012; 481: 295-305.
134. Yang L, Han Y, Nilsson-Payant BE, et al. A Human Pluripotent Stem Cell-based Platform to Study SARS-CoV-2 Tropism and Model Virus Infection in Human Cells and Organoids. *Cell Stem Cell*. 2020; 27: 125-36 e7.
135. Soussi T. Handbook of p53 mutation in cell lines. 2010.
136. Ma-Lauer Y, Carbajo-Lozoya J, Hein MY, et al. p53 down-regulates SARS coronavirus replication and is targeted by the SARS-unique domain and PLpro via E3 ubiquitin ligase RCHY1. *Proc Natl Acad Sci U S A*. 2016; 113: E5192-201.
137. Jacob A, Vedaie M, Roberts DA, et al. Derivation of self-renewing lung alveolar epithelial type II cells from human pluripotent stem cells. *Nature Protocols*. 2019; 14: 3303-32.
138. Li J, Liu Y and Zhang X. Murine coronavirus induces type I interferon in oligodendrocytes through recognition by RIG-I and MDA5. *J Virol*. 2010; 84: 6472-82.
139. Moreno-Eutimio MA, López-Macías C and Pastelin-Palacios R. Bioinformatic analysis and identification of single-stranded RNA sequences recognized by TLR7/8 in the SARS-CoV-2, SARS-CoV, and MERS-CoV genomes. *Microbes Infect*. 2020; 22: 226-9.
140. Li Y, Chen M, Cao H, Zhu Y, Zheng J and Zhou H. Extraordinary GU-rich single-strand RNA identified from SARS coronavirus contributes an excessive innate immune response. *Microbes Infect*. 2013; 15: 88-95.
141. Becker S, Dailey L, Soukup JM, Silbajoris R and Devlin RB. TLR-2 is involved in airway epithelial cell response to air pollution particles. *Toxicology and Applied Pharmacology*. 2005; 203: 45-52.
142. Bérubé J, Bourdon C, Yao Y and Rousseau S. Distinct intracellular signaling pathways control the synthesis of IL-8 and RANTES in TLR1/TLR2, TLR3 or NOD1 activated human airway epithelial cells. *Cellular Signalling*. 2009; 21: 448-56.
143. Wang W, Wang WH, Azadzoi KM, et al. Activation of innate antiviral immune response via double-stranded RNA-dependent RLR receptor-mediated necroptosis. *Sci Rep*. 2016; 6: 22550.
144. Dauletbaev N, Cammisano M, Herscovitch K and Lands LC. Stimulation of the RIG-I/MAVS Pathway by Polyinosinic:Polycytidylic Acid Upregulates IFN-beta in Airway Epithelial Cells with Minimal Costimulation of IL-8. *J Immunol*. 2015; 195: 2829-41.
145. Palchetti S, Starace D, De Cesaris P, Filippini A, Ziparo E and Riccioli A. Transfected poly(I:C) activates different dsRNA receptors, leading to apoptosis or immunoadjuvant response in androgen-independent prostate cancer cells. *J Biol Chem*. 2015; 290: 5470-83.
146. Laura G, Liu Y, Fernandes K, et al. ORMDL3 regulates poly I:C induced inflammatory responses in airway epithelial cells. *BMC Pulm Med*. 2021; 21: 167.

147. Bianchi F, Alexiadis S, Camisaschi C, et al. TLR3 Expression Induces Apoptosis in Human Non-Small-Cell Lung Cancer. *Int J Mol Sci*. 2020; 21.
148. Guillot L, Le Goffic R, Bloch S, et al. Involvement of Toll-like Receptor 3 in the Immune Response of Lung Epithelial Cells to Double-stranded RNA and Influenza A Virus*. *Journal of Biological Chemistry*. 2005; 280: 5571-80.
149. Groskreutz DJ, Monick MM, Powers LS, Yarovinsky TO, Look DC and Hunninghake GW. Respiratory syncytial virus induces TLR3 protein and protein kinase R, leading to increased double-stranded RNA responsiveness in airway epithelial cells. *J Immunol*. 2006; 176: 1733-40.
150. Tissari J, Siren J, Meri S, Julkunen I and Matikainen S. IFN-alpha enhances TLR3-mediated antiviral cytokine expression in human endothelial and epithelial cells by up-regulating TLR3 expression. *J Immunol*. 2005; 174: 4289-94.
151. Janovec V, Hodek J, Clarova K, et al. Toll-like receptor dual-acting agonists are potent inducers of PBMC-produced cytokines that inhibit hepatitis B virus production in primary human hepatocytes. *Sci Rep*. 2020; 10: 12767.
152. Meas HZ, Haug M, Beckwith MS, et al. Sensing of HIV-1 by TLR8 activates human T cells and reverses latency. *Nat Commun*. 2020; 11: 147.
153. Cherfils-Vicini J, Platonova S, Gillard M, et al. Triggering of TLR7 and TLR8 expressed by human lung cancer cells induces cell survival and chemoresistance. *J Clin Invest*. 2010; 120: 1285-97.
154. Banerjee A, El-Sayes N, Budylowski P, et al. Experimental and natural evidence of SARS-CoV-2 infection-induced activation of type I interferon responses. *iScience*. 2021: 102477.
155. Osterlund PI, Pietilä TE, Veckman V, Kotenko SV and Julkunen I. IFN regulatory factor family members differentially regulate the expression of type III IFN (IFN-lambda) genes. *J Immunol*. 2007; 179: 3434-42.
156. Thomson SJP, Goh FG, Banks H, et al. The role of transposable elements in the regulation of IFN-lambda1 gene expression. *Proceedings of the National Academy of Sciences of the United States of America*. 2009; 106: 11564-9.
157. Cooper JR, Abdullatif MB, Burnett EC, et al. Long Term Culture of the A549 Cancer Cell Line Promotes Multilamellar Body Formation and Differentiation towards an Alveolar Type II Pneumocyte Phenotype. *PLOS ONE*. 2016; 11: e0164438.
158. Neufeldt CJ, Cerikan B, Cortese M, et al. SARS-CoV-2 infection induces a pro-inflammatory cytokine response through cGAS-STING and NF-κB. *bioRxiv*. 2020: 2020.07.21.212639.

Supplementary

Supplementary A

LB agar and medium formulation and preparation

LB medium recipe:

- 4 g NaCl
- 4 g Tryptone
- 2 g Yeast Extract
- 400 mL dH_2O (MilliQ)

To prepare 400 mL of LB medium, the solid ingredients (see Table X) were added to an autoclaved bottle and filled up to 400 mL with dH_2O. The LB medium was autoclaved on liquid cycle and the bottle allowed to cool down on the bench. For ampicillin-resistant medium, 100 µg/mL ampicillin (1:1000) was added to the LB medium after cooling down to a temperature of about 50-55°C. The LB medium was stored at 4°C until usage.

LB agar recipe:

- 5 g NaCl
- 5 g Tryptone
- 2.5 g Yeast Extract
- 15 g Agarose
- 500 mL dH2O (MilliQ)

To prepare app roximately 20 agar plates, solid ingredients (see Table X) were added to an autoclaved bottle and filled up to 500 mL with deionized H_2O (dH_2O, MilliQ). The LB agar medium was autoclaved on liquid cycle and the bottle allowed to cool down on the bench. For ampicillin-resistant plates, 100 µg/mL ampicillin (1:1000) was added to LB agar medium after cooling down to a temperature of about 50-55°C. Next to a flame, the plates were filled 1/2 – 2/3 full and allowed to cool down to room temperature for a few hours. When cool, the plates were sealed in a big and stored at 4°C until usage.

Supplementary B

Molecular weights of SARS-CoV-2 viral proteins

Suppl. Table 1) A list of the molecular weight (kDa) of all transfected SARS-CoV-2 viral proteins, compared to Krogan's lab.

SARS-CoV-2 viral protein	Molecular Mass [kDa]
NSP1	19.8
NSP5	33.8
NSP13	66.9
NSP15	38.8
ORF3A	31.1
ORF6	7.3
ORF9B	10.8
(GFP)	28

Concentration of Lentiviral stocks

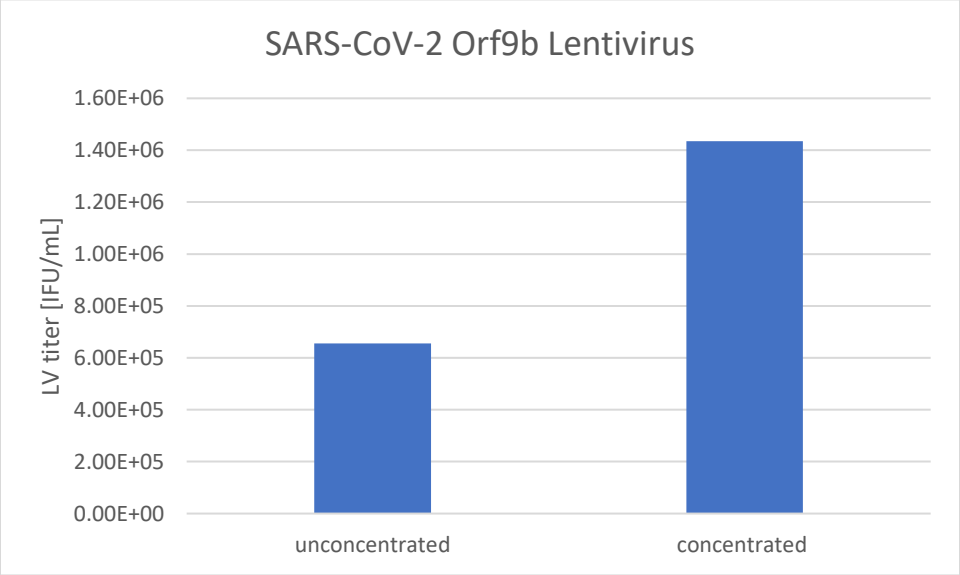

Suppl. Figure 1) Lentiviral titer of SARS-CoV-2 Orf9b Lentivirus before and after concentration with Lenti-X Concentrator (Takara Bio). *1:10 concentration of lentiviral stock using Lenti-X Concentrator. Titer determination by p24 measurement using Lenti-X GoStix Plus®.*

Optimization of lentiviral transduction of THP-1 cells

Puromycin kill curve

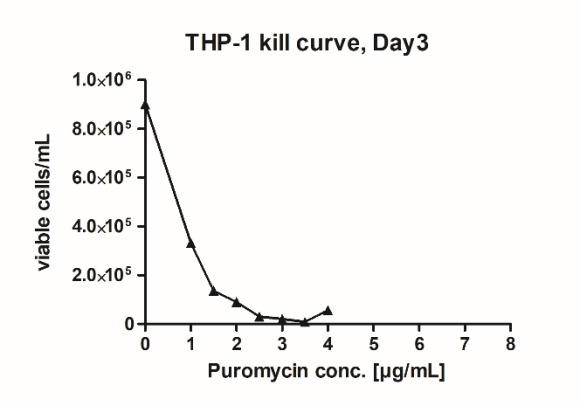

Suppl. Figure 2) Puromycin kill curve of THP-1 cells. *Cells were incubated with a range of puromycin concentrations (0-4 µg/mL) for 3 days and number of viable cells determined by Trypan Blue Exclusion. The concentration for selection after lentiviral transduction was determined to be 2.5-3 µg/mL.*

Doxycycline titration over time

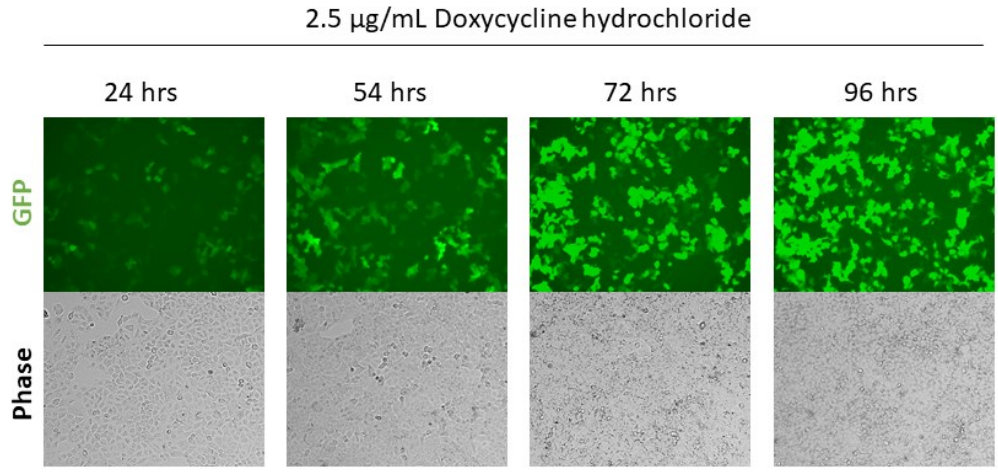

Suppl. Figure 3) Doxycycline titration over time. *A549-GFP cells were incubated with 2.5 µg/mL Doxcycycline for 24-96 hours and analysed by fluorescence microscopy (EVOS™).*

Second validation and doxycycline titration of A549-NSP5 and A459-NSP13 cell lines

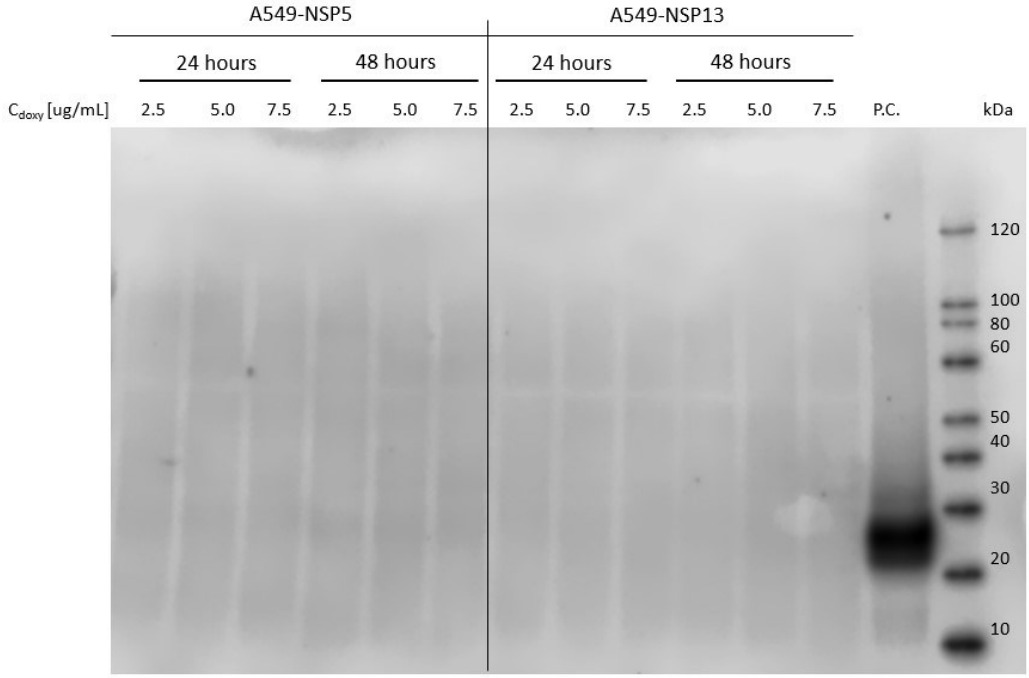

Suppl. Figure 4) Western blot analysis of transduced A549-NSP5 and -NSP13 cell lysates. *Cells were seeded in a 24-well plate the day before. The cells were then incubated with doxycycline at 2.5, 5.0 or 7.5 µg/mL for 24 or 48 hours, respectively and lysed in 150 uL RIPA buffer with protease inhibitor cocktail. After SDS-PAGE gel electrophoresis, transfer onto membrane and blocking with 5% BSA, the membrane was incubated with Mouse Anti-Strep-II antibody and Goat-anti-Mouse HRP antibody and chemiluminescence visualized with Li-Cor Odyssey scanner. The positive control (P.C.) included transduced A549-Orf3a lysate.*

Supplementary C

Cell viability of mock controls

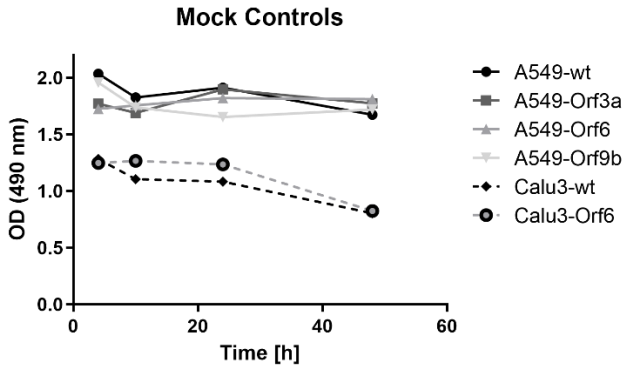

Suppl. Figure 5) Optical Density (O.D.) (490nm) values for mock controls during MTS cell viability assay. *The mock controls were used to normalize measures from the treated cells.*

Mirjam Dürkoop

Studying the immunomodulatory effects of SARS-CoV-2 viral proteins in human lung epithelial cell lines

NTNU
Kunnskap for en bedre verden

CEMIR
Centre of Molecular Inflammation Research